Combining Nanoparticles and Surfactants to Stabilize CO_2 Foam for CCUS

Master Thesis in Reservoir Physics

By

Aleksandra Magdalena Soyke

Department of Physics and Technology

University of Bergen

April 2020

Abstract

CCUS (Carbon Capture, Utilization and Storage) is regarded as an important contributor in the ongoing energy transition. Anthropogenic CO_2 emissions can be mitigated by capturing CO_2 from point sources followed by permanent storage in geological formations. It is critical to utilize all the available storage volume in the formation because of limited optimal storage sites. Pure CO_2 injection has previously demonstrated poor sweep efficiency and reduced overall CO_2 storage capacity due to viscous fingering and gravity override. These challenges can be overcome by foaming the injected CO_2 for improved mobility control. The main objectives of this thesis were to investigate the ability of foaming agents (i.e. nanoparticles and/or surfactants) to stabilize CO_2 foam in sandstone, and subsequently determine the effect of oil on CO_2 foam flow properties.

Laboratory steady state co-injections of CO_2 and different foaming solutions were performed to investigate the ability of nanoparticles to generate and stabilize CO_2 foam when combined with nonionic surfactants. Results showed a synergistic effect when including nanoparticles, even at low concentrations (150 ppm), compared to surfactants only. Injection rate scans showed the most significant effects of nanoparticles at a higher injection rate (8 feet/day), where apparent viscosity increased by 26% leading to increased CO_2 sweep efficiency. Foam generation was stronger at low gas fraction (0.6) compared with high gas fraction (0.9), regardless of foaming agent. The residual water saturation during co-injections decreased with approximately 30% when including nanoparticles compared with surfactants only, indicating increased CO_2 storage capacity.

Unsteady state CO_2 injections were conducted to study dynamic foam generation and coalescence processes using nonionic and anionic surfactants, separately or in combination with nanoparticles. Generally, foam generation was observed using both types of surfactants and apparent viscosity increased by two orders of magnitude compared with pure CO_2 injection (without foaming agent). Foam generation contributed to improved sweep efficiency and the average residual water saturation decreased by 60% relative to pure CO_2 injection, and therefore increased the CO_2 storage capacity. Results showed stronger foam generation using anionic surfactants compared to nonionic surfactants. A correlation between foam strength and coalescence rate was observed, where strong foams coalesced faster than weaker foams. Nanoparticles stabilized foams generated with anionic surfactants, identified with delayed foam coalescence both at high (1500 ppm) and low (150 ppm) nanoparticle concentrations. No stabilizing effect was observed when using nonionic surfactants and nanoparticles.

Emulsion formation and destabilizing effect of oil on foaming agents were investigated during steady and unsteady state injections at miscible conditions. Oil and CO_2 were co-injected, and the experimental design facilitated significant generation of oil-in-water emulsions. Results showed generation of a stronger foam/emulsion system using nonionic surfactants compared to anionic surfactants, with observation of 165% higher apparent viscosity when using nonionic surfactants. Combining nanoparticles and nonionic surfactants, apparent viscosity decreased by approximately 50% indicating a weaker foam/emulsion system. Anionic surfactants in combination with nanoparticles showed a stronger and more stable system as the apparent viscosity increased by approximately 30% compared to using anionic surfactants separately. Nanoparticles demonstrated a stabilizing effect on foam/emulsion systems when combined with anionic surfactant. Overall, CO_2 foam generation by surfactants and by surfactants combined with nanoparticles caused delayed gas breakthrough and improved sweep efficiency compared to pure CO_2 injection, demonstrating the potential for CO_2 foam to improve carbon utilization and storage processes.

Acknowledgements

First of all, I would like to express my gratitude to my supervisors Professor Martin Fernø and Researcher Jarand Gauteplass at the Department of Physics and Technology at the University of Bergen, for giving me the opportunity to work on an interesting research project. Thank you, Martin and Jarand, for the support, guidance and valuable discussions. In addition, I would like to thank PhD candidate Tore L. Føyen for experimental guidance, collaboration, patience, and for willingly sharing valuable experience and knowledge.

Thanks to all my friends and fellow students contributing to five memorable years at the University of Bergen. Thank you for sharing your knowledge and experience, for always being positive and for memorable trips together.

I would also like to thank my family. Thank you for your endless love and support. Without you, I would never be where I am today.

Last but not least, thank you Chris Joakim for supporting and motivating me during these years. Thank you for making me laugh and for always believing in me.

Bergen, April 2020

Aleksandra Soyke

Table of Contents

Abstract III

Acknowledgements V

Part I. Introduction and Theory 1

1. Introduction 3

2. Fundamentals of Reservoir Engineering 5

2.1. Relative Permeability and Wettability 5

2.2. Capillary Pressure 6

2.3. Oil Recovery 6

2.4. Physical Properties of CO_2 7

2.5. Miscibility 9

2.6. Diffusion and Dispersion 10

2.7. Oil Swelling 11

3. Carbon Capture, Utilization and Storage (CCUS) 13

3.1. CO_2 Storage in Saline Aquifers 13

3.2. CO_2 EOR and Storage in Hydrocarbon Reservoirs 15

4. CO_2 Foam for Mobility Control in Sediments 17

4.1. Foam Characteristics 18

4.2. Foam Generation 19

4.3. Foam Stability 21

4.4. Foam Flow Behavior 22

4.5. CO_2 Foaming Formulas 23

Part II. Experimental Procedure 25

5. Material and Methods 27

5.1. Rock Material and Preparation 28

5.2. Fluid Properties 29

5.3. Experimental Setup 31

5.4. Unsteady State CO_2 Injection 33

5.5. Steady State Co-Injection 34

5.6. Cleaning and Preparation Procedure 35

Part III. Results and Discussion 37

6. CO_2 Foam Generation and Stability 39

6.1. The Effect of Foaming Agent on CO_2 Foam Generation and Stability 39

7. CO_2 Foam Generation and Coalescence 45

7.1. Baseline 45
7.2. The Effect of Surfactant Type and Concentration on CO_2 Foam Generation and Coalescence 47
7.3. The Effect of Nanoparticles on CO_2 Foam Generation and Coalescence 53
8. The Effect of Oil on CO_2 Foam 57
8.1. Baseline 57
8.2. Foam Generation and Stability 59
8.3. Foam Coalescence 61
Part IV. Conclusion and Future Work 58
9. Conclusions 67
10. Future Work 69
Part V. Nomenclature, Abbreviations, Appendix and References 71
Nomenclature 73
Abbreviations 75
References 77
Appendix 85
A. Core Analysis 85
B. Permeability Variations 87
C. Surfactant and Nanoparticle Concentration Calculations 89
D. Rate Scan Results 91
E. Sand Packs 93
F. Uncertainties 99

Part I. Introduction and Theory

1. Introduction

Energy plays an important role in everyone's life and due to increased population and prosperity global energy consumption has increased over the last decade. According to BP Statistical Review of World Energy (2019), the primary energy consumption grew at a rate of 2.9% in 2018. Almost double the 10-year average of 1.5% per year. As a result of this high energy consumption, the emissions of greenhouse gas, CO_2, has increased by 1.7% since 2018 and are the highest in history (IPCC, 2018). To mitigate the emissions, development of renewable and clean energy solutions are critical focus areas. Still, 80% of global energy today comes from fossil fuels and will continue to be an important energy source in the decades to come. Therefore, other measures are necessary to reduce the emissions and meet the increasing energy demand.

Carbon capture and storage (CCS), is a known technology for mitigation of CO_2 emissions by capturing anthropogenic CO_2 and storing it in geological formations (IPCC, 2005). The method is considered safe, can store CO_2 for thousands of years and has been successfully applied since 1970s. CCS contributes to mitigation of climate problems, however, the technology is currently expensive and not profitable. To use the technology in a profitable way, CO_2 may be utilized to produce other products, which is called carbon capture, utilization and storage (CCUS).

CO_2 can, among other things, be utilized to enhance oil recovery from new and mature hydrocarbon fields. CO_2 for enhanced oil recovery (EOR) is a known technology which has been performed for over 40 years, but due to severe density and viscosity differences between the injected CO_2 and the displaced oil, challenges like gravity override, viscous fingering and early gas breakthrough has been observed and led to poor sweep efficiency (Mo et al., 2012). These flow instabilities can be mitigated by generating CO_2 foam to reduce CO_2 mobility (Talebian et al., 2014).

CO_2 foams are thermodynamically unstable and foaming agents are necessary in order to generate stable foams (Sheng, 2013). Surfactants are the most commonly used foaming agents due to their ability to generate stronger foams, but the long-term stability of surfactant-induced CO_2 foam is difficult to obtain. Using nanoparticles to stabilize foam may increase the long-term stability of CO_2 foams, especially at harsh reservoir conditions, such as high temperature and salinity (Enrick et al., 2012). Generation of a stable foam is essential to increase oil recovery but also to improve the potential CO_2 storage capacity by replacing initial reservoir fluids with CO_2.

Feasibility of nanoparticles to stabilize CO_2 foam has been studied during this thesis. Surfactants and a combination of surfactants and nanoparticles were used as foaming agent to identify the effect of nanoparticles on foam. Steady state co-injections of CO_2 and foaming agents were performed to determine ability of nanoparticles to generate and stabilize foam, whereas unsteady state CO_2 injections were conducted to study foam coalescence. In addition, the use of nanoparticles to stabilize foam in presence of oil was investigated.

2. Fundamentals of Reservoir Engineering

Understanding the fundamental petrophysical properties and concepts of reservoir engineering is necessary in order to understand CO_2 flow behavior through a porous medium in the context of CCUS. This chapter describes the fundamentals of reservoir engineering as well as the physical properties and behavior of CO_2 essential for this thesis.

2.1. Relative Permeability and Wettability

Relative permeability is a dimensionless term describing flow of a fluid in the presence of another. When a single fluid is present in a porous media, its relative permeability equals 1. The presence of more than one fluid, however, inhibits the fluid flow and the relative permeability is less than 1. Relative permeability can be defined as

$$k_{rf} = \frac{K_f}{K} \tag{1}$$

where k_{rf} is the relative permeability of fluid f , K_f is the effective permeability of fluid f and K is the absolute permeability of the porous media (Warner, 2015). Relative permeability can also be described as a function of fluid saturation. In general, the relative permeability of a fluid increases with increasing fluid saturation. The functionality between relative permeability and saturation is also a function of wettability (Zolotuchin, 2000).

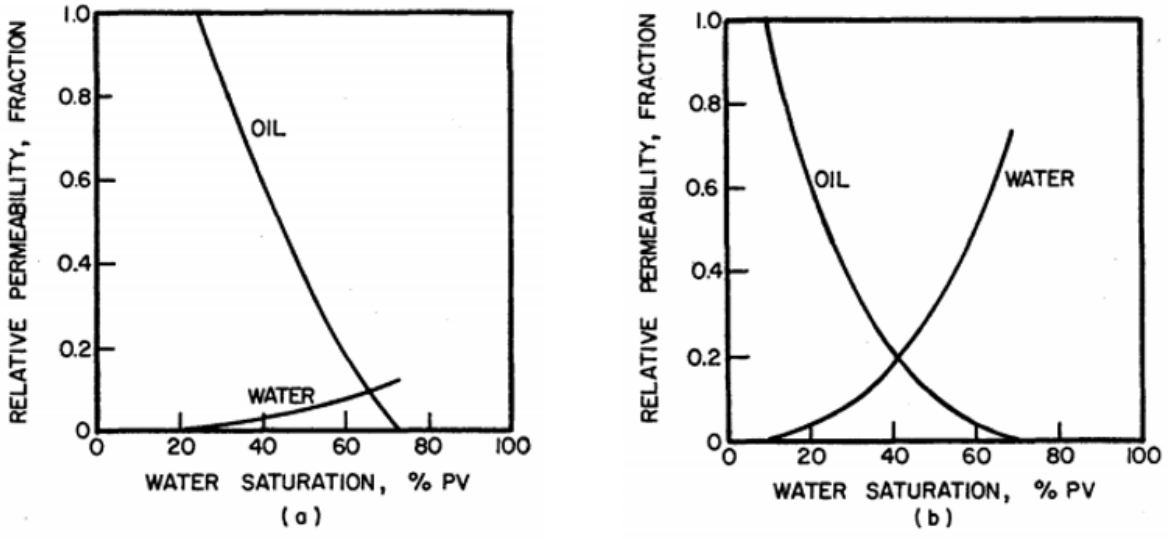

Figure 2.1 Typical relative permeability curve for (a) strongly water-wet rock and (b) strongly oil-wet rock (Anderson, 1987b).

Wettability can be defined as the tendency of one fluid to spread on or adhere to a solid surface in the presence of other immiscible fluids (Anderson, 1986). When two immiscible fluids are present near a solid surface, one of the fluids will have greater cohesive force than the other. The fluid with the greatest cohesive forces is the wetting fluid. In a rock/oil/brine system, wettability is a measure of the preference that the rock has, to either oil or water. When the rock is water-wet, there is a tendency for water to be in contact with the majority of the rock surface and occupy the smaller pores. Similarly, in an oil-wet system, the rock is preferentially in contact with oil and the water will flow through the

bigger pores. Figure 2.1 illustrates the relative permeability for water-wet and oil-wet systems. When the water occupies the smaller pores the water flow is low, hence there is a low relative permeability of water (Anderson, 1987b). In addition to relative permeability, wettability has been shown to influence waterflood behavior, capillary pressure, irreducible water saturation, residual oil saturation, dispersion and electrical properties (Fernø et al., 2010).

2.2. Capillary Pressure

Capillary pressure is the pressure difference across the interface between two immiscible fluids arising from capillary forces due to the interfacial tension between the surfaces of the fluids (Anderson, 1987a). Capillary pressure is defined as

$$Pc = p_{nw} - p_w \tag{2}$$

or

$$Pc = \frac{2\sigma cos\theta}{r} \tag{3}$$

where Pc is the capillary pressure, p_{nw} and p_w are the pressures of the non-wetting and wetting fluids respectively, σ is the interfacial tension, θ is the wetting angle between the fluids and r is the pore radius.

Equation 2 shows that an increase in pressure of the non-wetting phase results in an increase of the capillary pressure, a process called drainage. When pressure of the wetting phase increases, the capillary pressure decreases, called imbibition. Additionally, capillary pressure depends on the wettability (Eq.3). Drainage-like processes with water as the wetting phase were performed during this thesis.

2.3. Oil Recovery

Generally, oil production operations are divided into three stages: primary, secondary and tertiary recovery (Sheng, 2011). Primary oil recovery refers to the amount of oil produced by natural driving mechanisms such as rock and fluid expansion, depletion, water drive or gas cap drive. Secondary recovery involves the introduction of artificial energy into the reservoir to maintain reservoir pressure and increase volumetric sweep efficiency. This recovery refers to techniques such as water or gas injection (Romero-Zerón, 2012). Primary and secondary recovery, also called conventional recovery, are both associated with low oil recovery, where approximately 35% of the oil originally in place (OOIP) is recovered (Lake, Johns, Rossen, & Pope, 2014). Low recovery during the primary stage is caused by a rapid decrease in reservoir pressure, while the recovery during the secondary stage is low mainly because of poor volumetric sweep efficiency and uneconomic water production due to unfavorable mobility ratio between oil and the injected fluid and reservoir heterogeneity (Zolotuchin, 2000). In order to produce the remaining amount of oil, the enhanced oil recovery (EOR) techniques can be implemented. Usually, EOR refers to the tertiary recovery but the techniques have also been implemented in the secondary stage of the production (Lake, 2014).

EOR is the production of oil by injection of fluids and energy not normally present in the reservoir (Lake, 2014). EOR techniques are implemented to increase the oil production from mature hydrocarbon fields after performing conventional recovery methods such as depletion and waterflooding. During the last decades, there has been a decline in new oil discoveries and most of the current world oil production comes from mature fields. At the same time, the global energy demand has grown significantly. Therefore, it is believed that EOR techniques will play a significant role in meeting a continuously growing energy demand (Alvarado et al., 2010).

The main goal of the EOR techniques is to increase the overall displacement efficiency by increasing the microscopic and macroscopic displacement efficiency (Romero-Zerón, 2012). Both efficiencies refer to the mobilization of the trapped oil in a reservoir. The microscopic efficiency refers to mobilization of oil at the pore scale, while the macroscopic efficiency describes how well the displacing fluid is sweeping through the reservoir and displacing the oil towards the production well (Sehbi et al., 2001). By reducing the capillary forces, interfacial tension between oil and the displacing fluid, and/or viscosity of oil, the amount of trapped oil decreases and the microscopic displacement efficiency improves. Generating a more favorable mobility ratio between oil and the displacing fluid improves the macroscopic displacement efficiency (Green et al., 1997).

Generally, enhanced oil recovery methods can be divided into five groups. Mobility-control, chemical, thermal, miscible and other processes. The aim of mobility-control is to generate and maintain a favorable mobility ratio and improve the macroscopic displacement efficiency. Chemical processes refer to the use of chemicals such as surfactants to reduce interfacial tension (IFT) and enhance the microscopic displacement efficiency. Thermal techniques are based on injection of thermal energy into the reservoir to reduce the viscosity of the oil and to improve the overall displacement efficiency. The objective of miscible processes is to inject fluids that are miscible with oil. This is for instance, to swell the oil and increase the recovery. Other processes refers to methods like immiscible CO_2 injection, mining and microbial-based methods (Green et al., 1997). The methods can be implemented together such as the method described in this thesis, where CO_2 foam for mobility control is made with energy support from chemicals.

2.4. Physical Properties of CO_2

Carbon dioxide is a preferred fluid for EOR methods in particular for onshore basins in the US. Physical properties of CO_2, such as viscosity and density vary with temperature and pressure (Lee et al., 2013). Since the reservoir conditions (pressure and temperature) differ from the ambient conditions, it is essential to understand the behavior of CO_2 at the different conditions. At standard temperature and pressure (T = 15 °C, P = 1.013 bar) carbon dioxide is a gas. With increasing temperature and pressure CO_2 changes phase into supercritical condition (Chang, 2013). Supercritical carbon dioxide is characterized by a higher density and viscosity compared to other compressed gases and CO_2 at gas phase (Bachu et al., 2005). Injection of supercritical CO_2 alleviate gravity segregation and viscous fingering, which makes it favorable for EOR (Lee et al., 2013). CO_2 becomes a supercritical fluid when the reservoir conditions exceed the critical temperature and pressure (T_{crit} = 31°C, P_{crit} = 73.9 bar) (Figure 2.2). Figure 2.3 illustrates viscosity and density of CO_2 as a function of temperature and pressure.

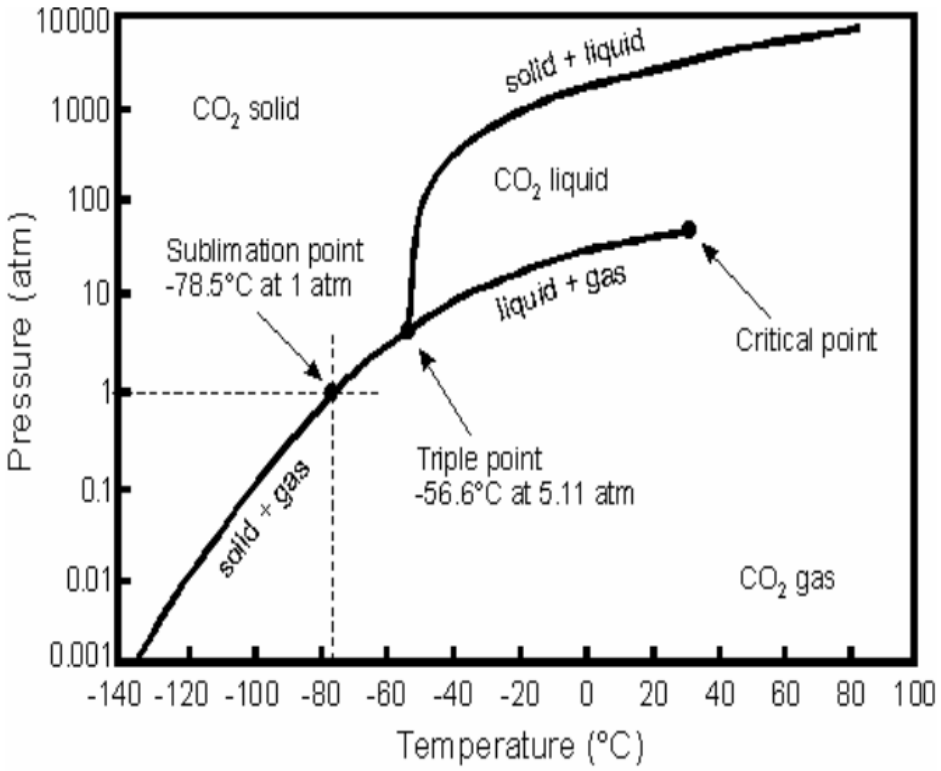

Figure 2.2 CO_2 Phase diagram. CO_2 becomes a supercritical fluid at T = 31°C and P = 73.9 bar (Picha, 2007).

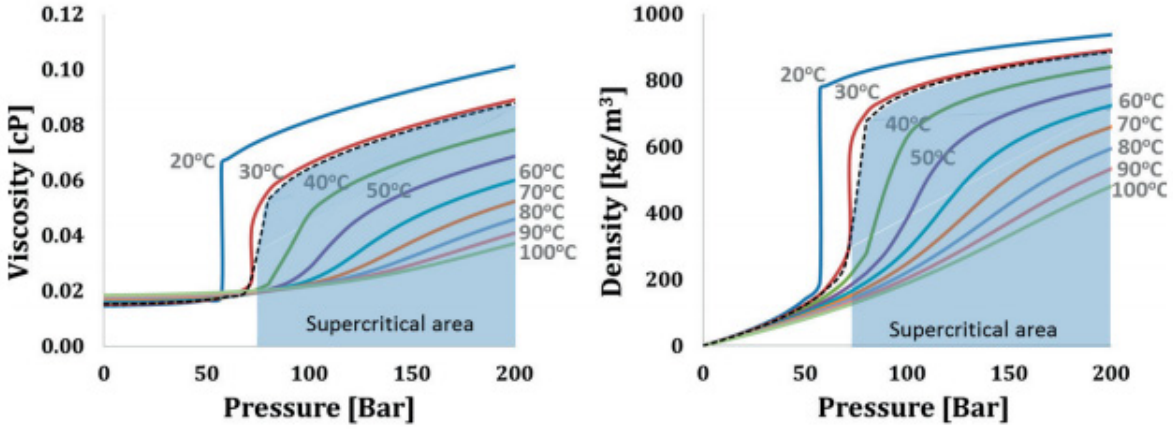

Figure 2.3 Viscosity and density of CO_2 as a function of temperature and pressure. The black dotted line represents the critical point. The blue area represents the supercritical phase of CO_2 (Brattekås, 2014).

2.5. Miscibility

One of the advantages of using CO_2 for EOR is its ability to mix with oil and generate a miscible displacement at relatively low pressures compared to other gases (Holm et al., 1974). Miscibility is defined as the ability of two or more fluids to mix and form a single homogenous phase without the existence of an interface. However, if there is a phase boundary between the fluids, they are referred to as immiscible. Miscible displacement involves elimination of interfacial tension between the fluids and allows recovery of the capillary trapped oil in the swept regions (Holm, 1986). Unfortunately, because of instabilities caused by viscous fingering, local heterogeneities in the reservoir and water blocking, it is not possible to completely recover the oil in place in the swept areas (Muller et al., 1991). Still, miscible displacement can recover up to 70% more oil than an immiscible process (Kulkarni et al., 2004).

Generally, the concept of miscible displacement is divided into two types: first-contact and multi-contact displacement. First-contact miscibility can be achieved when a proportion of the injected solvent and reservoir oil form a single phase. First-contact miscibility will only be generated by injection of highly hydrocarbon rich gases such as propane and butane. These are expensive and not economically beneficial. CO_2 is not first-contact miscible, however, multi-contact miscibility can be achieved at specific pressures and temperatures. Multi-contact miscible displacement is based on two mechanisms: vaporizing gas drive and condensing gas drive. Both mechanisms involve transfer of hydrocarbon components between the injected solvent and reservoir oil. In vaporizing gas drive, hydrocarbons vaporize from the oil into the injected lean gas and thereby makes it heavier. When the gas has vaporized a sufficient amount of hydrocarbon components, the fluids become miscible. In condensing gas drive, enriched gas injected into the reservoir will enrich the oil with heavier hydrocarbon components until the fluids become miscible (Holm, 1986; Parra-Ramirez et al., 2001).

Minimum Miscibility Pressure (MMP)

To allow CO_2 or any other gas to mix with the reservoir oil a minimum miscibility pressure is required. This is the lowest pressure at which two or more fluids are miscible (Mungan, 1981). This minimum pressure depends on the reservoir temperature, the oil composition and the properties of the injected gas and can be determined by different laboratory experiments. The most common experiment for MMP determination is the slim tube experiment, where oil is displaced by gas in a thin tube filled with unconsolidated sand and the pressure is measured. The MMP is defined at the pressure corresponding to maximum oil recovery value (Yellig et al., 1980).

The minimum miscibility pressure varies depending on different field projects. In general, it increases with temperature and heavy components (Ahmed, 1994; Zhang et al., 2016). It is worth noting that the reservoir pressure must be equal or higher than MMP to generate miscibility. CO_2 injected below the minimum miscible pressure will result in immiscible displacement and low recovery (Poettmann et al., 1991).

The oil used during the experiments performed in this thesis was n-Decane. Song et al. (2011) estimated the MMP for a CO_2/n-Decane system by using high spatial resolution magnetic resonance imaging (MRI). Figure 2.4 illustrates the MMPs of a CO_2/n-Decane system at different pressure and temperature conditions.

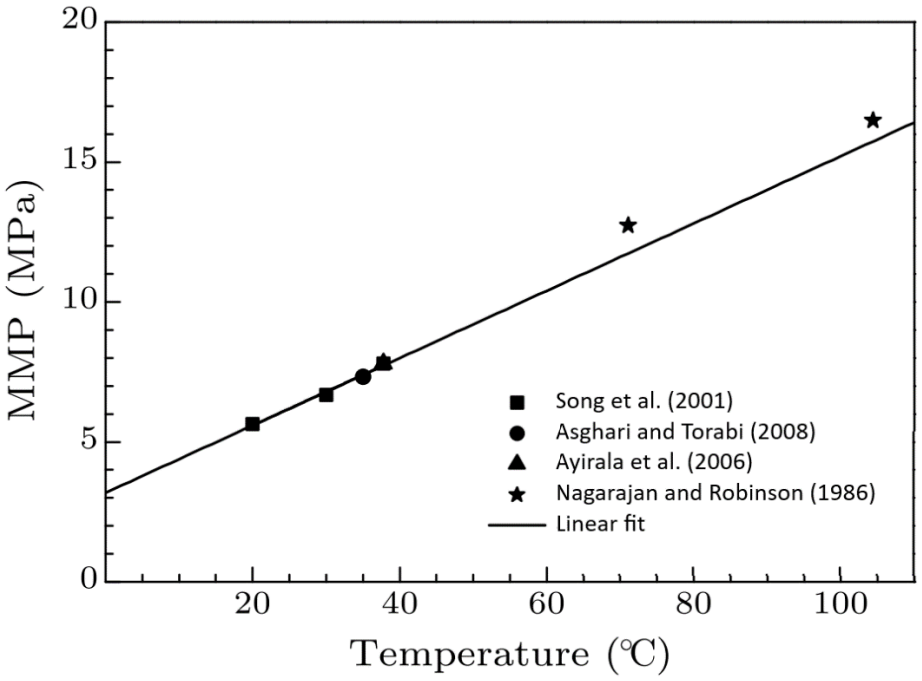

Figure 2.4 MMPs of a CO_2/n-Decane system as a function of temperature. Correlation line fitted based on the experiments performed by Song et al. (2011), and compared with the MMPs measured by Asghari and Torabi (2008), Ayiral et al. (2006) and Nagarajan and Robinson (1986). Modified from (Song et al., 2011).

2.6. Diffusion and Dispersion

Molecular diffusion and mechanical dispersion are the main mechanisms responsible for the mixing of the gas and oil that occurs in a miscible displacement process. These phenomena ensure that the hydrocarbon components transfers from one fluid to the other. During the mass transfer, miscibility may be lost by dissipating the miscible fluid or by fingering through the miscible zone. Hence, it is important to understand the processes and their influence on the fluid flow to obtain an optimal oil recovery (Perkins et al., 1963; Shrivastava et al., 2002).

Molecular diffusion describes the transport of molecules across a sharp interface because of the concentration differences between the two phases (Figure 2.5). Molecular diffusion can occur in gases, liquids and dense phases. Molecules move from a region of higher concentration to a region of lower concentration due to a random motion that occurs until equilibrium between the two phases transpires. As a result, the sharp interface vanishes and becomes a diffuse mixed zone grading from one pure fluid to the other (Perkins et al., 1963; Skjæveland et al., 1992). In addition to mixing the fluids, diffusion contributes to swelling of the oil droplets that are isolated and blocked by water and thereby allow higher oil recoveries (Grogan et al., 1987).

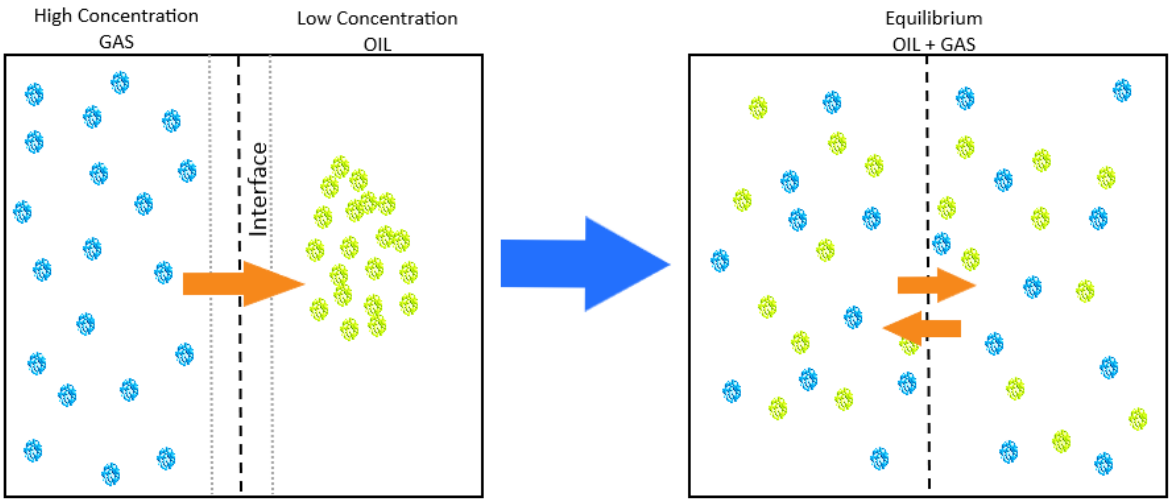

Figure 2.5 Molecular diffusion. Molecules move from high-concentration regions to low-concentration regions through a sharp interface until equilibrium and miscibility is achieved.

Dispersion is the combined effect of two physical phenomena; diffusion and convection induced mixing. As CO_2 transports through a system, dispersion contributes to reduction of the concentration gradient. Several variables such as heterogeneity of media, viscosity differences and density differences can affect the dispersion (Perkins et al., 1963). Generally, the phenomena of dispersion are categorized based on scale: pore/microscopic, core/macroscopic and field/megascopic scale. Mechanisms such as molecular diffusion and flow in a single pore describes the dispersion on a microscopic scale, while large-scale heterogeneities such as stratification and high-permeable channels are likely for macroscopic and megascopic scale. At laboratory core scale, all sorts of mixing may occur, however, the main mechanisms for homogenous media such as sandstones, are molecular diffusion and single-pore flow. Carbonates and heterogeneous media are dominated by the macroscopic scale diffusion processes (Skjæveland et al., 1992).

2.7. Oil Swelling

When CO_2 is injected into a reservoir at the conditions required to achieve miscibility, the gas mixes with and dissolves into the reservoir oil. Dissolution of carbon dioxide in the crude oil results in a reduction in viscosity and swelling of the oil. This contributes to increased oil volume, hence improved flow properties and enhanced production (Jha, 1985; Mungan, 1981). The degree of swelling depends on pressure, temperature and oil composition. The solubility of CO_2 and the swelling factor increases with pressure and decreases with temperature at temperatures above critical (Mangalsingh et al., 1996). Oil swelling is caused by the solubility of CO_2 in hydrocarbon oil. Carbon dioxide displaces the methane and expands the oil. CO_2 is not able to displace all the methane, therefore, the amount of methane in the oil determines the oil swelling efficiency. An increased amount of methane in the oil reduces the effect of the swelling process (Skjæveland et al., 1992).

The effectiveness of oil swelling also depends on the injection strategy. Usually, CO_2 is injected into the reservoir in tertiary displacement, after the performance of a waterflood. At that point, the saturation of water is high, and the water blocks the direct contact between the oil and the injected gas. Water blocking reduces the effect of oil swelling and prevents development of miscibility, which results in lower oil recovery. An earlier study shows that the trapped oil can be mobilized and recovered despite water blocking. After a sufficient time, the injected gas will diffuse through the blocking water and

swell the oil (Figure 2.6). Even though the trapped oil can be produced through the blocking water, the oil swelling is more efficient, and the oil production is higher if the gas is injected in the secondary displacement. At the time of secondary flood, the water saturation is lower than at tertiary flood (Campbell et al., 1985; Grogan et al., 1987).

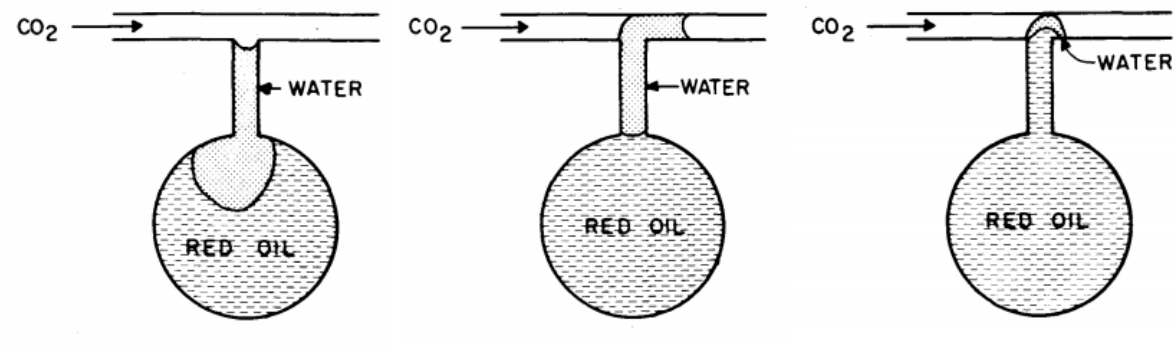

Figure 2.6 Oil swelling due to CO_2 molecular diffusion through blocking water. After a sufficient time the residual oil expands and pushes the blocking water out of the pore (Campbell et al., 1985).

3. Carbon Capture, Utilization and Storage (CCUS)

Carbon capture, utilization and storage (CCUS) is a process in which CO_2 is captured, utilized for production of a new product and transported to a storage location for long-term isolation from the atmosphere. CCUS is a technological option for mitigating climate change and at the same time increasing oil recovery to meet the growing energy demand on earth. In this thesis, utilization of CO_2 for increased oil recovery is discussed, but CO_2 may also be utilized in other technologies such as mineralization to form carbonate or bicarbonate solids for construction materials, production of useful fuels and chemical feedstocks and photosynthesis-based technologies (Laumb et al., 2013).

3.1. CO_2 Storage in Saline Aquifers

Injection of CO_2 into saline aquifers is one of three main methods for geological storage of CO_2 in order to decrease anthropogenic greenhouse gas emissions into the atmosphere. The two others are storage in depleted hydrocarbon reservoirs and un-mineable coal seams (Bachu, 2003; IPCC, 2005). Previous studies have shown that saline aquifers have the highest potential capacity globally for CO_2 storage and can store emissions from large stationary sources for at least a century (Celia et al., 2015). When CO_2 is injected into a geological formation, it becomes trapped due to four main trapping mechanics: stratigraphic and structural trapping, residual trapping, dissolution trapping and mineral trapping.

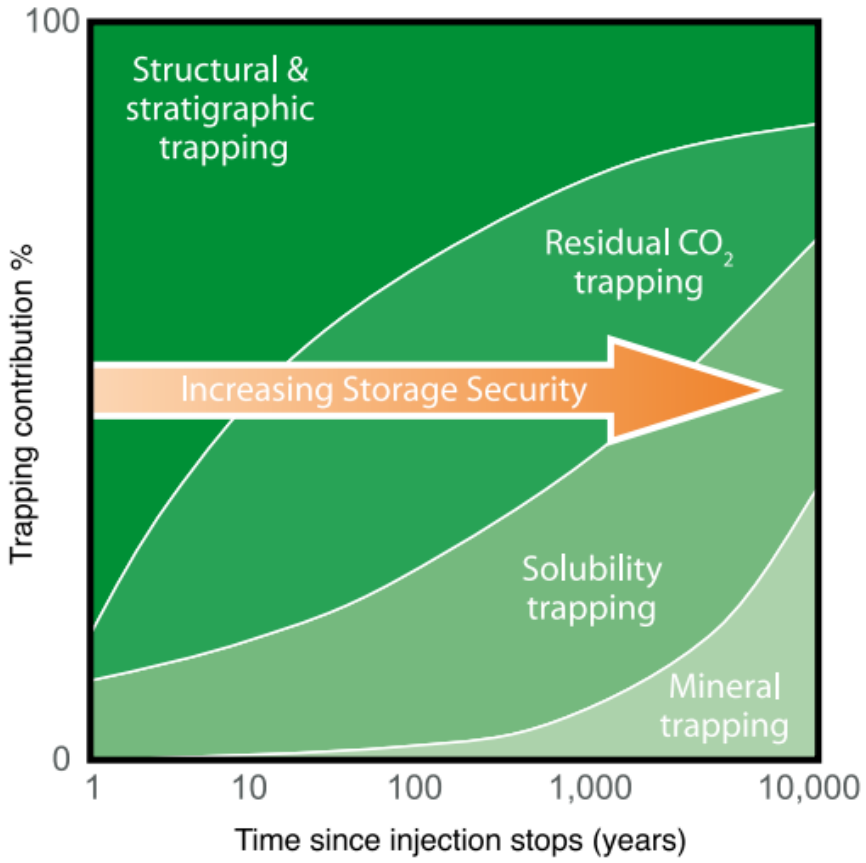

Figure 3.1 The security of CO_2 storage is a combination of all trapping mechanisms and increases over time (IPCC, 2005).

Stratigraphic and structural trapping means trapping of CO_2 in a formation with a low-permeable caprock, preventing CO_2 from migrating upwards (Shukla Potdar et al., 2016). Residual trapping refers to the trapping of CO_2 within the rock pores due to capillary forces (Niu et al., 2014). Dissolution trapping means mixing of CO_2 in the formation water. Once CO_2 is fully dissolved, it no longer exists as a separate phase and it is not migrating upwards in the formation (Benson et al., 2008). Mineral trapping is a slow reaction between CO_2 and calcium and/or magnesium to form solid carbonate minerals and is regarded as the most safe and permanent form of geological storage (Gunter et al., 1993). The storage security (Figure 3.1) depends on a combination of all trapping mechanisms and increases with time.

CCS is a known technology with several pilot and commercial projects over the past two decades. The first commercial CO_2 storage project was the Sleipner project in the North Sea, where Statoil (now Equinor) and their partners separated CO_2 from natural gas production at Sleipner Vest Field and injected it back into a deep saline aquifer in the Utsira Sand formation. Since 1996 more than 20 million tonnes of CO_2 has been captured and stored underground (Equinor, 2019; Leung et al., 2014). A similar project started in 2008, where CO_2 was reinjected into a sandstone saline aquifer in Snøhvit field in the North Sea (Shi et al., 2013). Previous projects and research show that CCS is expected to account for the mitigation of approximately 20% of the total CO_2 emissions, therefore, further development and knowledge related to CCS has been in focus over the last years (Benson et al., 2008; Mac Dowell et al., 2017). The first full-scale CCS Project in Norway (Northern Light, planned for operation in 2024), and the CLIMIT program established by the Research Council of Norway and Gassnova are examples of measures that have been taken in order to achieve climate objectives (Bekken et al., 2013).

According to IPCC special report on the impacts of global warming of 1.5 °C above pre-industrial levels, CCS is necessary to mitigate climate change (IPCC, 2018). However, injection of CO_2 for pure storage in offshore saline aquifers is currently expensive, has unproved stratigraphically gas seals, lacks proper infrastructure in terms of pipelines and wells, and thus has a low economic benefit (Bentham et al., 2005). An approach to offset the costs of CCS is to find beneficial uses for the injection of CO_2. The most common utilization of CO_2 is for enhanced oil recovery (Celia et al., 2015).

3.2. CO_2 EOR and Storage in Hydrocarbon Reservoirs

Injection of CO_2 for increased oil recovery is an EOR method that was first implemented in 1972 in the US (Verma, 2015). The use of CO_2 has grown dramatically since the 70s (Brock et al., 1989) and the technology has been performed with commercial success (Lee et al., 2013). The aim of CO_2 injection, as well as injection of other gases, is to improve both the microscopic and macroscopic displacement efficiency. This can be achieved by decreasing the interfacial tension between gas and oil to generate miscibility, reducing the viscosity and density of the oil to achieve a more favorable mobility ratio and swelling the oil (Johns et al., 2013). CO_2 is preferred compared to other gases because it forms a dense or supercritical phase at typical reservoir conditions, which results in more stable displacement front and higher oil recovery (Lee et al., 2013). Although CO_2-EOR is considered a successful technique, there are still disadvantages associated with the high mobility ratio between gas and oil that leads to early gas breakthrough, viscous fingering and poor sweep efficiency. In addition, the low density of CO_2 causes gravity override. Figure 3.2 shows the issues associated with CO_2 gas injection. These problems can be alleviated by foaming the injected CO_2 (Enrick et al., 2012).

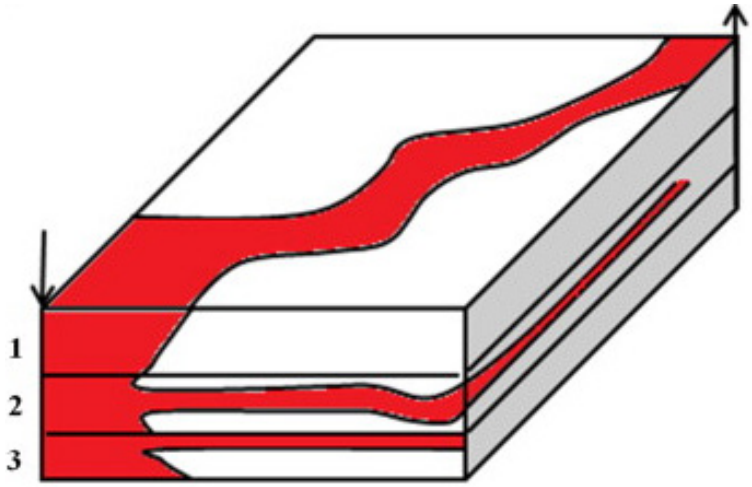

Figure 3.2 Issues associated with CO_2 injection. (1) Poor sweep efficiency, (2) Viscous fingering, (3) Gravity override (Hanssen et al., 1994).

In addition to utilizing CO_2 for increased oil recovery, CO_2 may also be stored in mature hydrocarbon reservoirs. Depleted oil and gas reservoirs are safe candidates for CO_2 storage for several reasons. Firstly, oil and gas have been stored in these formations before, which indicate that the traps are secure. The geological structure and physical properties of most of the fields have been studies extensively and advanced computer models have been developed to predict the movement, displacement behavior and trapping of hydrocarbons. Finally, already existing wells and infrastructure may be used for CO_2 storage operations (IPCC, 2005; Le Gallo et al., 2002). Unlike storage in saline aquifers, the storage capacity in depleted oil and gas reservoirs is low. The capacity is limited by the need to avoid exceeding the pressures that can damage the caprock and storage in shallow reservoirs may be problematic due to the physical properties of CO_2 (Kovscek, 2002).

4. CO_2 Foam for Mobility Control in Sediments

Carbon dioxide injection is a commonly used enhanced oil recovery method. Injection of CO_2 can enhance the production by mobilizing the trapped oil in the reservoir. Even though it is a common and successful method, the unfavorable mobility ratio between the reservoir oil and the injected gas leads to instability problems such as gas fingering, gravity override and gas breakthrough, resulting in low sweep displacement efficiency and low oil recovery (Mo et al., 2012). The instability issue can be reduced by injection of CO_2 foam (Figure 4.1). Foam refers to as a collection of gas bubbles dispersed in a liquid and have a widespread occurrence in the daily life and in the petroleum industry (Schramm, 1994b). Foam injection increases the viscosity of CO_2, thus reduces the mobility ratio and improves the macroscopic sweep efficiency (Talebian et al., 2014).

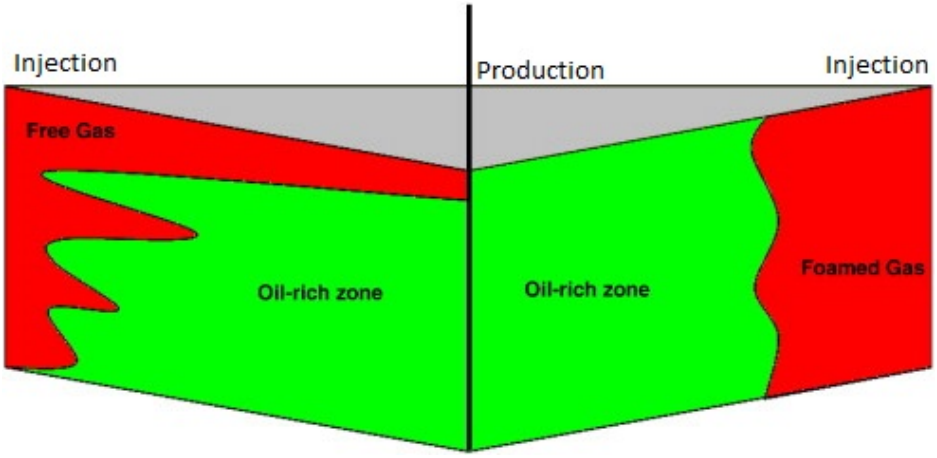

Figure 4.1 Comparison of gas flooding (left) and foam flooding (right). Modified from (Farajzadeh et al., 2012)

This chapter discusses the CO_2 foam used for mobility control in sediments and includes the, characteristics of the foam, generation and stability of the foam, foam flow behavior and foaming formulas.

4.1. Foam Characteristics

Foam is defined as a colloidal dispersion, a two-phase system in which a gas phase is dispersed in a continuous liquid phase (Tadros, 2017). Such foams are unstable systems that will collapse with time. In petroleum engineering, a gas – liquid mixture is referred to as foam, while a liquid – liquid mixture refers to as emulsion (Enrick et al., 2012). In a foam, gas bubbles are separated by a thin, continuous liquid film called lamella. Figure 4.2 illustrates a generalized foam system where gas bubbles are separated by lamellae. A connection of three lamellae is termed as plateau border. Even though CO_2 is in a liquid/supercritical phase at reservoir conditions and for all injections conducted in this thesis, the mixture of CO_2 and brine is characterized as CO_2 foam (Schramm, 1994b).

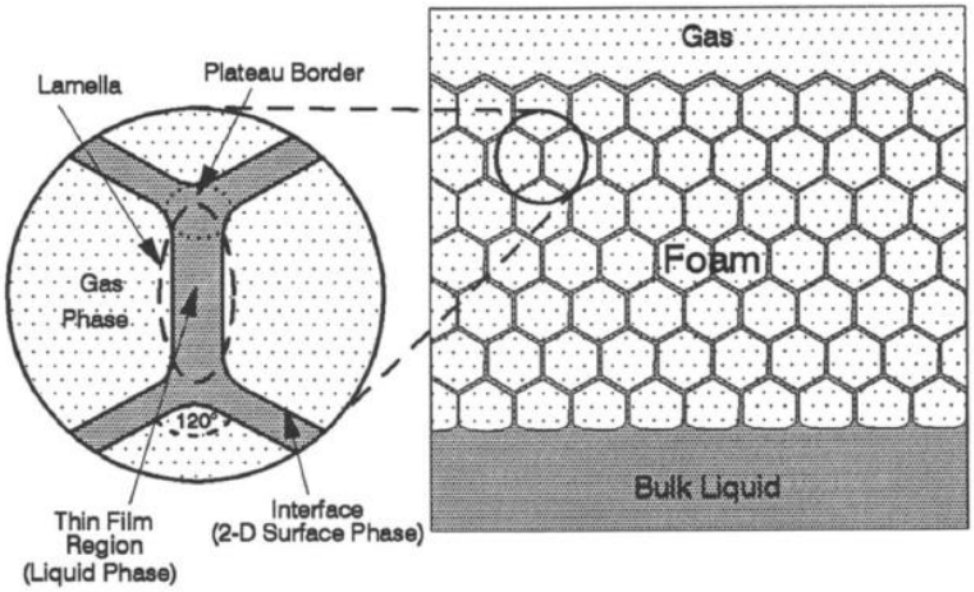

Figure 4.2 An illustration of a generalized foam system (Schramm, 1994b).

To achieve dispersion of small bubbles within the liquid, gas bubbles need to be injected faster than drainage of the interstitial liquid films. A foam formed by a gas-liquid mixture will quickly coalescence and the foam structure collapse. More stable foam can be formed by adding energy into the system. A foaming agent can be added into the system to reduce the surface tension between gas and liquid phase, and thereby increase the interfacial area with a minimum of mechanical energy input, which improves the stability of the foam. In addition, a protective film is formed to prevent coalescence (Schramm, 1994b). Most common foaming agents are surfactants, but finely divided solids like nanoparticles have recently proven successful for foam stabilization (Li et al., 2010; Mo et al., 2012).

4.2. Foam Generation

Foams for enhanced oil recovery can be generated by a continuous co-injection of gas and liquid containing a foaming agent or by injection of alternating slugs of liquid with a foaming agent and gas (Gauglitz et al., 2002). In porous media, foam is generated if gas bubble injection is quicker than the drainage of the liquid between the bubbles (Schramm, 1994b). During the lifetime of the foam, new lamella forms, while others collapse. The lamella generation rate in a porous media depends on the pore geometry and is proportional to the flow rate, while the rate of decay depends on processes that cause coalescence of the bubbles, e.g. limiting capillary pressure. A lamella will break if the foaming agent is ineffective or due to rapture of lamella, meaning that two bubbles approach each other as a result of poor foam quality, flow rate and pore geometry. In addition, the ability of a lamella to form may be inhibited due to presence of oil, pore geometry or wettability of the media. To generate an effective foam for enhanced oil recovery, the lamella generation rate needs to be equal or higher than the decay rate (Enrick et al., 2012; Heller, 1994).

Foam generation in a porous media is caused by three main mechanisms; leave-behind, snap-off and lamella division. The generation mechanism of the foam influences the foam texture (bubble size and distribution), which has an impact on the flow properties and apparent viscosity of the foam. The understanding of the generation mechanisms is crucial in predicting the efficiency of the foam (Hirasaki et al., 1985; Ransohoff et al., 1988).

The leave-behind mechanism occurs when two gas fronts enter a liquid-filled pore from two different directions (Figure 4.3). The liquid is squeezed between the two gas fronts, resulting in the creation of a lamella oriented in the flow direction of the gas. The leave-behind mechanism does not generate new, separate gas bubbles and the gas remains a continuous phase. The foam is relatively weak, and its stability depends on the presence of the surfactants in the liquid phase. Frequent occurrence of the mechanism results in large numbers of lamellae blocking the gas pathway and decreasing the relative permeability of gas (Ransohoff et al., 1988).

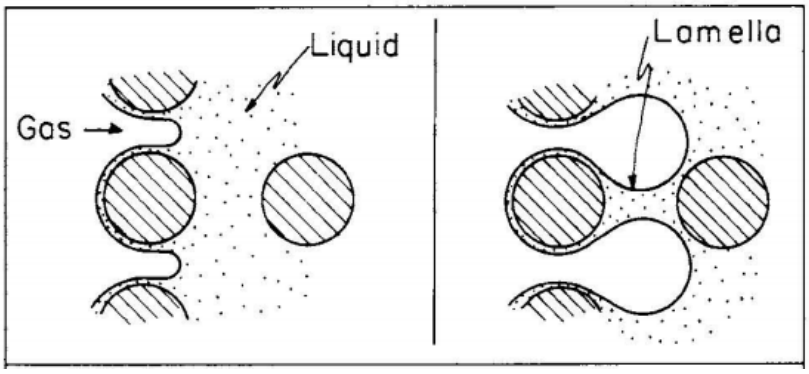

Figure 4.3 Schematic of the leave-behind mechanism (Ransohoff et al., 1988).

Snap-off, the dominant foam generation mechanism, occurs during multiphase flow in porous media regardless of the presence of surfactant. During the process, a gas finger moves into a liquid-filled pore through a narrow pore throat. Due to a decrease of capillary pressure on the downstream side, liquid accumulates into the throat and separate the continuous gas phase (Figure 4.4). An increased discontinuity of the gas phase influences the flow properties of the gas (Kovscek et al., 1994). Snap-off generates a strong foam because the gas flow resistance in a porous media is greater with a discontinuous phase than with a continuous phase (Ransohoff et al., 1988).

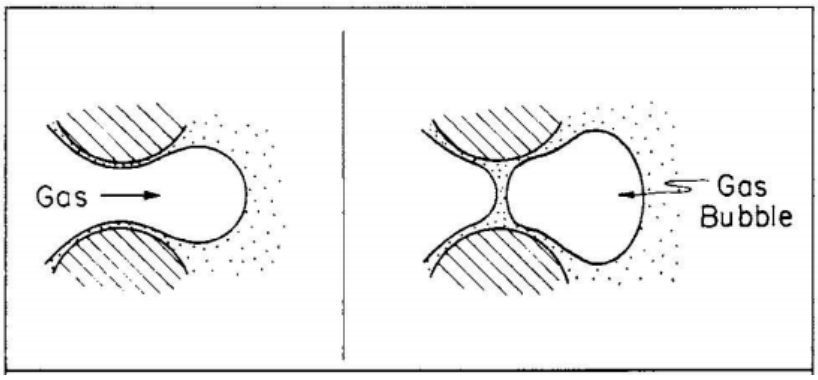

Figure 4.4 Schematic of the snap-off mechanism (Ransohoff et al., 1988).

During the lamella division mechanism, an already existing lamella enters a liquid-filled pore with multiple pore throats. As the lamella moves through the pore, it may spread into different directions creating new lamella (Figure 4.5). Division occurs only if the gas bubble is bigger than the pore body. This mechanism is called secondary foam generation as the pre-existence of a lamellae is required. Due to creation of separate bubbles, foam generated by the lamella division is considered to be strong (Kovscek et al., 1994).

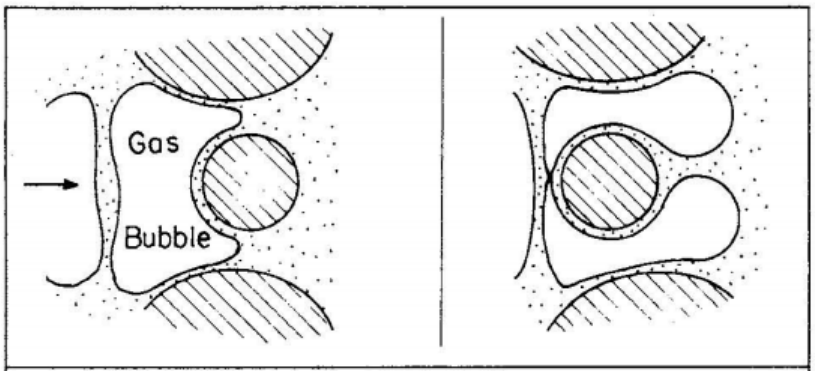

Figure 4.5 Schematic of the lamella division mechanism (Ransohoff et al., 1988).

Foam generation depends on injection velocity or pressure gradient and surfactant concentration. Earlier studies of foam generation showed that there is a minimum gas velocity or pressure gradient threshold to generate foam, which depend on the length of the system and the gas fractional flow. Greater foam quality, f_g (defined in Chapter 4.4), requires a greater velocity to generate foam. Generally, the minimum gas velocity required to generate foam increases with increasing foam quality and decreases with increasing surfactant concentration (Rossen et al., 1990; Yu et al., 2018).

4.3. Foam Stability

Generally, foams continually generate and collapse through time and are thermodynamically unstable. To achieve a favorable sweep efficiency, foam needs to be stable during the flood. The stability of foam is the ability to resist bubble breakdown due to coalescence or bubble collapse and depends on different factors (Chambers, 1994). Generally, foam strength improved with increased foam texture (number of lamellae). The stability of foam in a porous media depends both on the petrophysical properties of the rock such as permeability and fluid saturation and foam film properties (Farajzadeh et al., 2012).

The Effect of Permeability

Permeability is an important property that controls the foam stability in a porous media because of its relation to the pressure gradient. To generate a fine-textured and strong foam, a minimum pressure gradient is required. Pressure gradient decreases with increasing permeability, therefor stronger and more stable foams are generated in high-permeable zones (Gauglitz et al., 2002). Because of heterogeneity in the majority of the reservoirs, foam will flow into the high-permeable zones. This event can lead to foam blockage in the high-permeable areas and thereby resulting in flow diversion and enhanced oil production from the low-permeable, previous unswept regions (Farajzadeh et al., 2012; Veeningen et al., 1997).

The Effect of Temperature and Pressure

In a reservoir, both temperature and pressure are higher than at ambient conditions, therefor it is important to understand how these properties influence the stability of the foam. An increase temperature results in increased surfactant solubility in the liquid phase, leading to less surfactant in the gas-liquid interface. Additionally, higher temperature increases liquid drainage, which destabilizes foams (Maini et al., 1986; Sheng, 2013). An increasing pressure, however, will stabilize the foam by making the gas bubbles smaller, liquid films larger and slow down liquid drainage. High pressure stabilizes the foam as long as it is below a specific, maximum value (limiting capillary pressure). If the pressure exceeds this value the gas bubbles are exposed to high stress and will rapture (Sheng, 2013).

The Effect of Oil

An understanding of the interaction between oil and foam is essential for EOR applications. The presence of oil in the porous media will destabilize the foam by spontaneously spreading on the foam film and driving it out, resulting in an unstable oil film that easily breaks (Ross et al., 1944). Oil may also spontaneously emulsify and sever the stabilizing foam interface. The surfactant concentration which stabilize the foam can be reduced due to absorption into the oil phase (Sheng, 2013). In addition, oil in the porous media can prevent generation of the foam when the oil saturation is above a critical foaming saturation or when the wettability of the rock is oil-wet (Friedmann et al., 1986). Lamella prefers water-wet reservoir conditions, and foam generation can be achieved with help of an surfactant that can alter the wettability (Sanchez et al., 1992). In general, presence of oil makes foam generation and stability difficult, and light oils tend to destabilize foam more than heavy oils (Schramm, 1994a).

4.4. Foam Flow Behavior

Understanding foam flow through a porous media is essential for an effective enhanced oil recovery application and CO_2 storage. The behavior of foam in a porous media can be described by investigation of properties like foam quality and apparent viscosity. Also, the efficiency of the foam can be determined by calculating the mobility reduction factor (MRF) (Chang et al., 1998).

Foam Quality

Foam quality is the most important parameter describing foam flow in a porous media as it directly affects the mobility of the foam. Foam quality is the ratio between the gas flow rate and the sum of the gas and the liquid flow rates:

$$f_g = \frac{q_g}{q_g + q_{liq}} \tag{4}$$

where f_g is the foam quality, and q_g and q_{liq} is the gas flow rate and liquid flow rate, respectively (Farajzadeh et al., 2012). Foam quality can also be described as the ratio of gas volume to foam volume. Mobility conformance foams typically have foam qualities in the range of 75% to 90%. Foams with lower foam qualities consist of separate gas bubbles and have low viscosity. As the gas fraction increases, the size of the gas bubble increases resulting in an unstable foam. At foam qualities typically above 90-95% foams are no longer effective (Chambers, 1994; Sheng, 2013).

Apparent Viscosity

The benefit of using foam for EOR is its high apparent viscosity compared to its constituents (Sibree, 1934). Apparent viscosity is defined as the relationship between the flow rate and the pressure drop for the flow of foam through a capillary (Hirasaki et al., 1985). Using Darcy's law, apparent viscosity of foam, μ_{app}, can be described as:

$$\mu_{app} = \frac{KA\Delta P}{q_{tot}L} \tag{5}$$

where K is the absolute permeability of the porous media, A is the cross section area, ΔP is the pressure drop across the media, q_{tot} is the volumetric flow and L is the length of the porous media (Falls et al., 1989).

Mobility Reduction Factor

Mobility reduction factor (MRF) is a dimensionless measure of foam effectiveness and can be defined as the ratio between the apparent viscosity of foam and the viscosity of pure gas (Heller, 1994; Svorstol et al., 1996):

$$MRF = \frac{\mu_{app}(foam)}{\mu_g(gas\ before\ foam)} \tag{6}$$

where μ_{app} is the apparent viscosity defined in Eq. (5) and μ_g is the viscosity of the gas. Low MRF values indicate an ineffective and weak foam, while high MRF values indicate strong foam that is more effective in reducing gas mobility (Zhang et al., 2009). It is noteworthy that both apparent viscosity and mobility reduction factor are average values calculated over periods of steady state pressure drop (Svorstol et al., 1996).

4.5. CO_2 Foaming Formulas

Foams can be generated as a result of mixing gas with brine. Unfortunately, foams are thermodynamically unstable and collapse easily. To generate more stable foams with longer lifetime, a foaming agent is necessary (Sheng, 2013). Surfactants are commonly used as foaming agents because of their low costs and high availability. However, the long-term stability of a surfactant-induced CO_2 foam is difficult to obtain. Nanotechnology has demonstrated that small solid particles such as fumed silica can absorb at the fluid/fluid interfaces to stabilize bubbles in foams. Using nanoparticles to stabilize CO_2 foam may therefore overcome the long-term instability and high mineral adsorption rates associated with commercial surfactants (Enrick et al., 2012). Both surfactants and nanoparticles were used as foaming formulas during this thesis and will be described below.

Surfactants as Foaming Agent

Surfactant, or a surface-active agent, is a substance, which lowers the surface tension between two immiscible fluids and allows them to mix. This property is caused by the amphiphilic structure of a surfactant, meaning that one part of the surfactant is hydrophilic while the other part is hydrophobic as shown in Figure 4.6. A surfactant adsorbs up to the gas-liquid interface and reduce IFT (Lake, 2014; Schramm, 1994b).

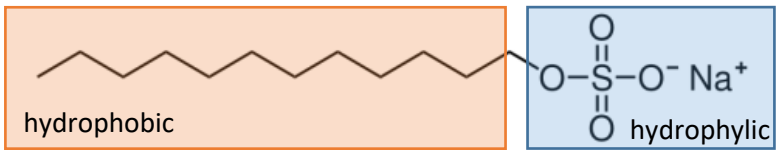

Figure 4.6 Illustration of surfactant with and hydrophobic and hydrophilic part. Modified from (Lake, 2014)

There are an enormous variety of surfactants and they can be classified into four groups depending on their electric charge: anionic (negatively charged), cationic (positively charged), non-ionic (neutral charged) and amphoteric (positively and negatively charged) (Schramm, 2000). Anionic surfactants are soluble in the water-phase. They efficiently reduce IFT and are stable at high temperatures. They have relatively low production costs and are therefore frequently used for EOR. They should, however, not be used in carbonate reservoirs due to their negatively charged surface which may react with the positively charged rock surface. Cationic surfactants are the preferred surfactants for carbonate reservoirs. Non-ionic surfactants are usually used as co-surfactants and amphoteric surfactants are rarely used for EOR, but both could be implemented for sandstone and carbonate reservoirs (Enrick et al., 2012; Zolotuchin, 2000). Both non-ionic and anionic surfactants have been used during the experimental work described in this thesis.

In order to generate a strong and stable foam, surfactants should satisfy primary characteristics. Firstly, a surfactant should have a strong molecular interaction with both fluids to achieve a low IFT (Lake, 2014). Secondly, the surfactant should remain stable at high temperatures. Generally, surfactants are soluble in brine, but most surfactants become less soluble as the temperature increases, thus resulting in inefficient IFT reduction. Adsorption and retention of the surfactant in a porous media lead to a reduction in the surfactant concentration, which decrease the ability to reduce the IFT. In addition, it is important that the surfactant does not create viscous structures (agglomeration) that may disturb the flow through the porous media (Lake, 2014). The right surfactant needs to be selected to be able to decrease the interfacial tension. The type of surfactant needs to be carefully chosen for a specific field based on the current reservoir conditions (Kuehne et al., 1992).

Nanoparticles as Foaming Agents

Nanoparticles are small colloidal particles ranging from 1 – 100 nm in diameter. These are composed of a core and a chemically modified surface consisting of covalently linked surface molecules. The combination of the core and the surface molecules makes nanoparticles flexible and enables production of the well-defined particles with desired properties (Bennetzen et al., 2014). Unlike surfactants, nanoparticles are mechanically and thermally stable which makes them ideal for CCUS in the harsh environments that are found in saline aquifers and hydrocarbon reservoirs (Zhang et al., 2011).

Nanoparticles used for enhanced oil recovery includes oxides of aluminum, zinc, magnesium, iron, zirconium, nickel, tin and silicon. Previous studies show that aluminum and silicon oxides are good agents for increasing oil recovery (Ogolo et al., 2012) and silicon oxides generate a stable and strong foam (Rognmo et al., 2017). Nanoparticles used in this thesis are silica nanoparticles (silicon oxides) dissolved in brine. The particles are as small as several nanometers and can easily flow through a porous media without blocking the pores (Talebian et al., 2013). Silica nanoparticles are attractive for EOR application due to low fabrication costs and availability. Additionally, they are environmentally friendly as they constitute a natural part of a reservoir (Skauge et al., 2010).

Emulsions of Foaming Formula and Oil

Emulsions are colloidal dispersions of two immiscible liquids where one liquid is dispersed in another. In a reservoir, water (brine) and oil are liquid phases and two types of emulsions may be formed. Oil-in-water (o/w) emulsions are formed when individual oil droplets are dispersed in a continuous water phase, and water-in-oil (w/o) emulsions are formed when water droplets are dispersed in oil (Schramm et al., 1992). Similar to foams, emulsions are thermodynamically unstable, and an emulsifying agent is necessary to generate and stabilize emulsions. Surfactants and nanoparticles can be used to generate emulsions by decreasing IFT between oil and water (Bennetzen et al., 2014). To increase the stability of the emulsion, a combination of surfactants and nanoparticles has been proposed. Previous results showed that the most stable o/w emulsions can be obtained when the system contains oppositely charged nanoparticles and surfactants (Arab et al., 2018).

Generation of emulsions can positively influence displacement efficiency and oil recovery. Similar to CO_2 foams, emulsions flow to high permeable zones and divert the injected fluids to low permeable layers. Flow of emulsions in a porous media may also block pore throats by lodging between sand grains which results in permeability reduction and consequently increase in differential pressure (McAuliffe, 1973).

Part II. Experimental Procedure

5. Material and Methods

This part of the thesis describes rock material, fluids, experimental preparation and procedures performed during the experimental work. All experiments were performed at the Department of Physics and Technology at the University of Bergen. The objective of this thesis was to study CO_2 foam behavior in a porous media using different foaming agents, both at unsteady state CO_2 injections and steady state co-injections of CO_2 and foaming agent. In total 40 foam and baseline experiments were conducted (Table 5.1).

Table 5.1 Experimental Overview

Injection Strategy	**Initially in Pore Space (100% Saturation)**	**Injection Fluid**	**Number of Experiments**
Unsteady State CO_2 Injection	Brine (Baseline)	CO_2	1
		CO_2 + n-Decane	2
	Nonionic Surfactant	CO_2	4
		CO_2 + n-Decane	3
	Nonionic Surfactant + Nanoparticles	CO_2	8
		CO_2 + n-Decane	4
	Anionic Surfactant	CO_2	4
		CO_2 + n-Decane	2
	Anionic Surfactant + Nanoparticles	CO2	4
		CO_2 + n-Decane	2
Steady State Co-Injection	Brine (Baseline)	CO2 + Brine	1
	Nonionic Surfactant	CO_2 + Nonionic Surfactant	1
		CO_2 + n-Decane + Nonionic Surfactant	1
	Nonionic Surfactant + Nanoparticles	CO_2 + Nonionic Surfactant + Nanoparticles	2
		CO_2 + n-Decane + Nonionic Surfactant + Nanoparticles	1

5.1. Rock Material and Preparation

The experiments were performed on a cylindrical Bentheimer core plug. Bentheimer is a water-wet and homogeneous outcrop sandstone consisting mainly of quartz (92%), feldspar (5%) and clay (3%) (Peksa et al., 2015). Before the unsteady and steady state injections, the core plug was prepared by PhD candidate Tore L. Føyen and Researcher Jarand Gauteplass. Firstly, the core plug was rinsed with water and dried at 60 °C for at least 48 hours. Then, the length, diameter and weight were measured. The core was then saturated with brine (see Table 5.3) and the porosity and permeability (see Table 5.2) were measured as described in Appendix A.

Table 5.2 Rock Properties

Properties	**Values**
Diameter [cm]	3.64 ± 0.01
Length [cm]	24.6 ± 0.01
Porosity [%]	23.9 ± 0.1
Permeability [D]	1.41 ± 0.15
Pore Volume [ml]	68.23 ± 0.01

The same core sample was used for all co- and single-injections and absolute permeability was frequently measured between injections to evaluate possible residual CO_2 saturation. Permeability results are presented and discussed in Appendix B.

5.2. Fluid Properties

Surfactants or a combination of surfactants and nanoparticles were used as the foaming agent during unsteady state and co-injections. Two types of surfactants were used, a nonionic surfactant (SURFONIC L24-22) and an anionic surfactant (BIO-TERGE AS-40). The surfactants were dispersed in brine to obtain the desired concentration. The concentrations of the nonionic and anionic surfactant solutions were 5000 ppm and 3500 ppm, referred to as SFA5000, SFA3500 for nonionic surfactants and SFB5000, SFB3500 for anionic surfactants. Nanoparticles used during the experiments are Levasil CC301, a water-based epoxy silane-modified colloidal silica dispersion, referred to as NP. Two concentrations of NP were used 1500 and 150 ppm (parts per million) referred to as NP1500 and NP150. Surfactants and nanoparticles were mixed into different aqueous solutions. Concentration calculations are described in Appendix C.

After each experiment, the core plug was cleaned by injecting isopropyl alcohol (IPA) solution followed by brine. The IPA consisted of 87 wt.% isopropanol and distilled water and brine consisted of 3.5 wt.% sodium chloride (NaCl) dissolved in distilled water. To evaluate the effect of oil on foam behavior, a mineral oil, n-Decane, was used. Table 5.3 represents composition of fluids used during the unsteady state and co-injections and Table 5.4 shows the density and viscosity of brine, CO_2 and n-Decane at experimental conditions (P = 200 bar, T = 40 °C). The thermophysical properties of the foaming agent solutions were not measured but are assumed to be the same as for brine.

Table 5.3 Fluid Composition

Fluid	**Composition**
Brine	Distilled water + 3.5 wt.% NaCl
SFA5000	Brine + 5000 ppm Surfactant (*)
SFA3500	Brine + 3500 ppm Surfactant (*)
SFB5000	Brine + 5000 ppm Surfactant (**)
SFB3500	Brine + 3500 ppm Surfactant (**)
NP1500	Brine + 1500 ppm Nanoparticles
NP150	Brine + 150 ppm Nanoparticles
CO_2	>99.999% CO_2
n-Decane	$C_{10}H_{22}$
IPA	Distilled water + 87 wt.% Isopropanol

(*) Anionic Surfactant, SURFONIC L24-22
(**) Cationic Surfactant, BIO-TERGE AS-40

Table 5.4 Fluid Properties

Fluid	Density [g/ml]	Viscosity [cP]
Brine	1.016 (1)	0.655 (1)
CO_2	0.840 (2)	0.078 (2)
n-Decane	0.731 (2)	0.862 (2)

(1) Values obtained from (El-Dessouky, 2002)
(2) Values obtained from (Lemmon et al., 2012)

5.3. Experimental Setup

Figure 5.1 shows the schematics of the experimental apparatus. The same setup was used for all the experiments except the spiral tubing which was included during unsteady and steady state injections with presence of oil. A Bentheimer core plug was mounted in a biaxial Hassler core holder and vertically placed in a heating cabinet with a constant temperature of 40°C. The core plug was wrapped with nickel foil to reduce radial CO_2 diffusion and damage to rubber equipment, such as the core holder sleeve, the o-rings in the core holder and the back pressure regulator (Smithells et al., 1936).

Two Equilibar back pressure regulators (BPR) regulated by a N_2 tank were connected in series at the outlet of the system to maintain a desired pore pressure of 200 bar and to reduce pressure fluctuations. The confinement pressure was controlled by an ISCO pump, which injected hydraulic oil into the core holder to maintain a net overburden pressure of 70 bar. The pressure at the inlet and outlet of the core, the pressure of the BPR and the confinement pressure were monitored by four ESI pressure transducers with a range of 0 – 250 bar and 0 – 400 bar.

The fluids were injected into the core through three injection pumps connected at the inlet of the system. Brine and foaming agent solution were injected through a Quizix Q5000-10K pump, n-Decane was injected through a Quizix QX6000 pump and CO_2 was first pressurized to liquid phase by a Haskel gas booster and thereafter injected using a Quizix Q6000-10K pump. The pumps were controlled using the Quizix PumpWorks Software. The produced fluids were depressurized and separated at atmospheric conditions. The liquids were collected in a glass bottle and CO_2 was vented out through a water absorption column. The mass of the production fluids was continuously logged on a scale for calculation of the average water saturation in the core. The differential pressure in the core was measured using Alipsens Smart Differential Pressure Transmitter for calculation of foam apparent viscosity. All the equipment used during the experiments are listed in Table 5.5.

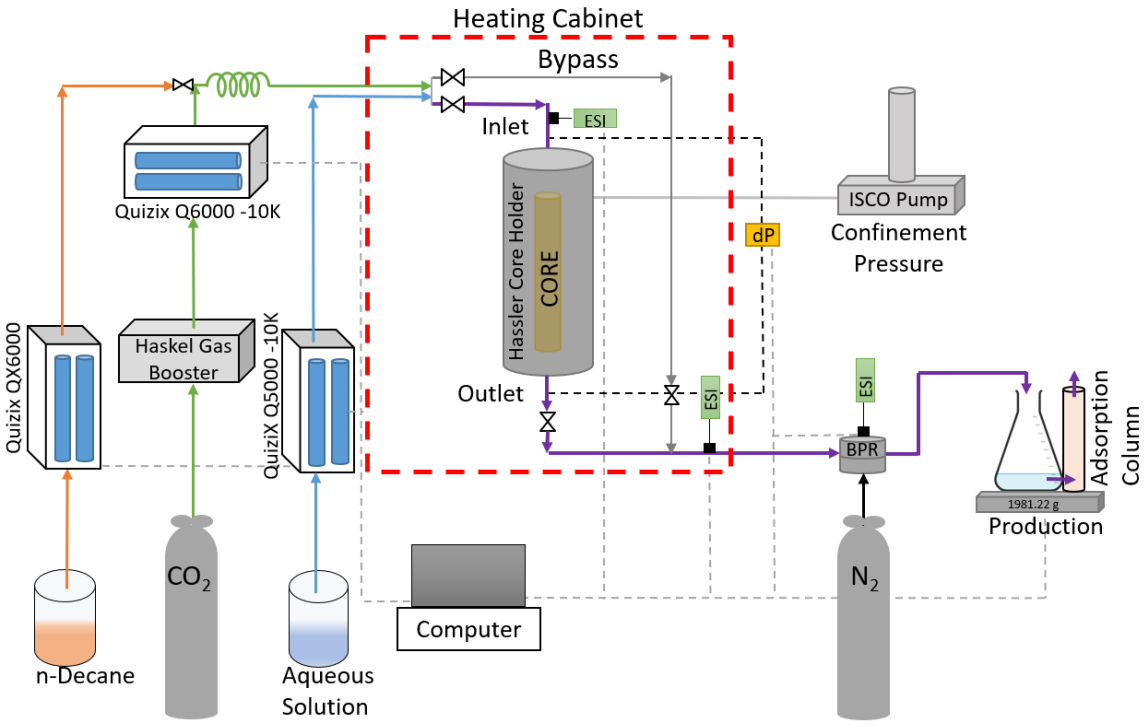

Figure 5.1 Illustration of the experimental setup. Orange, green and blue lines represent n-Decane, CO_2 and brine/foaming agent flow, respectively. The red dotted line represents the heating cabinet and the purple line indicates fluid flow during the experiments.

Table 5.5 List of equipment used for CO_2 foam experiments in core plugs

Heating Cabinet
Hassler Core Holder
Quizix Q6000 pump for gas injection
Quizix Q5000 pump for injection of aqueous solutions
Quizix QX6000 pump for injection of n-Decane
ISCO Syringe Pump for confinement pressure
Back Pressure Regulator (BPR) regulated by a N_2 tank
ESI Pressure Transducers for pressure measurements (range 0 – 250 bar for inlet and outlet pressure, 0 – 400 bar for BPR and confinement pressure)
Differential Pressure Transmitter (range 0 -16 bar)
Weight scale for saturation measurements
Production Beaker
Adsorption column
CO_2 tank used for gas injection
N_2 tank used for BPR regulation
Haskel gas booster to pressurize the injected gas
Swagelock valves, tubing and fittings
Automatic valves
Computer to operate Quizix pump, ESI pressure transducers and differential pressure transducers, automatic valves and weight

5.4. Unsteady State CO_2 Injection

Generation and coalescence of CO_2 foam in sandstone pores was investigated during unsteady state CO_2 injections. The injections were performed with different foaming agent solutions, with, and without the presence of oil. Prior to a CO_2 injection, the core was saturated with a foaming agent solution. A minimum of 3 PV foaming agent solution was injected into the core at a maximum injection rate of 100 ml/h to satisfy adsorption, displace brine and fully saturate the core. Thereafter CO_2 was injected into the system at a superficial velocity of 4 feet/day. The CO_2 was first injected through the bypass to displace fluids in the tubing, thereafter it was injected into the top of the core. A total of 10-12 PV CO_2 was injected through the core. Differential pressure in the core and the weight of the produced fluids were logged continuously during the injection for calculation of apparent viscosity and residual water saturation. After a completed experiment, the core was cleaned by injecting a cleaning solvent followed by brine as described in Chapter 5.6. The permeability of a clean core was measured before it was re-saturated with a foaming agent solution. A minimum of two experiments were performed for each foaming agent solution.

During injections with presence of oil, n-Decane and CO_2 were co-injected into a core that had been pre-saturated with a foaming agent solution. The fluids were injected at a total superficial velocity of 4 feet/day with two different CO_2 and n-Decane molar fractions$\left(x_{CO_2} = 0.95 \; and \; x_{CO_2} = 0.9\right)$, corresponding to 0.1 and 0.3 volume fraction of n-Decane. The injections were performed at constant pressure and temperature conditions of 200 bar and 40 °C. The n-Decane – CO_2 mixture was therefore considered miscible. In order for n-Decane and CO_2 to mix, the fluids were injected through a spiral tubing and bypass before injection into the core. Similar to the experiments performed without oil, differential pressure and weight were measured. After each injection, 4-5 PV CO_2 was injected into the core to displace the residual oil, thereafter the core was cleaned as described in Chapter 5.6.

5.5. Steady State Co-Injection

Steady state co-injections were performed by simultaneously injecting CO_2 and a foaming agent solution into a pre-saturated core. The core was pre-saturated by injecting 3 PV foaming agent solution to displace the initial brine. The fluids were injected at four total superficial velocities (u) and two foam qualities (f_g). The velocities were 16, 8, 4 and 1 feet/day and the gas fractions (f_g) were 0.6 and 0.9. Each injection rate was held constant until steady state flow and pressure were obtained, around 4 PV. Figure 5.2 represents the injection scheme used during the steady state co-injections. Differential pressure and weight of the produced fluids were continuously logged during the fluid flood for calculation of apparent viscosity and water saturation. Apparent viscosity was calculated for each gas fraction and rate. In addition to investigating the effect of various foaming formulas on foam strength, the impact of injection rate and foam quality was observed.

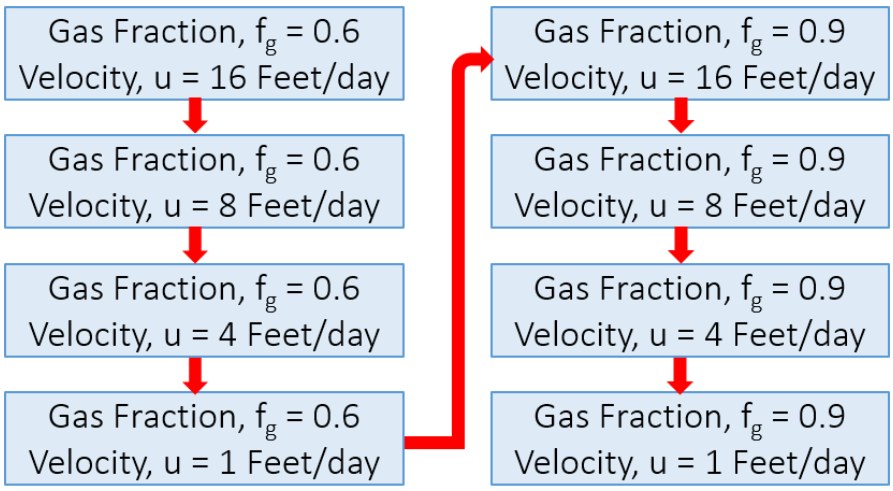

Figure 5.2 Injection scheme used during steady state co-injections. CO_2 and foaming agent solution were co-injected into a pre-saturated with foaming agent core, starting at a low gas fraction (0.6), decreasing the injection rate (16, 8, 4 and 1 feet/day) and continuing with high gas fraction (0.9) and the same injection rates.

Two steady state co-injections with presence of oil were performed. The procedure was similar to the procedure without oil as described above. In addition to CO_2 and foaming agent solution, n-Decane was injected into the system. CO_2 and n-Decane were mixed as described in Chapter 5.4. The molar fraction during the steady state co-injections was $x_{CO_2} = 0.95$, corresponding to 0.1 volume fraction of n-Decane. The mixture was injected following a similar injection scheme to the one described above, except for the lowest injection velocity of 1 ft/day because of the limitations of the Quizix QX pump.

5.6. Cleaning and Preparation Procedure

The same core plug has been used during all the unsteady and steady state injections. Therefore the preparation and the cleaning of the core before a new experiment was important. After a completed injection, the core plug contained residues of foaming agent, CO_2 and oil. In order to start a new injection and avoid impact on the upcoming experiment the remaining fluids had to be flushed out of the core. The core was cleaned following this procedure:

1) 4 – 5 PV of cleaning solvent (IPA, composition described in Chapter 5.2) was injected through the core at a maximum rate of 100 ml/h to displace the CO_2
2) 4 – 5 PV brine was injected to displace the IPA-solution
3) A minimum of 3 PV foaming agent solution was injected into the core to displace brine and saturate the core.

For the experiments with oil, 4-5 PV CO_2 was injected as a first step in the cleaning process to displace the residual oil at miscible conditions.

Part III. Results and Discussion

6. CO_2 Foam Generation and Stability

Foam generation and stability using different foaming agents were evaluated by steady state co-injections. The objective was to investigate potentially synergic effects between surfactants and nanoparticles to stabilize foam and to reduce the CO_2 mobility. CO_2 and foaming agent were injected simultaneously into a core with a constant injection rate, until steady state flow and pressure were obtained. All reported results used the same pressure and temperature condition: P = 200 bar, T = 40 °C.

6.1. The Effect of Foaming Agent on CO_2 Foam Generation and Stability

To evaluate the feasibility of a foaming agent to generate and stabilize foam and to reduce CO_2 mobility, co-injections of different foaming agents and CO_2 were performed. The fluids were co-injected at a constant volumetric injection rate and gas fraction until steady state flow and pressure occurred. Foam behavior was investigated at four different injection rates (16, 8, 4 and 1 feet/day) and two gas fractions (0.6, 0.9), using nonionic surfactant (SFA) and combinations of SFA and nanoparticles.

Two co-injections without foaming agent were performed as a baseline for subsequent injections. During baseline, CO_2 and brine were co-injected at a total injection rate of 4 feet/day and a gas fraction f_g= 0.6 until steady state flow occurred. Then the gas fraction was increased to f_g = 0.9. Only one injection rate was conducted because foam generation was not expected for co-injections in absence of foaming agent. Unsteady state baseline (Chapter 7.1) and injections performed by Rognmo et al. (2017) confirmed that no foam was generated, also for higher injection rates. Apparent viscosity during baseline was 1.2 cP for f_g = 0.6 and 1.4 cP for f_g = 0.9.

Results from steady state co-injections using various foaming formulas showed a strong foam generation for all of the foaming agents (Figure 6.1). Apparent viscosity at 4 feet/day was two orders of magnitude higher than the baseline, showing the feasibility of foaming agents to generate foam. Regardless of foaming agent solution, shear thinning behavior was observed, meaning the apparent viscosity decreased with the increased injection rate. This behavior is favorable for field applications because it reduces injectivity problems in the near-well regions and contribute to in-depth mobility control (Alvarez et al., 2001). Additionally, apparent viscosity was higher at lower gas fraction (f_g = 0.6) when compared with higher gas fraction (f_g = 0.9) for all three foaming agents. At high gas fraction the lamella may be thin and will easily collapse or there might be no sufficient volume of foaming agent to form lamella (AlYousif et al., 2018).

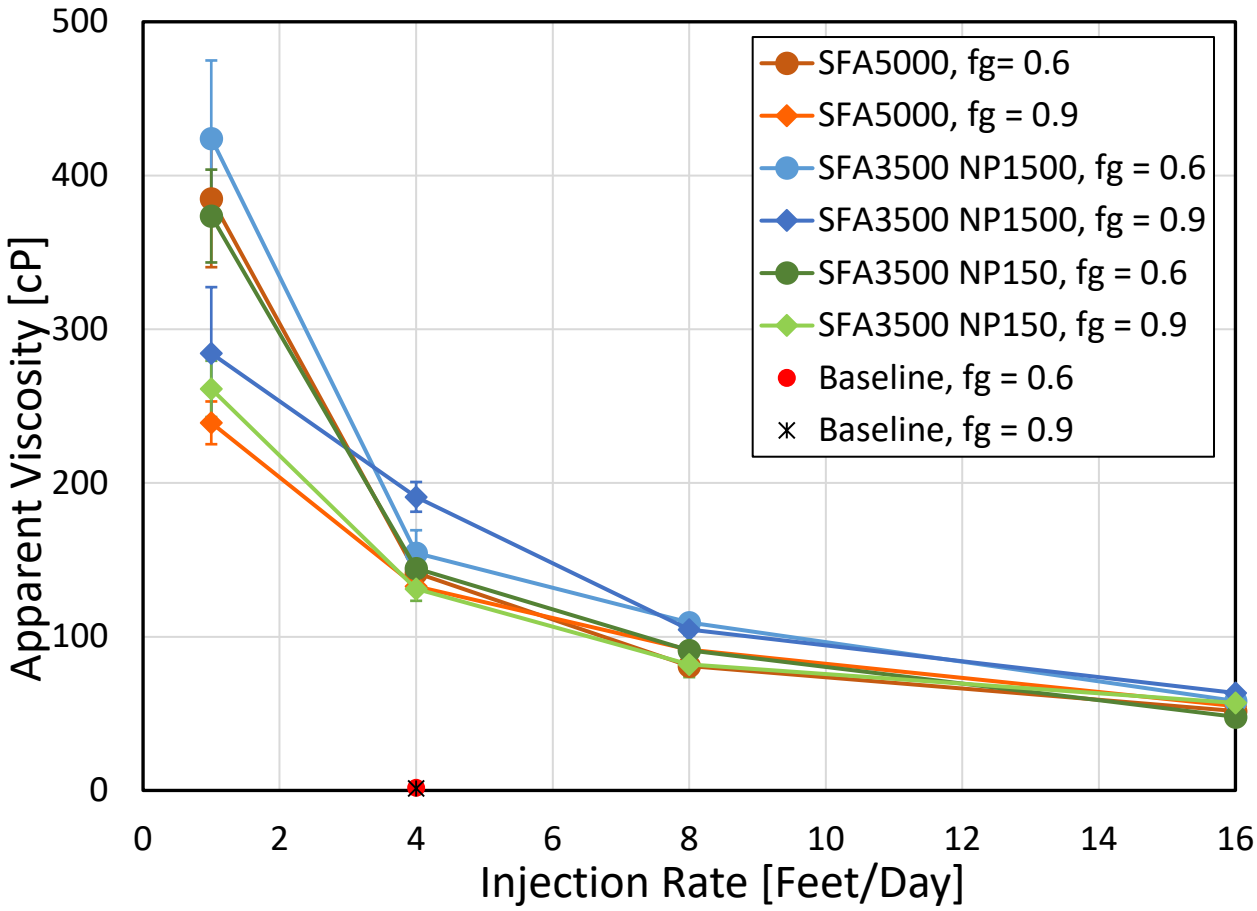

Figure 6.1 Apparent viscosity as a function of injection rate during steady state co-injection using surfactant (orange curves) and a combination of surfactant and nanoparticles (blue and green curves) as foaming formula. Experiments performed at two gas fractions (0.6 (circle) and 0.9 (diamond)) show an increase in foam strength for lower gas fraction. Shear thinning behavior was observed using all of the three foaming formulas and stronger foam was observed during the injection with presence of nanoparticles.

Results also showed the impact of foaming agent on foam stability (Figure 6.2). The measured differential pressure increased and remained stable during co-injection, but fluctuations during the low injection rates were observed. Fluctuations were caused by the effect of the BPR on the system pressure and similar effect was observed in previous studies (Skjelsvik, 2018). Uncertainties in the calculated apparent viscosity due to fluctuations are shown as error bars in Figure 6.1. Figure 6.2 show a decrease in differential pressure with a decreasing injection rate during co-injection using SFA3500 NP1500. Identical behavior was observed for the two other foaming agent solutions and curves are shown in Appendix D.

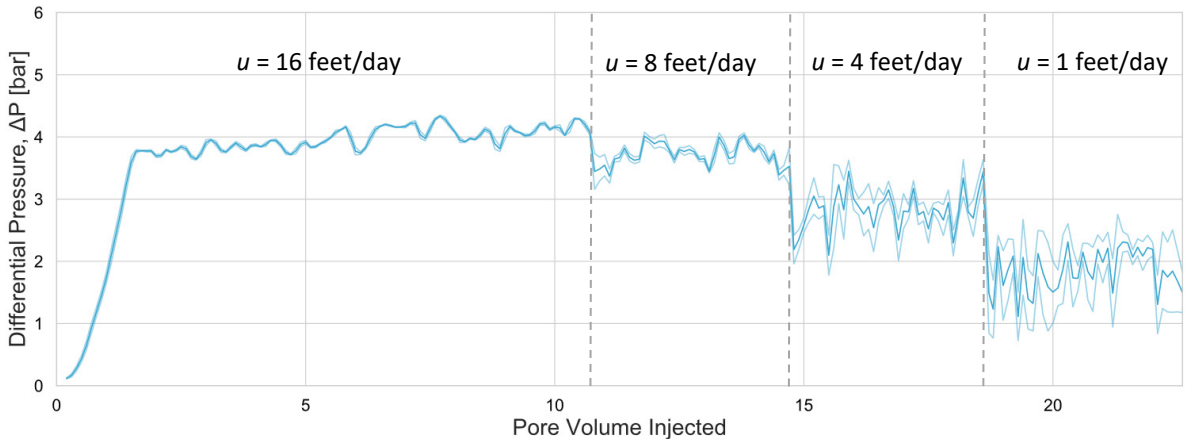

Figure 6.2 Pressure drop with standard deviation as a function of pore volume injected for different injection rates during co-injection using SFA3500 NP1500. Pressure drop was highest at highest superficial velocity.

Comparison of foam generation shows a positive effect of including nanoparticles for both low and high gas fractions. By using a foaming agent consisting of 3500 ppm SFA and 1500 ppm nanoparticles the apparent viscosity increased with 10% for low gas fraction (0.6) and 15% for high gas fraction (0.9) compared to 5000 ppm SFA only. Simultaneously, water saturation at gas breakthrough decreased from $S_w = 0.30$ using SFA to $S_w = 0.20$ using a combination of SFA and nanoparticles (Figure 6.3). This indicated improved water displacement efficiency which is advantageous for increased CO_2 storage. It should be noted that the core was not re-saturated between adjustments of injection rate and breakthrough occurred during co-injection at 16 feet/day and f_g = 0.6.

The reduction of the nanoparticle concentration to 150 ppm also showed positive results for several injection rates. At low gas fraction, the apparent viscosity increased with 5-10% at an injection rate of 4 and 8 feet/day, while at high gas fraction it increased with 4-10% at an injection rate of 1 and 16 feet/day. Foam generation at other rates were similar to the results in absence of nanoparticles. Water saturation measurements show a decrease from $S_w = 0.3$ using surfactants to $S_w = 0.24$ using a combination of surfactants and a low concentration (150 ppm) of nanoparticles (Figure 6.3). This indicates that the total amount of foaming agent might be reduced without decreasing the effectiveness of the foam, which can be an economic advantage.

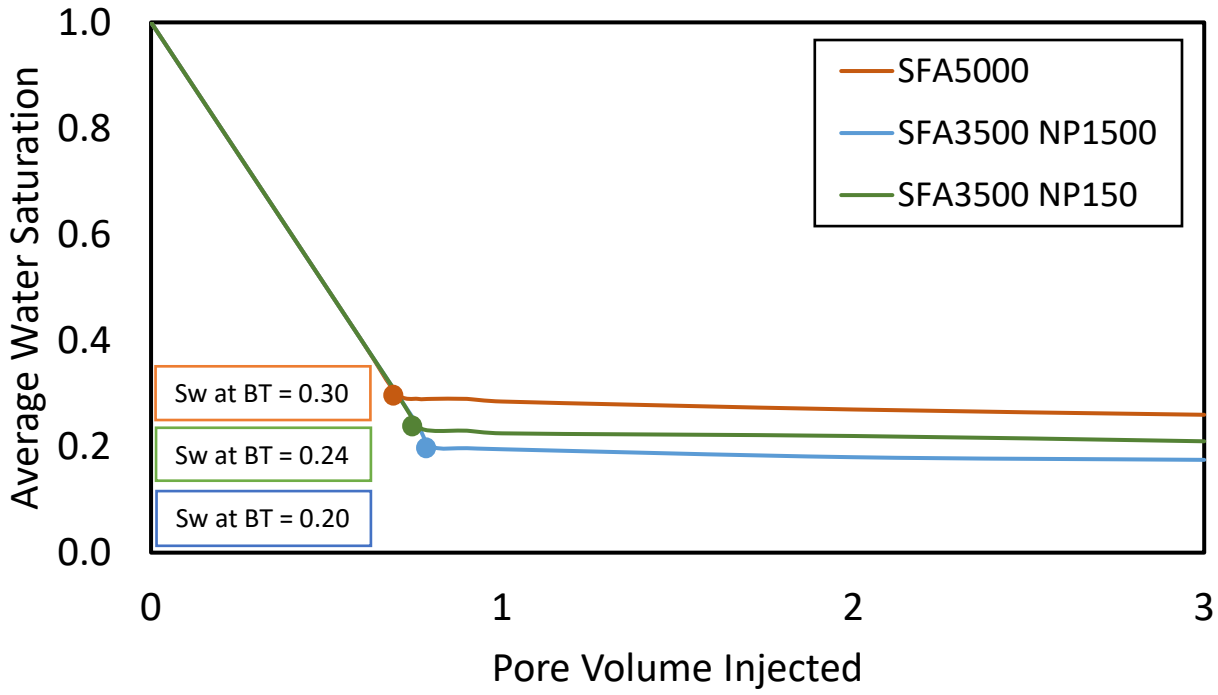

Figure 6.3 Average water saturation during co-injection of CO_2 and foaming agent. Fluids were co-injected at a total injection rate of 16 feet/day and the gas fraction f_g = 0.6. Presence of nanoparticles improved water displacement. Water saturation at breakthrough decreased from 0.3 using surfactants to 0.24 and 0.20 in combination with nanoparticles.

Foam effectiveness can be described by the mobility reduction factor (MRF). A dimensionless factor that measure the ability of the CO_2 foam to reduce gas mobility. High MRF values indicate substantial foam generation and efficient mobility reduction. Results obtained from steady state co-injections showed that the combination of surfactants and nanoparticles improves mobility reduction of CO_2 (Figure 6.4). The effect of nanoparticles was noticeable at both high and low injection rates and gas fractions. Using 3500 ppm surfactants in combination with 1500 ppm nanoparticles, the MRF increased with 10 – 30%, while using 150 ppm nanoparticles, the MRF increased with 2 – 13% compared to using 5000 ppm surfactants.

Results show that the MRF increased with approximataly 20% when nanoparticle concentration increased from 150 to 1500 ppm. Previous studies of the effect of nanoparticles on MRF show similar increase when the concentration increased from 0.1 to 0.3 wt.% (Singh et al., 2015).

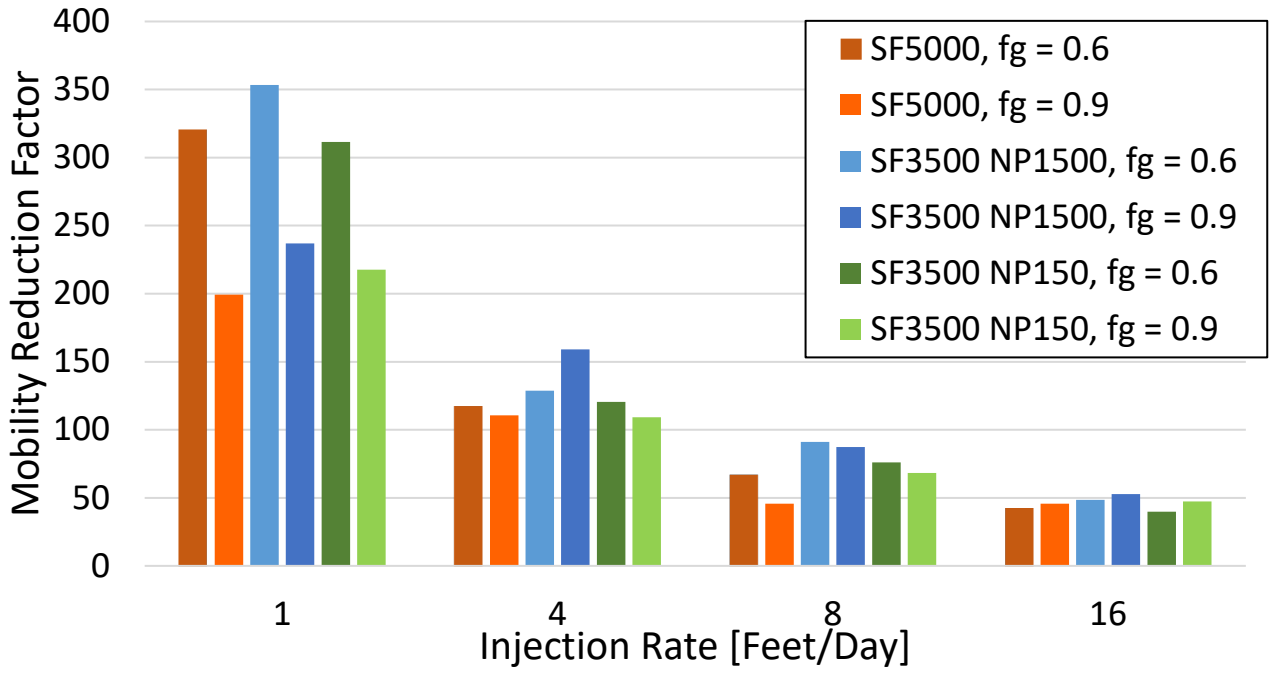

Figure 6.4 The mobility reduction factor (MRF) at different injection rates and gas fractions using three different foaming formulas. The MRF decreased as the injection rate increased.

7. CO_2 Foam Generation and Coalescence

Foam generation and coalescence rates for different foaming agents were studied during unsteady state CO_2 injections. A particular focus was to identify synergistic effects between surfactants and nanoparticles, to increase foam stability and to delay coalescence. Two types of surfactants were used separately and in combination with nanoparticles. Results demonstrate the influence of the foaming agents on foam generation and coalescence rate. All reported results used the same pressure and temperature condition: P = 200 bar, T = 40 °C.

7.1. Baseline

An unsteady state CO_2 injection without presence of foaming agent was performed to benchmark subsequent CO_2 injections with foaming agents in terms of foaming ability and foam stabilization. A constant superficial velocity of 4 feet/day was applied.

To identify the foam generation, the apparent viscosity was calculated using Eq. (5). Apparent viscosity is proportional to differential pressure across the core, meaning that an increase in differential pressure results in a higher apparent viscosity for identical injection rate. Figure 7.1 shows the apparent viscosity (orange curve) as a function of the pore volume CO_2 injected for the baseline injection. An increase in apparent viscosity was observed at the start of the CO_2 injection. The value increased to μ_{app} = 1.7 cP after 0.18 PV CO_2 injected followed by a linear drop at 0.32 PV injected and stabilization at μ_{app} ≈ 1.1 cP. Although there was observed an increase in pressure, it was assumed that foam did not generate due to the lack of foaming agent present. Increased pressure may be caused by relative permeability effects when two immiscible fluids are present in a porous media.

The avarage water saturation was calculated using the weight of the produced water during CO_2 injection, with the assuption that the core was initially 100% saturated with brine. As the CO_2 was injected into the core, brine was displaced and residual water sautration decreased (Figure 7.1). Similar to apparent viscosity, a significant change was observed at the beginning of the injection. Water saturation decreased from S_w= 1 to S_w= 0.68 after 0.32 PV injected, thereafter it gradually decreased to S_w= 0.6. Calculated water saturations indicated a gas breakthrough at 0.32 PV CO_2 injected.

A comparison of the curves shows changes in both apparent viscosity and water saturation after 0.32 PV injected. A reduction of the apparent viscosity indicates less flow resistans in the system while changes in water saturation shows that both brine and CO_2 were produces after 0.32 PV, hence the gas breakthrough. Gas breakthorugh occurred early in comparison to the measurements with foaming agent (see Chapter 6.1) , which was expected due to the low viscosity of CO_2 compared to the brine (Lee et al., 2013).

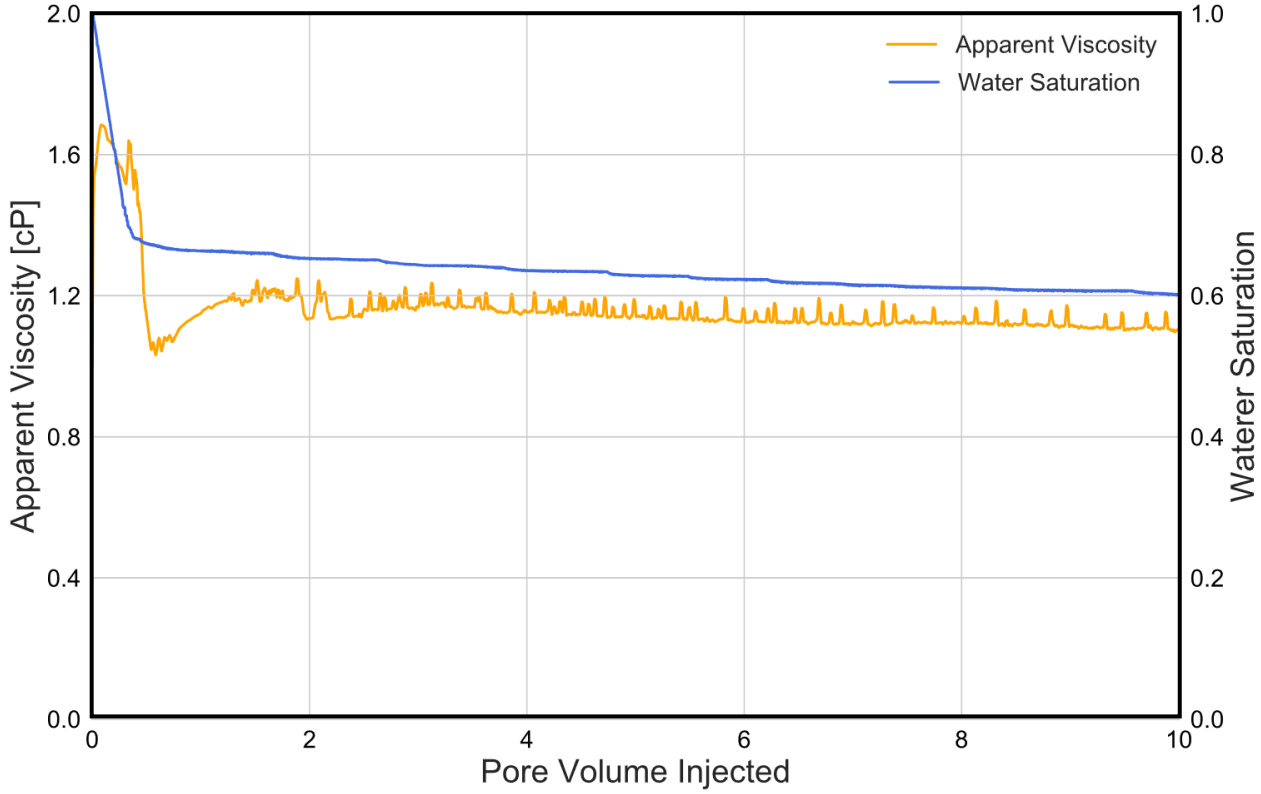

Figure 7.1 Apparent viscosity (orange curve) and water saturation (blue curve) as a function of pore volume injected for unsteady state CO_2 injection to a brine-saturated core without foaming agent. An increase in apparent viscosity due to relative permeability effects was observed at the start of the injection followed by a linear reduction and stabilization. Simultaneously, water saturation decreased from $S_w = 1$ to $S_w = 0.68$ and gas breakthrough after PV = 0.32.

The baseline experiment showed that a foaming agent is necessary in order to generate a strong and stable CO_2 foam. Injection without a foaming agent results in no foam or a weak foam that rapidly breaks (Sheng, 2013). Additionally, baseline results showed an early gas breakthrough and poor sweep efficiency as a results of unfavorable mobility ratio, which are disadvantages for both CO_2-EOR and CO_2 storage.

7.2. The Effect of Surfactant Type and Concentration on CO_2 Foam Generation and Coalescence

Nonionic and anionic surfactants were investigated as foaming agents. Anionic surfactants are widely used for EOR applications as they have a good stability, a low adsorption on sandstone and a low fabrication cost. The reduction in interfacial tension (IFT) is higher for anionic surfactants compared to nonionic surfactants. However, nonionic surfactants generally have a higher salinity tolerance (Becher, 1990; Sheng, 2011).

The foaming properties (generation and coalescence) were evaluated using two surfactants (anionic and nonionic) and two concentrations (3500 and 5000 ppm) with identical experimental conditions and superficial velocities as the baseline (Chapter 7.1). The core was initially 100% saturated with a foaming agent solution prior to the CO_2 injection. During the CO_2 injection, differential pressure and weight of the produced fluids were continuously measured for apparent viscosity and water saturation calculations. The effect of surfactant type and concentration was evaluated based on apparent viscosity (Figure 7.2 and Figure 7.3) and water saturation data (Table 7.1). Results were divided into four parts to compare different foam behavior observed during the CO_2 injections.

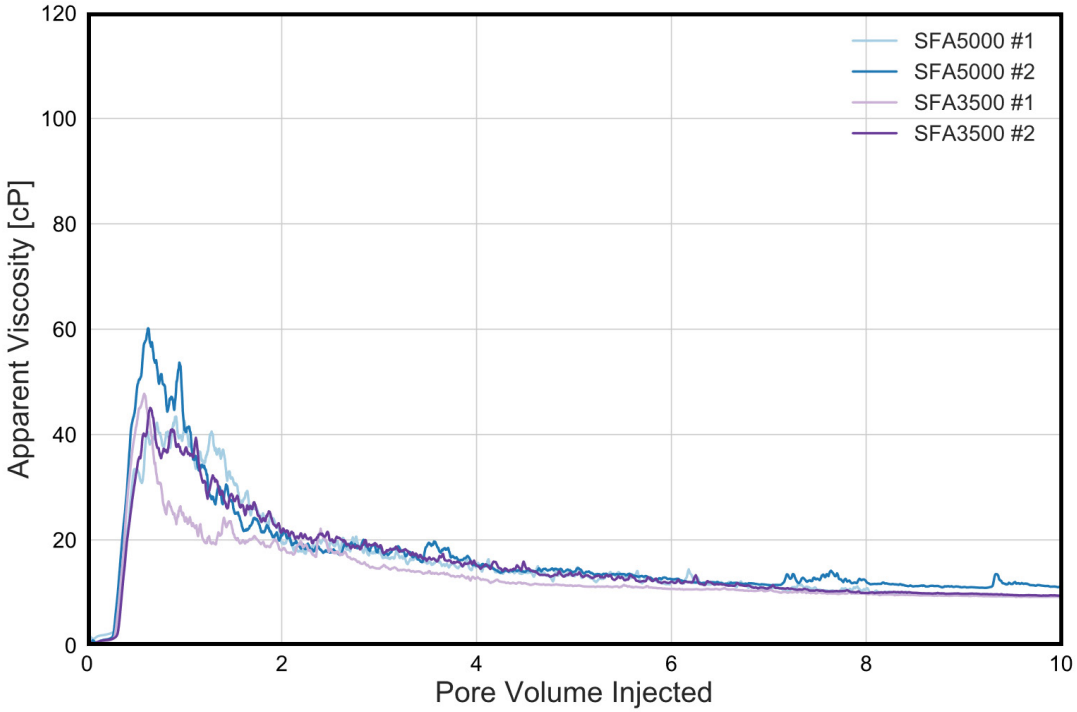

Figure 7.2 Apparent viscosity as a function of pore volume injected during unsteady state CO_2 injection with the nonionic surfactant using two concentrations (3500 ppm: purple lines and 5000 ppm: blue lines). Results show an increase in apparent viscosity during the experiments with high surfactant concentration. Over time, the apparent viscosity decreases to approx. 10 cP regardless of concentration.

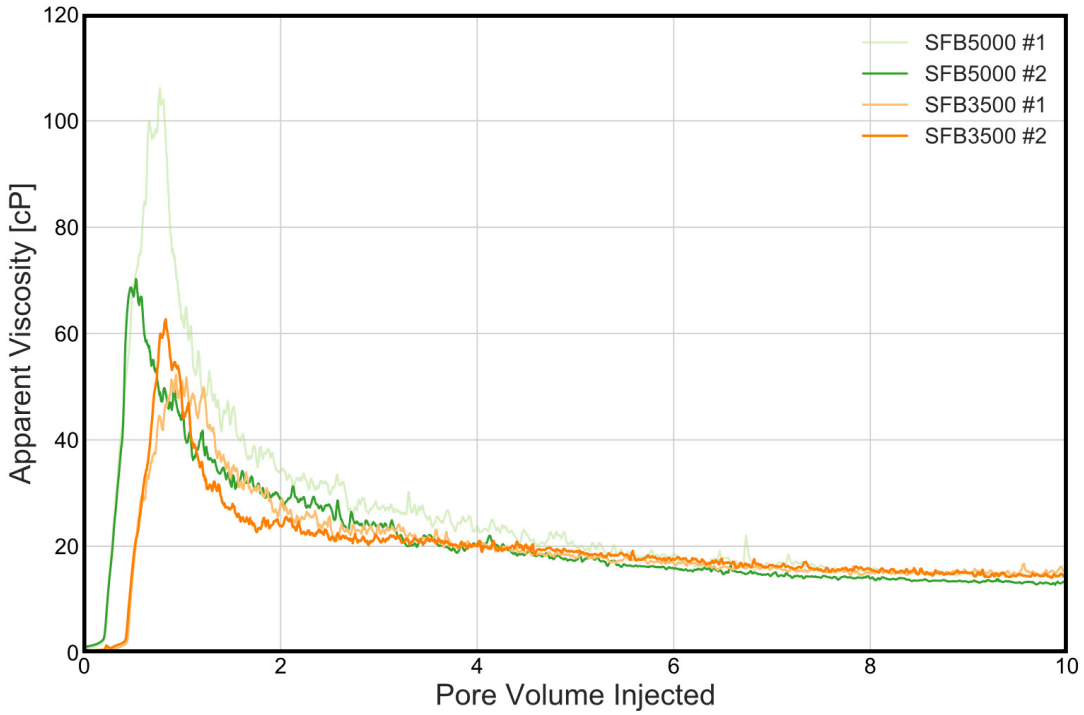

Figure 7.3 Apparent viscosity as a function of pore volume injected during unsteady state CO_2 injection with the anionic surfactant using two concentrations (3500 ppm: orange lines and 5000 ppm: green lines). Results show an increase in apparent viscosity and an earlier foam generation during experiments with high surfactant concentration. Over time, the apparent viscosity decreases to approx. 14 cP regardless of concentration.

In general, results show an increased apparent viscosity after 0.2 PV CO_2 injected for high-concentration solutions using both surfactants. Anionic surfactants show a delay of 0.23 PV injected in foam generation for low concentration solutions, whereas nonionic surfactants generate foam at the same time for both concentrations. Previous results show a delayed onset of foam generation with decreasing surfactant concentration and a correlation with the foam strength. Weaker foams require more PV injected before lamellae sufficiently stabilize and foam generates (Chou, 1991; Hadian Nasr et al., 2020). The results also show that over time the apparent viscosity decreased to an approximately equal value regardless of the concentration. Comparison of the two surfactants show a stronger foam generation using anionic surfactant which was expected due to their good stability, ability to reduce the IFT and low adsorption on sandstone (Sheng, 2011).

Apparent viscosity curves have been divided into four parts for a better understanding of the process and the influence of foaming agents: induction time (1), peak (2), half-life (3) and endpoint (4), see Figure 7.4. *Induction time* describes the time from when CO_2 entered the core to foam generation (pressure / apparent viscosity increase) was observed. *Peak* is the maximum apparent viscosity and *half-life* is defined as the half-life of the peak. The *endpoint* is the apparent viscosity after 10 PV CO_2 injected. Foam generation and coalescence rates were determined by calculating the linear slope of the curve between points 1 and 2 for generation, and 2 and 3 for coalescence (see Figure 7.4). Additionally, apparent viscosity has been compared with the water saturation data to evaluate when and how much water was displaced during the CO_2 injection. Water saturation at peak as well as gas breakthrough time for each experiment are shown in Table 7.1.

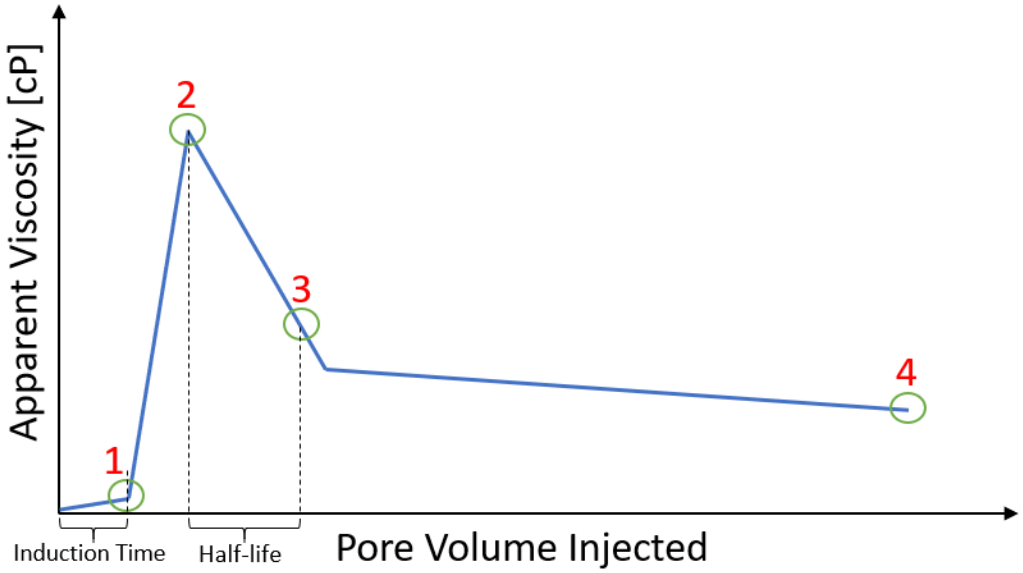

Figure 7.4 Illustration of division of apparent viscosity curve for foam behavior analysis. The graph has been divided into four parts: (1) Induction time described by time from when CO_2 entered the core to foam generation was observed, (2) Peak defined as the maximum apparent viscosity, (3) Half-life, time required to reduce apparent viscosity to half of the peak value, (4) Endpoint defined as the apparent viscosity after 10 PV injected.

The effect of surfactant type and concentration can be determined based on the information in Table 7.1. Using SFA, change in concentration did not affect induction time. The average induction time before the foam generation was 0.29 PV and the generation rate was 188.0 ± 2.5 cP/PV for both concentrations. Using SFB, however, there were observed different induction times and the time varied between 0.20 and 0.43 PV injected for SFB5000 and SFB3500, respectively. A recent study showed that delayed foam generation caused an inefficient water displacement (Føyen et al., 2020) but this was not observed during the injections possibly because the generation occurred before the gas breakthrough. There were no big changes in the generation rate. The average generation rate was 194.6 ± 7.2 cP/PV. For both surfactants, the peak was highest for high concentration solutions (5000 ppm), which indicated stronger foam generation with an increased surfactant concentration.

The half-life time and coalescence rate varied for all the CO_2 injections, regardless of surfactant type or concentration. Comparison of two identical injections showed variations in peak and coalescence rate and a correlation between them was observed (Figure 7.5). High peak resulted in a high coalescence rate meaning a rapid decrease in apparent viscosity and thus a short half-life. When foam is generated, and apparent viscosity is high, the number of foam films subsequently decreases because most of the liquid phase has been drained out due to efficient displacement. For low apparent viscosity, however, foam films do not decrease as much and the coalescence rate is lower (Huh et al., 1989).

Table 7.1 Parameters for CO_2 foam behavior using surfactants as foaming agents

	Nonionic Surfactant (SFA)				Anionic Surfactant (SFB)			
	5000 #1	**5000 #2**	**3500 #1**	**3500 #2**	**5000 #1**	**5000 #2**	**3500 #1**	**3500 #2**
Induction Time [PV]	0.28	0.27	0.29	0.30	0.20	0.20	0.43	0.43
Generation Rate [cP/PV]	185.4	187.4	191.3	188.1	202.4	192.6	197.8	185.6
Peak Value [cP]	43.4	60.2	52.4	49.5	106.1	70.3	52.3	62.7
Half – life [PV]	1.06	0.75	0.43	1.29	0.36	0.81	1.14	0.35
Coalescence Rate [cP/PV]	20.3	39.7	57.8	17.8	138.9	43.1	21.8	86.0
Endpoint [cP]	8.7	10.5	10.1	10.0	13.2	13.0	15.5	14.4
S_w at Peak	0.27	0.39	0.40	0.35	0.31	0.31	0.31	0.33
BT time [PV]	0.70	0.69	0.72	0.67	0.67	0.67	0.66	0.68
S_w at BT	0.30	0.31	0.28	0.33	0.33	0.33	0.34	0.32
S_w at Endpoint	0.21	0.25	0.24	0.23	0.24	0.24	0.22	0.22

To generate a strong and stable foam, high peak value and low coalescence rates are desired properties. Foam generated during each CO_2 injection was classified into four distinct regimes of either weak or strong and stable or unstable (see Figure 7.5). The regime transitions were defined by the average peak and coalescence rate of all injections (including the CO_2 injections with nanoparticles as foaming agent described in Chapter 7.3). The average peak was 59.1 cP and foams with a higher peak were classified as strong. The average coalescence rate was 41.7 cP/PV and foams with a lower coalescence rate were classified as stable. The classification showed that SFB contributed to generate stronger but less stable CO_2 foam than SFA. As two identical injections demonstrated variation in peak and coalescence rate, the injections should be repeated to confirm the observation.

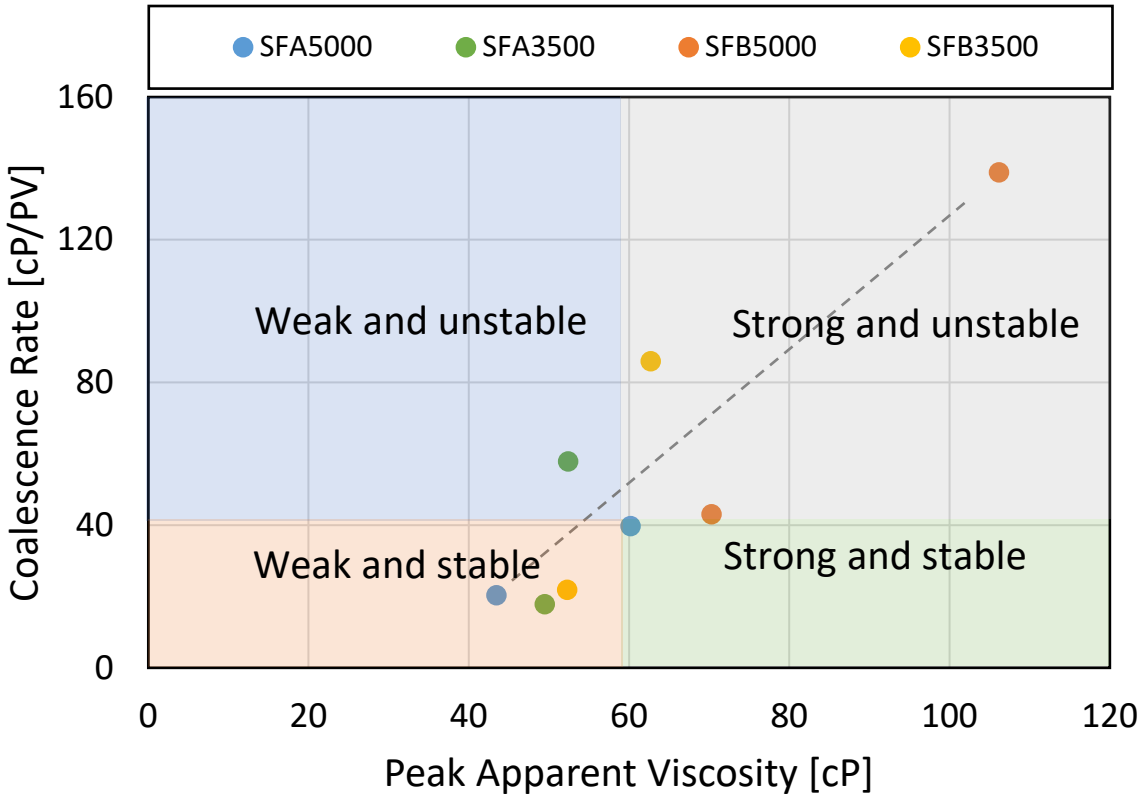

Figure 7.5 CO_2 foam classification based on viscosity peak value and coalescence rate. High peak indicated strong foam, and low coalescence rate indicated stable foam. A correlation between peak and coalescence rate was observed. Increase in peak resulted in increase in coalescence rate, meaning strong foams were less stable than weak foams.

After 10 PV injected the apparent viscosity was approx. 10 cP and 14 cP using SFA and SFB respectively and the average water saturation was 0.23 for both surfactants. Because anionic surfactant (SFB) show a better performance in term of apparent viscosity, lower water saturations were expected. This discrepancy could be explained by overestimation of water saturation due to permeability variations between the injections. It was observed that the absolute permeability with anionic surfactants was lower than with nonionic surfactants (Appendix B). Hence, the assumption that the core was 100% saturated with foaming agent might not be valid and the measured water saturations will in turn be overestimated. In this case, the water saturation for SFB will be lower and this means that a stronger foam contributes to a lower gas relative permeability and more efficient displacement.

Unsteady state CO_2 injections do not show significant differences in water displacement using different surfactant concentrations, even though variation in apparent viscosity was observed. Saturation data

show that gas breakthrough occurred after 0.68 ± 0.02 PV injected and the performance after breakthrough was similar assuming that the results for SFB were not overestimated.

Compared to baseline the presence of foaming agent had a positive impact on foam generation and water displacement efficiency. For baseline injection, no foam generation was observed. The apparent viscosity had a peak at 1.7 cP and decreased to 1.1 cP after 10 PV injected. Using surfactant as foaming agent the average peak was 62.1 cP and 11.9 cP after 10 PV injected. Water saturation data show a delay in gas breakthrough from 0.32 PV without a foaming agent to 0.68 PV with a foaming agent, hence a more favorable displacement efficiency. After 10 PV injected the average residual water saturation using surfactants was S_w = 0.23 compared to S_w = 0.60 for baseline, meaning that 60% less of the brine remained in the core and the potential CO_2 storage capacity increased by 60%. Similar results were observed in previous studies on CO_2 storage capacity in sandstone (Føyen et al., 2020). Results showed that the foam generation, regardless of surfactant type and concentration, contributed to decreasing the gas relative permeability, which can be beneficial for increased oil recovery and CO_2 storage capacity.

7.3. The Effect of Nanoparticles on CO_2 Foam Generation and Coalescence

Nanoparticles as foaming agents have shown promising results for foam mobility control due to their ability to stabilize foam (Talebian et al., 2013). Previous results show that nanoparticles on their own generate a weak foam, and contribute to foam stabilization when combined with surfactants (Rognmo, 2019). Synergic effects between nanoparticles and surfactants has been investigated during unsteady state CO_2 injections. Two concentrations (150 ppm and 1500 ppm) of silica nanoparticles were added to 3500 ppm of nonionic (SFA) and anionic (SFB) surfactant solutions. The experiments were performed under the same conditions and the same injection rate as without nanoparticles. The effect of nanoparticles was evaluated based on apparent viscosity (Figure 7.6 and Figure 7.7) and foam behavior was divided into four parts like the results without nanoparticles (Table 7.2).

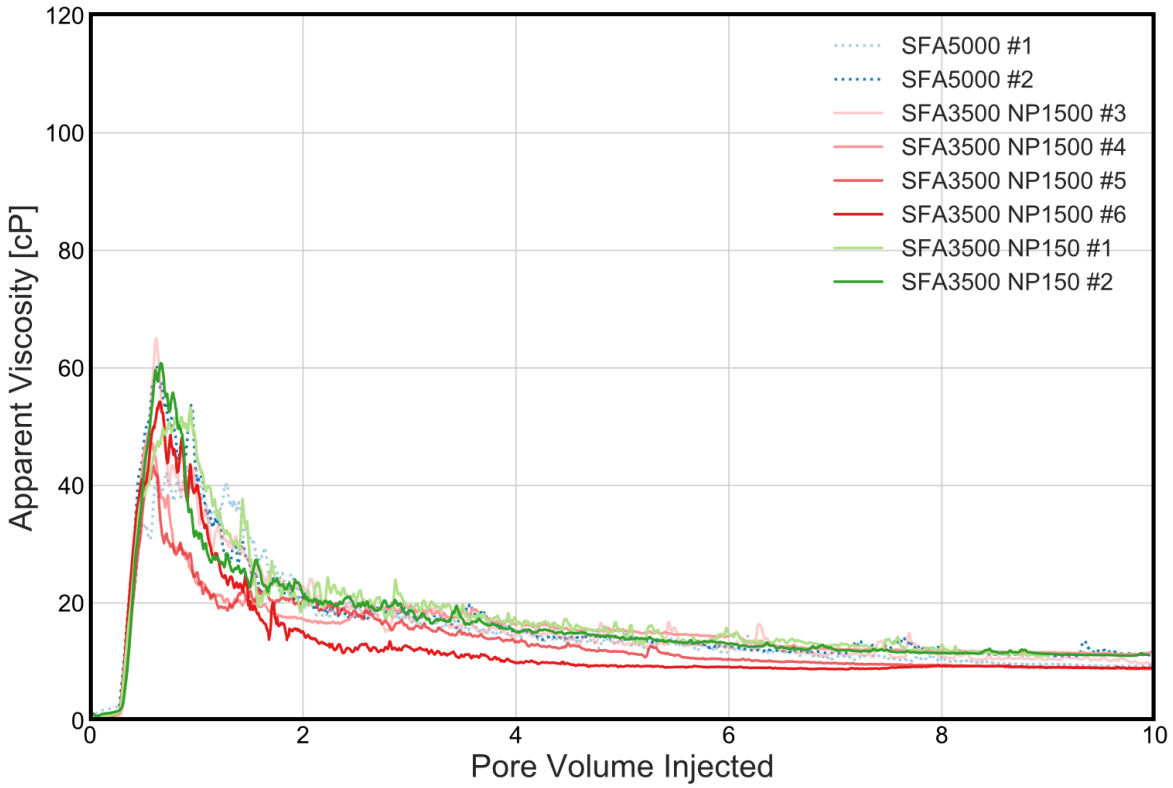

Figure 7.6 Apparent viscosity as a function of pore volume injected using two combinations of nonionic surfactant (SFA) and nanoparticles. 3500 ppm nonionic surfactant (SFA) in combination with high (1500 ppm) and low (150 ppm) concentration of nanoparticles (red and green curves respectively) show small differences in apparent viscosity compared to results using only surfactants (blue dotted curves).

Combination of nonionic surfactant (SFA) and nanoparticles do not show a stabilizing effect on foam as expected from steady state observations (Chapter 6). The induction time and generation time were similar to injections without nanoparticles. Foam generation was observed after 0.29 PV injected and the generation rate was 191.4 ± 6.6 cP/PV. The average peak was 52.9 cP and 57.1 cP for SFA3500 NP1500 and SFA3500 NP150 respectively. Similar to values obtained without nanoparticles. This can indicate that nanoparticles do not contribute to generation of a stronger foam when combined with SFA during transient unsteady state periods. Previous pore scale study using the same concentrations of surfactants and nanoparticles showed similar results (Benali, 2019). Half-life time and coalescence rate (Table 7.2) show negative impact of nanoparticles on foam stability. The average half-life time without nanoparticles was 0.88 ± 0.30 PV and the apparent viscosity decreased with a rate of 33.9 ±

18.7 cP/PV, while with nanoparticles the half-life time was 0.53 ± 0.13 PV and the coalescence rate was 50.5 ± 13.6 cP/PV. Calculated water saturation and breakthrough time during the CO_2 injections do not show effect of nanoparticles. The average breakthrough time was 0.68 and 0.67 PV and the average water saturation after 10 PV was S_w = 0.24 and S_w = 0.23 for SFA3500 NP1500 and SFA3500 NP150, respectively.

It is noteworthy that during steady state co-injections, nanoparticles in combination with SFA generated stronger foam and increased the stability of the foam. In general, simultaneous injection of CO_2 and foaming agent allows a stronger foam generation compared to unsteady state injections. Maximum apparent viscosity achieved during steady-state co-injections were between 150 – 220% higher compared with unsteady state injections. This is because a continuous injection of foaming agent prevents drainage of the liquid phase that decrease the number of lamellae (Raza, 1970). Previous studies show that gas relative permeability is lower during a steady state injection compared to unsteady state injection, meaning a more favorable mobility ratio and a better displacement is expected (Huh et al., 1989).

Synergy of anionic surfactants (SFB) and nanoparticles showed a stabilizing effect for both low and high nanoparticle concentrations (Figure 7.7). The induction time was 0.44 PV and was similar to induction time when using low concentration (3500 ppm) of anionic surfactant only (0.42 PV). This may indicate that nanoparticles contribute mostly to foam stabilization, and not foam generation. In addition, no change in the generation rate was observed and the peak was similar to that of using SFB3500, hence surfactants determine foam strength.

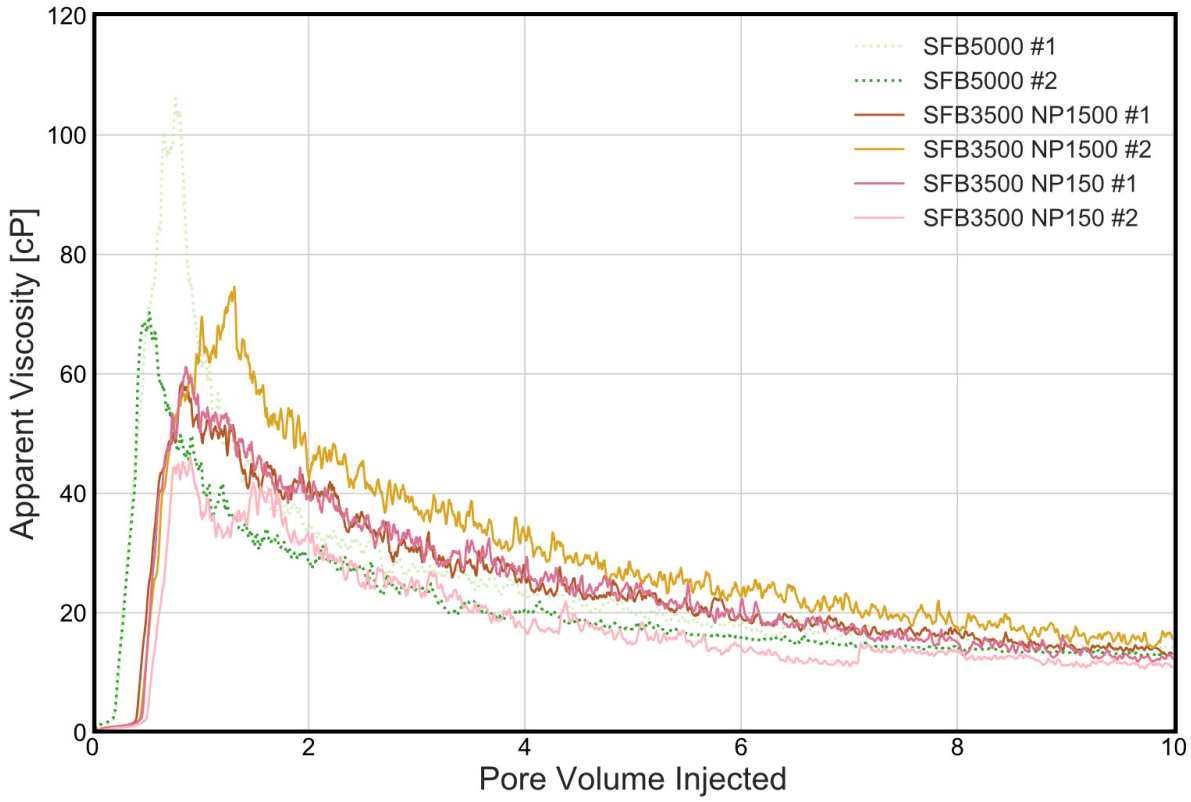

Figure 7.7 Apparent viscosity as a function of pore volume injected using two combinations of anionic surfactant (SFB) and nanoparticles (NP). 3500 ppm anionic surfactant (SFB) in combination with high (1500 ppm) and low (150 ppm) concentration of nanoparticles (brown and pink curves) show a stabilizing effect on apparent viscosity compared to results using only surfactants (green dotted curves).

Unlike for nonionic surfactants, nanoparticles showed a positive impact on half-life time and coalescence rate when combined with anionic surfactants. The average half-life time without nanoparticles was 0.67 ± 0.38 PV and the average coalescence rate was 72.4 ± 32.7 cP/PV. By including nanoparticles, the average half-life time increased with 230% to an average value of 2.22 ± 0.33 PV and the coalescence rate decreased to 13.3 ± 4.0 cP/PV. Low foam coalescence rates can contribute to in-depth mobility control further from the injection well in reservoirs and thus improved volumetric sweep. Although foam stabilization was observed, no changes in water saturation were observed. The gas breakthrough occurred after 0.67 PV and water saturation after 10 PV injected was 0.23.

Table 7.2 Parameters for CO_2 foam behavior using surfactants and nanoparticles as foaming agents

	Nonionic Surfactant (SFA) + Nanoparticles						**Anionic Surfactant (SFB) + Nanoparticles**			
	1500 #3	**1500 #4**	**1500 #5**	**1500 #6**	**150 #1**	**150 #2**	**1500 #1**	**1500 #2**	**150 #1**	**150 #2**
Induction Time [PV]	0.30	0.29	0.28	0.29	0.30	0.29	0.40	0.42	0.43	0.49
Generation Rate [cP/PV]	197.8	185.9	183.1	194.7	198.7	188.2	189.9	184.6	197.7	162.7
Peak Value [cP]	65.0	49.1	43.4	54.3	53.3	60.8	58.6	74.6	61.2	46.1
Half – life [PV]	0.58	0.41	0.49	0.54	0.77	0.40	2.62	1.84	2.30	2.14
Coalescence Rate [cP/PV]	53.0	53.3	43.5	46.9	32.7	73.4	10.9	19.0	12.6	10.5
Endpoint [cP]	9.1	11.8	8.5	8.7	11.0	11.2	13.3	12.6	11.5	11.3
S_w at Peak	0.38	0.43	0.39	0.34	0.30	0.34	0.32	0.32	0.32	0.35
BT time [PV]	0.67	0.68	0.68	0.69	0.65	0.67	0.66	0.64	0.67	0.65
S_w at BT	0.33	0.32	0.32	0.31	0.35	0.33	0.34	0.36	0.33	0.35
S_w at Endpoint	0.25	0.22	0.22	0.26	0.23	0.23	0.23	0.23	0.23	0.24

Comparison of the results using surfactants separately and in combination with nanoparticles shows differences in coalescence rate and half-life. Without nanoparticles, the use of nonionic surfactants (SFA) resulted in lowest coalescence rate, which means that a stable foam was generated. Including nanoparticles, a stabilizing effect was observed when combined with anionic surfactants (SFB). Combining SFB with nanoparticles, the average half-life time increased and the coalescence rate decreased (Table 7.2) compared to results without nanoparticles for both high (1500 ppm) and low (150 ppm) concentration of nanoparticles (Figure 7.8). A combination of SFA and nanoparticles, however, show higher coalescence rate and more unstable foam. Surface charge and hydrophobicity of the foaming agents affect particle interaction and can partially explain the differences in foam behavior observed here. However, detailed colloids and surface chemistry is beyond the scope of this thesis and such an investigation is reserved for future studies.

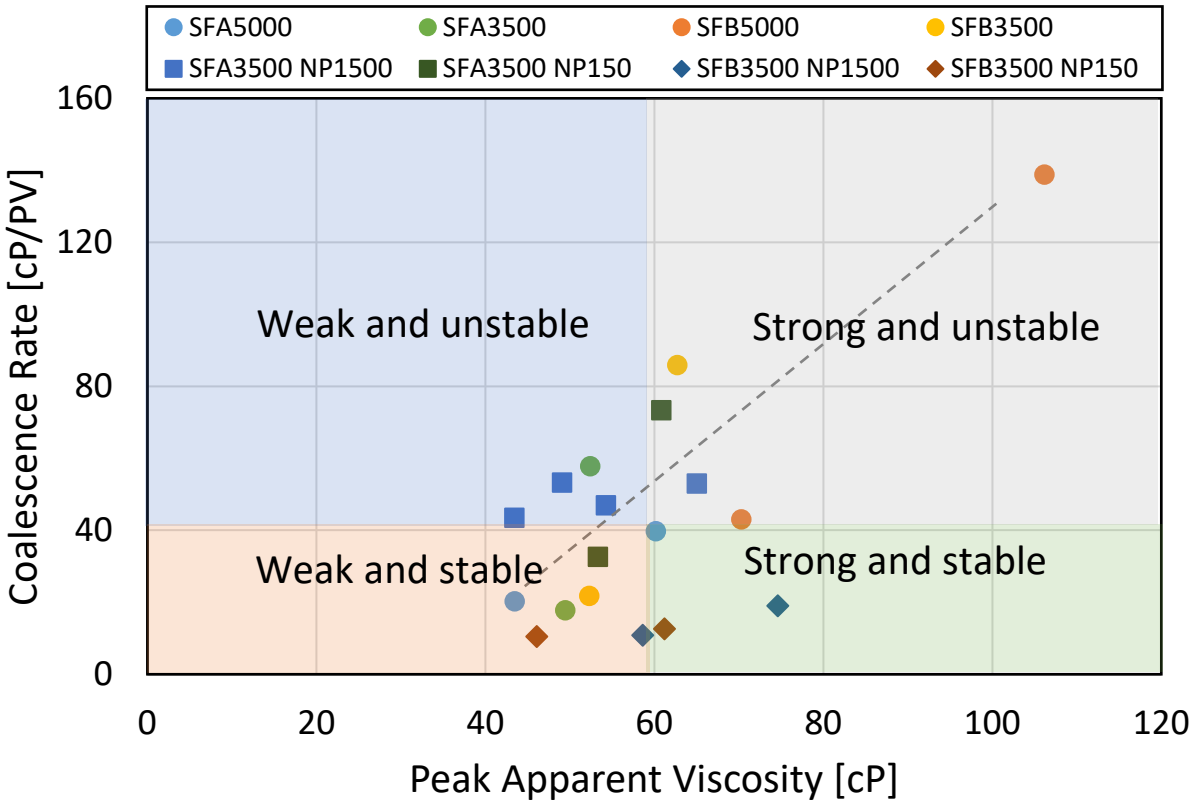

Figure 7.8 Coalescence rate as a function of peak showed a stabilizing effect of nanoparticles when combined with SFB as decrease in coalescence rate was observed. For SFA an increase in coalescence rate and peak was observed when in combination with nanoparticles.

Results obtained during unsteady state injections indicate that foam generation and stability is mostly dependent of surfactants. Previous results showed that nanoparticles play an essential role at harsh conditions with elevated temperatures and high salinity, where surfactants are less stable (Heldal, 2016). It was also reported that stability of silica nanoparticles increased with decreased pH (Eide et al., 2018). During this thesis, injections were performed at relatively low temperatures compared to previous experiments and at neutral pH, which may explain why the ability of nanoparticles to stabilize CO_2 foam was not significant.

8. The Effect of Oil on CO_2 Foam

Foam and emulsion generation, stability and coalescence in presence of oil were studied during unsteady and steady state injections. Presence of oil in a porous media has previously shown a negative effect on foam generation and stability. Oil destabilizes foam by spreading on foam films, adsorbing surfactant solution and might prevent foam generation (Jensen et al., 1987; Kuhlman, 1990). Recent studies showed that more stable CO_2 foams could be generated using nanoparticles as foaming agents (Dickson et al., 2004; Rognmo et al., 2018). Therefore, surfactants separately and in combination with nanoparticles were used to investigate the effect of oil in an attempt to provide more insight on interactions of oil on foam systems.

8.1. Baseline

Two CO_2/n-Decane miscible mixtures (10 and 30 volume % n-Decane) were injected into a brine (no foaming agent) saturated core to identify the effect of oil on fluid flow. Mixtures were injected at a total injection rate of 4 feet/day and identical experimental conditions as baseline without oil. Results showed an increase in apparent viscosity as the mixture entered the core followed by a linear drop after 0.75 and 0.65 PV injected (10 and 30% mixture) (Figure 8.1). Similar to injection without oil, the increase in apparent viscosity was caused by relative permeability effects when two or more immiscible fluids are present in a porous media. After several PV injected, the apparent viscosity varied between 0.7 and 1.5 cP and it was assumed that foam did not generate. A comparison of the mixtures showed that an increase in oil concentration led to higher apparent viscosity. The peak was 1.5 cP using 10% n-Decane and 2.5 cP using 30% n-Decane. After 10 PV injected, the apparent viscosity was approximately 0.95 and 1.15 cP for 10 and 30% n-Decane mixture respectively.

Fluctuations in differential pressure were observed during both co-injections with oil and might be caused by the effect of the BPR on system pressure and sudden slugs of oil entering the core due to incomplete miscibility. In addition, issues with the oil injection pump were observed at lower injection rates, which may explain pressure instabilities during baseline with 10% n-Decane. In previous studies, a spiral tubing (Figure 5.1) was added to ensure sufficient mixing of CO_2 and oil before entering the core (Kahrobaei et al., 2018). This was not used during baseline injections, therefore, it was assumed that complete miscibility was not achieved. Spiral tubing was mounted for subsequent injections to increase exposure time and improve fluid mixing.

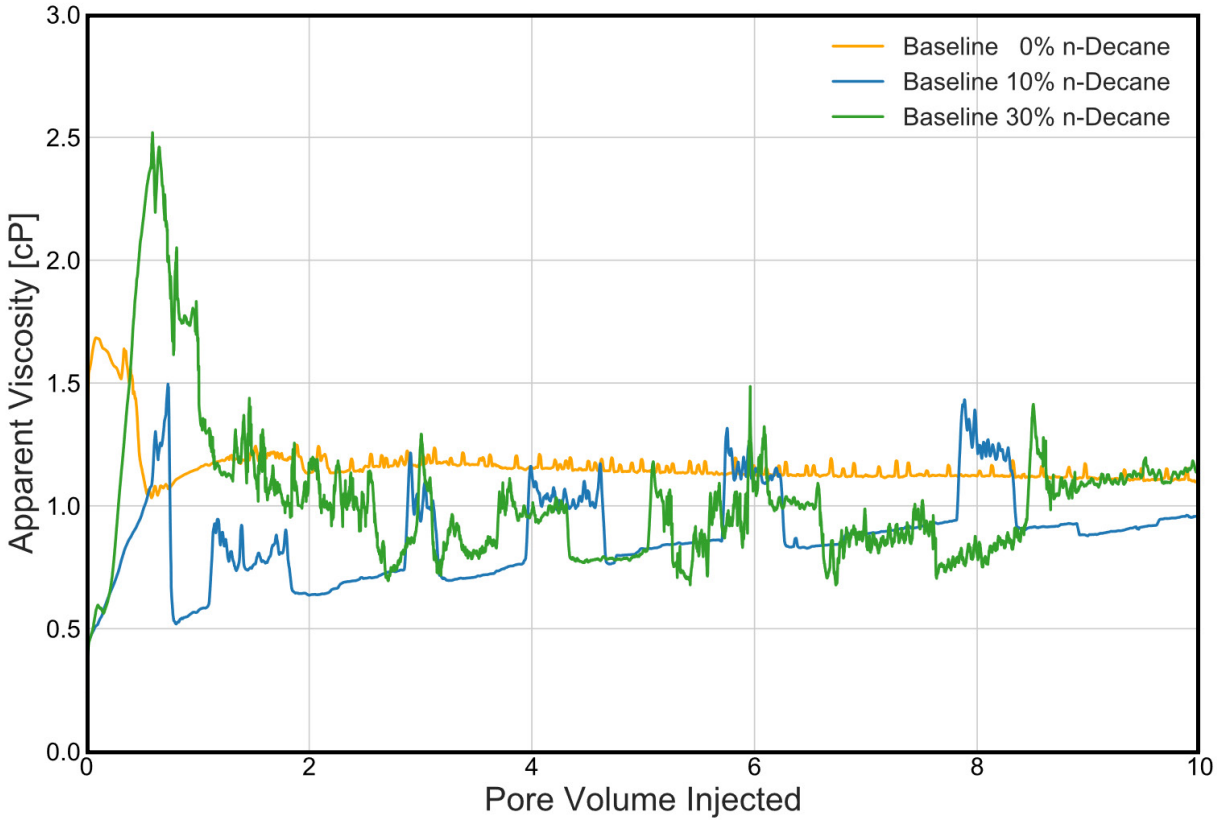

Figure 8.1 The baseline for two CO_2/n-Decane mixtures injected into a brine saturated core at a total injection rate of 4 feet/day. An increase in apparent viscosity as a result of relative permeability effects was observed for both mixtures. Fluctuations in apparent viscosity was observed, but the average apparent viscosity was 1 cP and no foam generation was observed.

8.2. Foam Generation and Stability

Foam generation and stability in presence of oil were studied during steady state co-injection of CO_2/n-Decane mixture (10% n-Decane) and two different foaming agents. Fluids were co-injected at three injection rates (4, 8 and 16 feet/day) and at two gas fractions (0.6 and 0.9) (gas fraction denotes fraction of CO_2/n-Decane mixture) at identical experimental conditions to those used in steady state co-injections without oil.

Results from steady state co-injections show a high apparent viscosity using both nonionic surfactant (SFA) and combination of nonionic surfactant and nanoparticles as the foaming agent (Figure 8.2). During co-injections, shear thinning behavior was observed using both foaming agents and differences in apparent viscosity due to gas fraction were noted. Unlike without oil (Chapter 6.1), the highest results occurred for high gas fraction (f_g = 0.9). Comparison of the results also shows higher apparent viscosity using surfactants only than combination between surfactants and nanoparticles. This differ from the results without oil, which might indicate that surfactants separately have a better ability to generate emulsions than when in combination with nanoparticles.

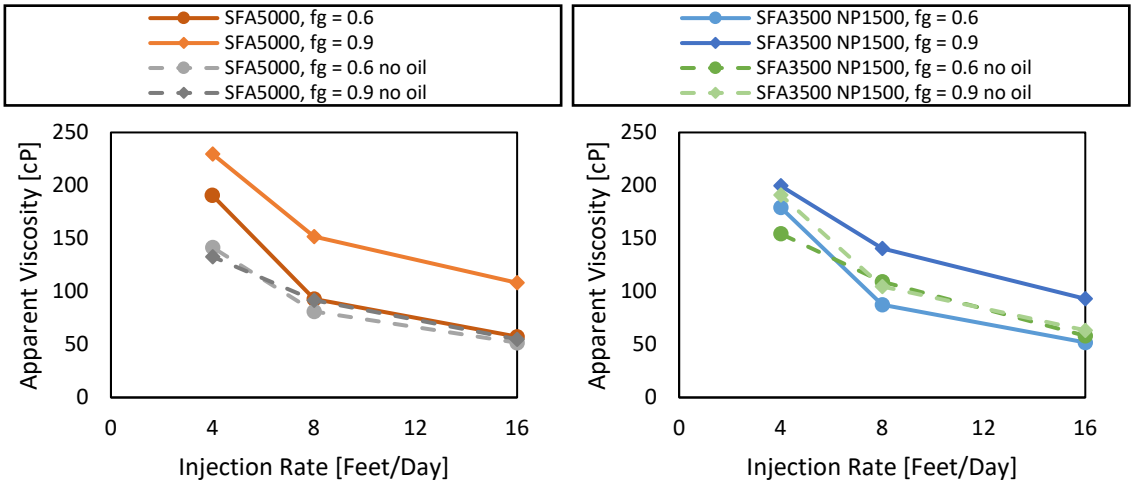

Figure 8.2 Apparent viscosity as a function of the injection rate during steady state co-injection with presence of oil. Nonionic surfactant (left) and a combination of nonionic surfactant and nanoparticles (right) were co-injected with CO_2/oil mixture at two gas fractions (0.6 (circle) and 0.9 (diamond)). Shear thinning behavior and increase in apparent viscosity with increased gas fraction was observed. Results without oil were plotted for comparison (dashed lines).

As oil has previously showed destabilizing effects on foam (Farajzadeh et al., 2012), apparent viscosity was expected to be lower with oil than during co-injection with absence of oil. Since apparent viscosity is proportional to differential pressure across the core (Eq. 5), a high apparent viscosity might be caused by other mechanisms that are contributing to increased differential pressure, such as generation of oil-in-water (o/w) emulsions. It was assumed that o/w emulsions were generated rather than w/o emulsions because both surfactants and the nanoparticles were hydrophilic, and water was the continuous phase (Schramm et al., 1992).

When oil and foaming agent come into contact, emulsions may form. Similar to foam, emulsions contribute to increased flow resistance and differential pressure. Previous studies also show shear thinning behavior for o/w emulsions and generation of stronger emulsions with increased oil concentrations (Mandal et al., 2015). This behavior was observed during co-injections, therefore it was assumed that in addition to the CO_2 foam also o/w emulsions were generated.

Simultaneous generation of CO_2 foam and o/w emulsions will influence the apparent viscosity and it is not possible to determine the effect of oil on foam only, but the overall feasibility of foaming agents to stabilize foam and emulsions can be investigated. Results show higher apparent viscosity when using 5000 ppm nonionic surfactant than when using a combination of 3500 ppm nonionic surfactant and 1500 ppm nanoparticles. Earlier, the opposite effect of nanoparticles in combination with nonionic surfactants to stabilize emulsions has been observed (Arab et al., 2018). Previous research hypothesized that at high surfactant concentrations, surfactant molecules either do not allow nanoparticles to enter oil-water interface or displace the nanoparticles from the interface (Pichot et al., 2012). As a result, the IFT reduction is only affected by surfactants and may explain the differences between SFA5000 and SFA3500 NP1500. To confirm this hypothesis, the effect of nanoparticles combined with lower surfactant concentrations should be further investigated.

8.3. Foam Coalescence

The destabilizing effect of oil on CO_2 foam was investigated during unsteady state injections. CO_2/n-Decane mixture was injected at a constant superficial velocity of 4 feet/day into foaming agent saturated core. Similar to steady state co-injections, there was observed an increase in the apparent viscosity. With known destabilizing effect of oil on CO_2 foam, generation of o/w emulsions was hypothesized. It was not possible to distinguish foams and emulsions based on differential pressure data, and the effect of oil on foam could not be quantified. Instead the influence of nanoparticles on foam/emulsion system was further investigated.

Injection of CO_2/n-Decane mixture into a core saturated with nonionic surfactant (SFA5000) increased the apparent viscosity with approximately 230% compared to CO_2 injection without oil (Figure 8.3). The average peak in absence of oil was 51.8 cP compared with 171.5 cP with presence of oil. Initially, lower apparent viscosity was expected as oil tends to destabilize foam and prevent foam generation, but similar behavior was observed in previous studies (Skjelsvik, 2018). It is believed that the increase was caused by increase in differential pressure due to generation of o/w emulsions and will be target for future studies to decipher the observed pressure increases.

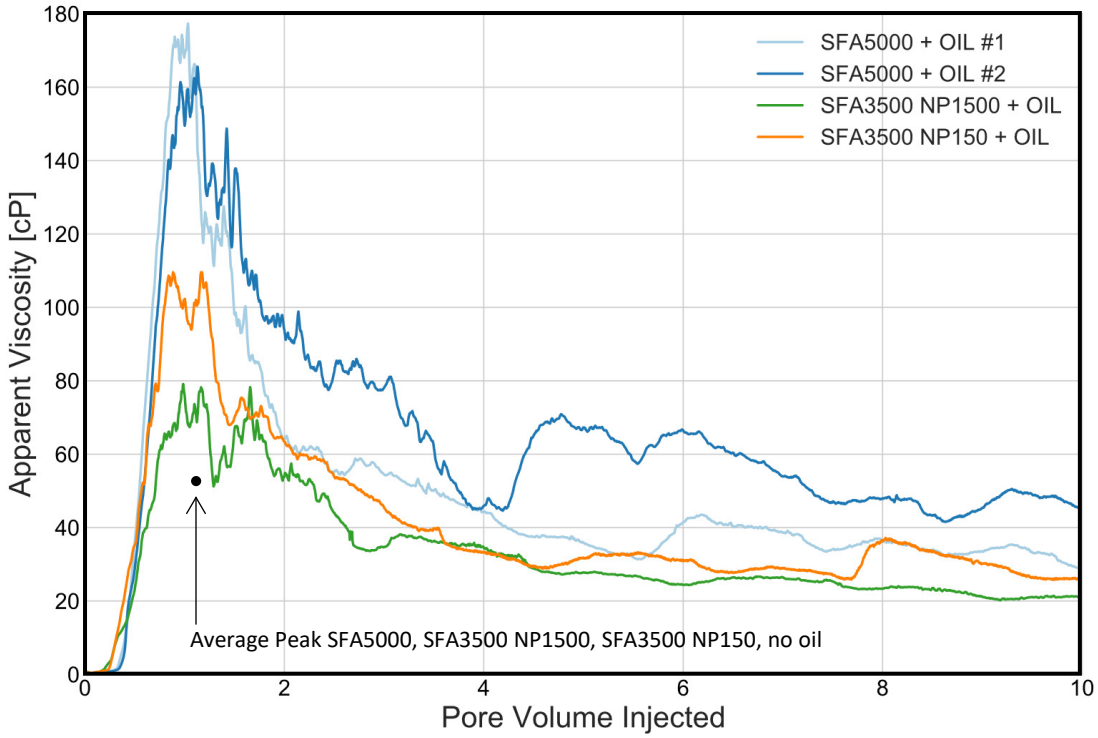

Figure 8.3 Apparent viscosity as a function of pore volume injected during CO_2/n-Decane mixture injection. Presence of oil resulted in high apparent viscosity values due to generation of foam/emulsions. Strongest foam/emulsions were generated using nonionic surfactant SFA5000. SFA3500 NP1500 generated weaker foam/emulsion system but a gentle slope was observed, hence a more stable system. The average peak in absence of oil was marked on the figure for comparison.

Investigation of foam/emulsion coalescence using nonionic surfactant as a foaming agent showed that even though high apparent viscosity was achieved the system was more unstable than without oil. The average coalescence rate was 105.2 cP/PV and 30.0 cP/PV for CO_2/n-Decane and CO_2 injection respectively. With nanoparticles added, however, a delayed foam/emulsion coalescence was observed with coalescence rates of 41.5 cP/PV (150 ppm) and 24.7 cP/PV (1500 ppm). Corresponding coalescence rates without oil were 53.1 cP/PV (150 ppm) and 49.2 cP/PV (1500 ppm), indicating a more stable system in presence of oil. Comparison of peak and coalescence rate in presence of oil showed a stronger but more unstable foam/emulsion system when using SFA5000 than when using SFA3500 NP1500/NP150.

Weaker foam/emulsion generation was observed using anionic surfactant (SFB) as a foaming agent compared to results without oil, as the maximum apparent viscosity decreased with approximately 30%. During injections without oil, the average peak was 88.2 cP, whereas with oil 64.7 cP (Figure 8.4). Similar behavior was observed during steady state co-injections of CO_2/n-Decane mixture and anionic surfactant in previous studies (Kahrobaei et al., 2018). It was concluded that CO_2 foam was generated in presence of oil, but the possible generation of o/w emulsion was not considered.

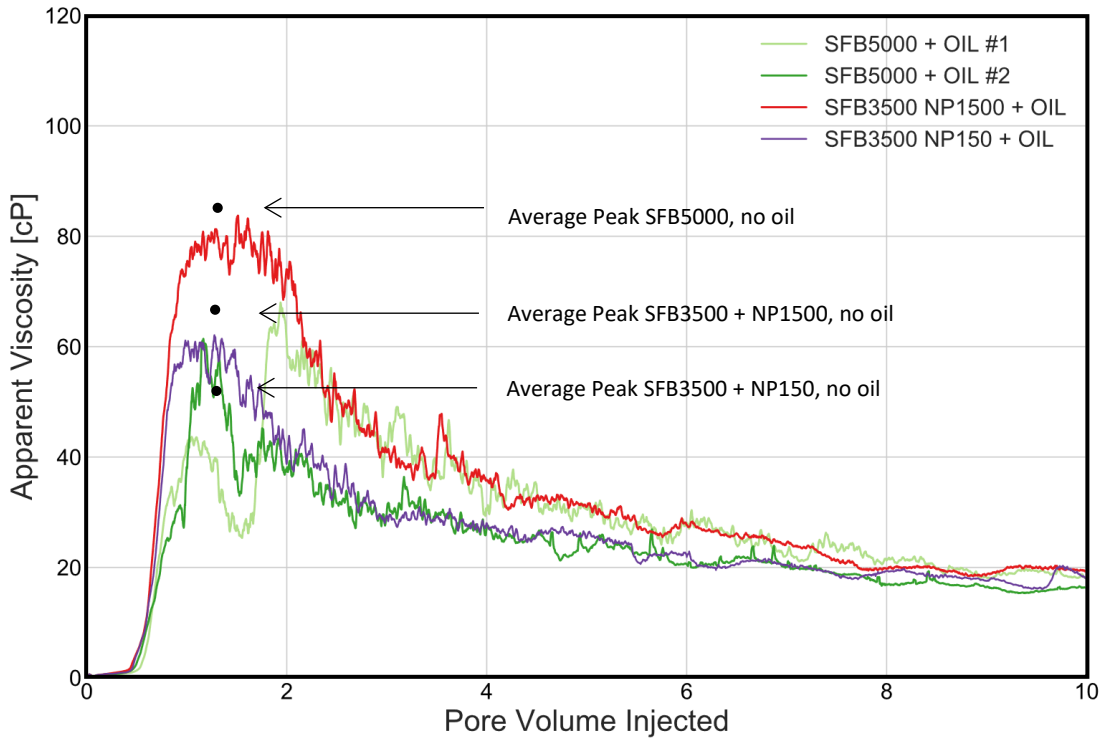

Figure 8.4 Apparent viscosity as function of pore volume injected during CO_2/n-Decane mixture injection. Presence of oil resulted in lower apparent viscosity using the anionic surfactant as foaming agent, but stronger foam/emulsion system was observed when including nanoparticles as foaming agent. Results showed similar coalescence rate (slope from peak to ½ peak) for all injections, however presence of nanoparticles showed a stabilizing effect on foam/emulsions. Average peaks with absence of oil was marked on the figure for comparison.

The combination of SFB and nanoparticles showed an increase in apparent viscosity using 1500 ppm nanoparticles. The peak increased from 64.7 cP for SFB5000 to 83.4 cP for SFB3500 NP1500. This might indicate that nanoparticles are feasible for stabilizing o/w emulsions. Lowering the nanoparticle concentration to 150 ppm showed a similar result as SFB5000, indicating that the total amount of foaming agent might be reduced. This can give an economical advantage. An increase in apparent viscosity was observed when comparing to results without oil. Peaks were 83.4 cP and 62.1 cP using SFB3500 NP1500 and SFB3500 NP150 respectively, while without presence of oil corresponding average peaks were 66.6 cP and 53.6 cP.

Average coalescence rate for all of the four injections was 21.1 ± 3.4 cP, but increased stability at high apparent viscosity (near peak) was observed using nanoparticles. To determine the observed stability, time at which apparent viscosity was equal peak ± 10% was calculated and showed an increase from 0.20 ± 0.01 PV to 0.84 ± 0.26 PV when using nanoparticles. The chosen limit was 10 % based on the fluctuations near the peak.

Foam/emulsion systems generated using SFA and SFB separately and in combination with nanoparticles were compared. The average peak was 165% higher when using SFA than when using SFB. The reason why nonionic surfactants generated a stronger foam/emulsion system could relate to the hydrophilic-lipophilic balance (HLB) number which is a measure of the degree to which a surfactant is hydrophilic or lipophilic. To generate an o/w emulsion, the HLB value should be between 8 and 18, but this value can vary based on the oil composition (Griffin, 1949). HLB values for SFA and SFB are 16.6 and 12, respectively (Ash, 2004; Huntsman, 2005). Based on the HLB range, both surfactants are o/w emulsifiers. To understand the reason why SFA generated stronger foam/emulsion systems, the chemical interactions between surfactant, oil and brine should be investigated.

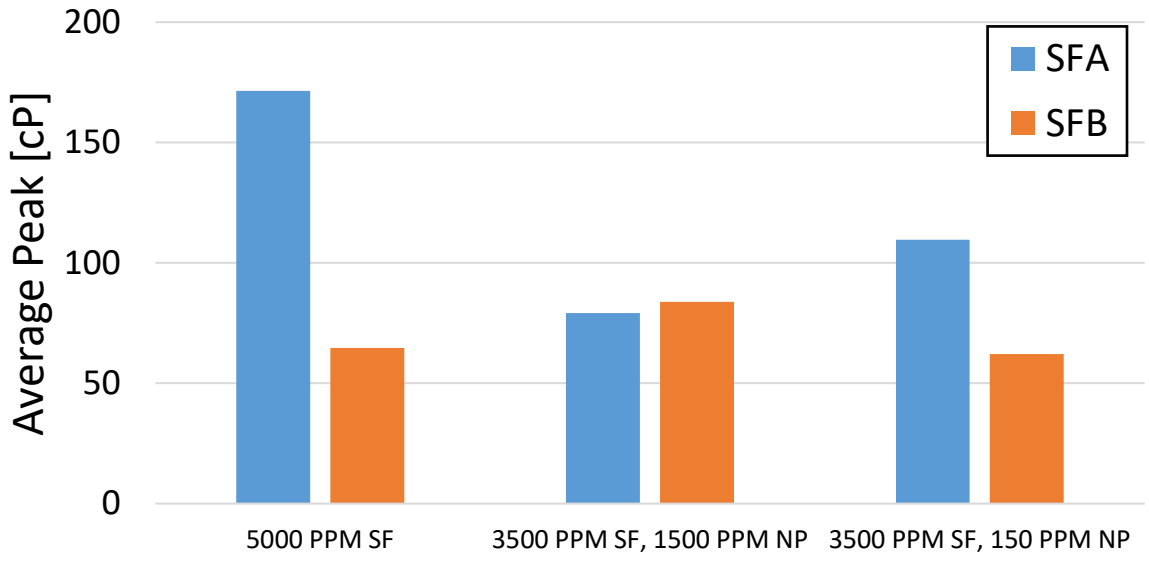

Figure 8.5 The average peak indicate stronger foam/emulsion generation using 5000 ppm SFA compared to using SFB. Combining nanoparticles with SFA a decrease in apparent viscosity was observed and combining nanoparticles with SFB showed a gentle increase when using 1500 ppm nanoparticles.

The use of nanoparticles in combination with SFA as a foaming agent resulted in a decrease in apparent viscosity, while the combination of nanoparticles and SFB showed an increase in apparent viscosity using 1500 ppm nanoparticles and no change using 150 ppm. Results showed a stabilizing effect of the nanoparticles when combined with anionic surfactants. The use of anionic surfactants and negatively charged nanoparticles have previously showed an increase in IFT reduction and generation of more stable foams compared to the use of anionic surfactants separately (Arab et al., 2018; Ma et al., 2008). Earlier studies also showed that the most stable o/w emulsions can be generated combining oppositely charged surfactant and nanoparticles (Arab et al., 2018). Even though the nanoparticles showed a stabilizing effect when combined with SFB, stronger systems were generated using SFA. Additional tests should be carried out in order to get a better understanding of the effect nanoparticles have in stabilizing o/w emulsions.

Part IV. Conclusion and Future Work

9. Conclusions

Utilization of nanoparticles to stabilize the CO_2 foam for CCUS was studied in this experimental thesis. Foam generation, stability and coalescence using different foaming agents were investigated in order to improve the understanding of surfactant and nanoparticle stabilized CO_2 foam at core scale. The following key observations and conclusions from this experimental study were drawn:

- Foam generation and stability: Stronger and more stable foam was generated with a continuous supply of foaming agent solution during steady state co-injections compared to unsteady state CO_2 injection. During the CO_2 injections, use of anionic surfactant (SFB) showed stronger foam generation compared to the use of nonionic surfactant (SFA) due to its good stability and low adsorption on sandstone. The combination of surfactants and nanoparticles did not result in stronger foam generation during the CO_2 injections for either surfactants, but co-injections of nonionic surfactants (SFA) in combination with nanoparticles showed improved foam generation even at low nanoparticle concentrations.

- Foam coalescence: A correlation between foam strength and coalescence was observed. Strong foam (high apparent viscosity) resulted in faster coalescence rate than weak foam (low apparent viscosity). Combining anionic surfactant (SFB) and nanoparticles, reduced coalescence was observed. This indicated that nanoparticles, even at low concentrations, had the ability to stabilize the CO_2 foam.

- Displacement efficiency: Generation of CO_2 foam reduced CO_2 mobility resulting in delayed gas breakthrough and improved displacement efficiency. Using surfactants as foaming agent, the average residual water saturation decreased by approximately 60% compared to pure CO_2 injection. Including nanoparticles, residual water saturation decreased by approximately 30% compared to surfactant stabilized foam. This indicated that nanoparticle stabilized foam could increase the potential CO_2 storage capacity.

- Effect of oil: Generation of o/w emulsions was observed during CO_2 and co-injections in presence of flowing oil. Nonionic surfactants (SFA) contributed to generation of stronger emulsions compared to anionic surfactants (SFB). Combining surfactants and nanoparticles, a stabilizing effect on emulsions was observed using anionic surfactant (SFB). Similar to the CO_2 foam, a rapid coalescence was observed for strong emulsion systems.

- Input to simulation models: Data generated for this experimental thesis, in particular steady state measurements at various gas fractions, can be used as foam modeling input for history matching, sensitivity studies and upscaling.

The key observations and conclusions show stabilizing effect of nanoparticles on CO_2 foam and oil-in-water emulsions which is advantageous for CCUS. Nanoparticles show a greater ability to stabilize foam when combined with anionic surfactants, but additional tests should be run to reach a firm conclusion.

10. Future Work

The experimental work presented in this thesis was a part of an ongoing CO_2 foam project, led by the Reservoir Physics group at the Department of Physics and Technology, University of Bergen. During this thesis, the ability of nanoparticles to stabilize CO_2 foam in combination with two different surfactants was investigated. The work has provided improved understanding of using nanoparticles for CO_2 foam generation and stabilization, but results should be further verified through additional laboratory work. The following is a list of suggestions for future work:

- Steady state co-injections should be performed using anionic surfactant to confirm that anionic surfactant is the preferred choice to combine with Levasil CC301 nanoparticles in sandstone.

- Combining nonionic surfactants with nanoparticles did not show stabilizing effects during CO_2 injections. In previous studies, it has been observed that if the surfactant concentration exceeds a certain value, nanoparticles do not contribute to foam generation or stability. Therefore, it would be preferable to repeat the experiments with reduced surfactant concentration.

- The generation of oil-in-water emulsions made it difficult to identify how oil affects CO_2 foam. Instead of injecting oil, it is suggested to investigate the effect of residual oil. The core plug should be drained with oil and flooded with water in order to obtain residual oil saturation, thereafter, it should be saturated with the desired foaming agent solution followed by CO_2 injection or co-injection as described in Chapter 5.

- As foam generates, collapses and regenerates it would be interesting to investigate foam behavior at different lengths in a porous media. It is suggested to use sand packs with several pressure ports to study foam behavior. Additionally, the influence of permeability should be investigated, as permeability is higher in unconsolidated systems. There was developed a setup for foam studies in sand packs during this thesis and this is described in Appendix E.

- The combination of nanoparticles with nonionic and anionic surfactants showed different effects on the CO_2 foam and o/w emulsions. In order to find the preferred surfactant and to increase the stability of CO_2 foam, colloids/surface chemistry and the interaction between surfactants and nanoparticles should be studied.

Part V. Nomenclature, Abbreviations, Appendix and References

Nomenclature

A	Cross sectional area
D	Diameter
f_g	Gas fraction
K	Absolute pemreability
K_f	Effective permeability
k_{rf}	Relative permeability
L	Length
m_{dry}	Mass of dry sand pack
m_{sat}	Mass of saturated sand pack
P	Pressure
P_c	Capillary pressure
ppm	Part per million by mass
Q	Flow rate
q_g	Gas flow rate
q_{liq}	Liquid flow rate
S_w	Water saturation
T	Temperature
V_B	Bulk volume
V_p	Pore volume
wt.%	Weight percent
x_{CO_2}	Molar concentration of CO_2
ΔP	Differential pressure
μ	Viscosity
μ_{app}	Apparent viscosity
ρ	Density
φ	Porosity

Abbreviations

BPR	Back Pressure Regulator
CCS	Carbon Capture and Storage
CCUS	Carbon Capture Utilization and Storage
EOR	Enhanced Oil Recovery
HLB	Hydrophilic-Lipophilic Balance
IFT	Interfacial Tension
MFC	Mass Flow Controller
MMP	Minimum Miscible Pressure
MRF	Mobility Reduction Factor
OOIP	Oil Originally in Place
POM	Polyoxymethylene
PPM	Part Per Million
PV	Pore Volume

References

Ahmed, T. H. (1994). *Prediction of CO2 Minimum Miscibility Pressures*. Paper presented at the SPE Latin America/Caribbean Petroleum Engineering Conference, Buenos Aires, Argentina. https://doi.org/10.2118/27032-MS

Alvarado, V., & Manrique, E. (2010). Enhanced Oil Recovery: An Update Review. *Energies, 3*(9), 1529-1575. doi:10.3390/en3091529

Alvarez, J., Rivas, H., & Rossen, W. J. S. j. (2001). Unified model for steady-state foam behavior at high and low foam qualities. *6*(03), 325-333.

AlYousif, Z., Kokal, S., Alabdulwahab, A., & Gizzatov, A. (2018). *CO2-Foam Rheology: Effect of Surfactant Concentration, Shear Rate and Injection Quality*. Paper presented at the SPE Kingdom of Saudi Arabia Annual Technical Symposium and Exhibition, Dammam, Saudi Arabia. https://doi.org/10.2118/192361-MS

Anderson, W. G. (1986). Wettability Literature Survey- Part 2: Wettability Measurement. *Journal of Petroleum Technology, 38*(11), 1246-1262. doi:10.2118/13933-PA

Anderson, W. G. (1987a). Wettability Literature Survey- Part 4: Effects of Wettability on Capillary Pressure. *Journal of Petroleum Technology, 39*(10), 1283-1300. doi:10.2118/15271-PA

Anderson, W. G. (1987b). Wettability Literature Survey Part 5: The Effects of Wettability on Relative Permeability. *Journal of Petroleum Technology, 39*(11), 1453-1468. doi:10.2118/16323-PA

Arab, D., Kantzas, A., & Bryant, S. L. (2018). Nanoparticle stabilized oil in water emulsions: A critical review. *Journal of Petroleum Science and Engineering, 163*, 217-242. doi:https://doi.org/10.1016/j.petrol.2017.12.091

Ash, M. (2004). *Handbook of green chemicals*: Synapse Info Resources.

Bachu, S. (2003). Screening and ranking of sedimentary basins for sequestration of CO2 in geological media in response to climate change. *Environmental Geology, 44*(3), 277-289. doi:10.1007/s00254-003-0762-9

Bachu, S., Freund, P., Gupta, M., Simbeck, D., & Thambimuthu, K. (2005). Annex I: properties of CO 2 and carbon-based fuels. *IPCC special report on carbon dioxide capture and storage. Cambridge University Press, New York*.

Barnes, K. B. (1936). *Porosity and Saturation Methods*. Paper presented at the Drilling and Production Practice, New York, New York. https://doi.org/

Becher, P. (1990). Microemulsions and Related Systems: Formulation, Solvency, and Physical Properties (Surfactant Science Series, Vol. 30). M. Bourrel and R. S. Schechter. Marcel Dekker, Inc., New York and Basel, 1988. pp. nil + 483. $99.75. *Journal of Dispersion Science and Technology, 11*(4), 431-432. doi:10.1080/01932699008943264

Bekken, S. G., Schöffel, K., Aakenes, S., Hatlen, T., Slagtern, Å., & Øi, L. E. (2013). The CLIMIT Program and its Strategy for Norwegian Research, Development and Demonstration of CCS Technology. *Energy Procedia, 37*, 6508-6519. doi:https://doi.org/10.1016/j.egypro.2013.06.581

Benali, B. (2019). Quantitative Pore-Scale Analysis of CO2 Foam for CCUS. In: The University of Bergen.

Bennetzen, M. V., & Mogensen, K. (2014). *Novel Applications of Nanoparticles for Future Enhanced Oil Recovery*. Paper presented at the International Petroleum Technology Conference, Kuala Lumpur, Malaysia. https://doi.org/10.2523/IPTC-17857-MS

Benson, S. M., & Cole, D. R. (2008). CO2 Sequestration in Deep Sedimentary Formations. *Elements, 4*(5), 325-331. doi:10.2113/gselements.4.5.325

Bentham, M., & Kirby, M. (2005). CO2 storage in saline aquifers. *Oil & gas science and technology, 60*(3), 559-567.

BP. (2019). BP Statistical Review of World Energy.

Brattekås, B. (2014). Conformance Control for Enhanced Oil Recovery in Fractured Reservoirs. In: The University of Bergen.

Brattekås, B., Føyen, T. L., Vabø, T., Haugland, H., Reite, S. I., Saunes, A. S., & Fernø, M. A. (2019). *Dos and Don'ts When Developing a System to Investigate Spontaneous Imbibition in Unconsolicdated Porous Media.* Paper presented at the E3S Web of Conferences.

Brock, W. R., & Bryan, L. A. (1989). *Summary Results of CO2 EOR Field Tests, 1972-1987*. Paper presented at the Low Permeability Reservoirs Symposium, Denver, Colorado. https://doi.org/10.2118/18977-MS

Campbell, B. T., & Orr, F. M., Jr. (1985). Flow Visualization for CO2/Crude-Oil Displacements. *Society of Petroleum Engineers Journal, 25*(05), 665-678. doi:10.2118/11958-PA

Celia, M. A., Bachu, S., Nordbotten, J. M., & Bandilla, K. W. (2015). Status of CO2 storage in deep saline aquifers with emphasis on modeling approaches and practical simulations. *Water Resources Research, 51*(9), 6846-6892. doi:10.1002/2015WR017609

Chambers, D. J. (1994). Foams for Well Stimulation. In *Foams: Fundamentals and Applications in the Petroleum Industry* (Vol. 242, pp. 355-404): American Chemical Society.

Chang, & Grigg, R. B. (1998). *Effects of Foam Quality and flow Rate on CO2-Foam Behavior at Reservoir Conditions*. Paper presented at the SPE/DOE Improved Oil Recovery Symposium, Tulsa, Oklahoma. https://doi.org/10.2118/39679-MS

Chang, R. (2013). *Chemistry* (11th ed. ed.). McGraw-Hill Science/Engineering/Math New York.

Chou, S. I. (1991). *Conditions for Generating Foam in Porous Media*. Paper presented at the SPE Annual Technical Conference and Exhibition, Dallas, Texas. https://doi.org/10.2118/22628-MS

Dickson, J. L., Binks, B. P., & Johnston, K. P. (2004). Stabilization of Carbon Dioxide-in-Water Emulsions with Silica Nanoparticles. *Langmuir, 20*(19), 7976-7983. doi:10.1021/la0488102

Eide, Ø., Føyen, T., Skjelsvik, E., Rognmo, A., & Fernø, M. (2018). *Nanoparticle Stabilized Foam in Harsh Conditions for CO2 EOR*. Paper presented at the Abu Dhabi International Petroleum Exhibition & Conference, Abu Dhabi, UAE. https://doi.org/10.2118/193212-MS

El-Dessouky, H. T. (2002). *Fundamentals of salt water desalination*. Amsterdam: Elsevier.

Enrick, R. M., & Olsen, D. K. (2012). Mobility and Conformance Control for Carbon Dioxide Enhanced Oil Recovery (CO2-EOR) via Thickeners, Foams, and Gels – A Detailed Literature Review of 40 Years of Research. *U.S. Department of Energy, National Energy Technology Laboratory (NETL)*.

Equinor. (2019). Sleipner partnership releases CO2 storage data. Retrieved from https://www.equinor.com/en/news/2019-06-12-sleipner-co2-storage-data.html

Falls, A. H., Musters, J. J., & Ratulowski, J. (1989). The Apparent Viscosity of Foams in Homogeneous Bead Packs. *SPE Reservoir Engineering, 4*(02), 155-164. doi:10.2118/16048-PA

Farajzadeh, R., Andrianov, A., Krastev, R., Hirasaki, G., & Rossen, W. R. (2012). *Foam-Oil Interaction in Porous Media: Implications for Foam Assisted Enhanced Oil Recovery*. Paper presented at the SPE EOR Conference at Oil and Gas West Asia, Muscat, Oman. https://doi.org/10.2118/154197-MS

Fernø, M. A., Torsvik, M., Haugland, S., & Graue, A. (2010). Dynamic Laboratory Wettability Alteration. *Energy & Fuels, 24*(7), 3950-3958. doi:10.1021/ef1001716

Friedmann, F., & Jensen, J. A. (1986). *Some Parameters Influencing the Formation and Propagation of Foams in Porous Media*. Paper presented at the SPE California Regional Meeting, Oakland, California. https://doi.org/10.2118/15087-MS

Føyen, T., Brattekås, B., Fernø, M. A., Barrabino, A., & Holt, T. (2020). Increased CO2 storage capacity using CO2-foam. *International Journal of Greenhouse Gas Control, 96*, 103016. doi:https://doi.org/10.1016/j.ijggc.2020.103016

Gauglitz, P. A., Friedmann, F., Kam, S. I., & Rossen, W. R. (2002). *Foam Generation in Porous Media*. Paper presented at the SPE/DOE Improved Oil Recovery Symposium, Tulsa, Oklahoma. https://doi.org/10.2118/75177-MS

Green, D. W., & Willhite, G. P. (1997). *Enhanced Oil Recovery*. Richardson, UNITED STATES: Society of Petroleum Engineers.

Griffin, W. C. J. J. S. C. C. (1949). Classification of surface-active agents by" HLB". *1*, 311-326.

Grogan, A. T., & Pinczewski, W. V. (1987). The Role of Molecular Diffusion Processes in Tertiary CO2 Flooding. *Journal of Petroleum Technology, 39*(05), 591-602. doi:10.2118/12706-PA

Gunter, W. D., Perkins, E. H., & McCann, T. J. (1993). Aquifer disposal of CO2-rich gases: reaction design for added capacity. *Energy Conversion and management, 34*(9-11), 941-948.

Hadian Nasr, N., Mahmood, S. M., Akbari, S., & Hematpur, H. (2020). A comparison of foam stability at varying salinities and surfactant concentrations using bulk foam tests and sandpack flooding. *Journal of Petroleum Exploration and Production Technology, 10*(2), 271-282. doi:10.1007/s13202-019-0707-9

Hanssen, J., Holt, T., & Surguchev, L. (1994). *Foam processes: an assessment of their potential in North Sea reservoirs based on a critical evaluation of current field experience.* Paper presented at the SPE/DOE Improved Oil Recovery Symposium.

Heldal, S. (2016). *An experimental study using nanoparticle-stabilized CO2-foam for EOR in sandstone.* Department of Physics and Technology, University of Bergen, Bergen.

Heller, J. P. (1994). CO₂ Foams in Enhanced Oil Recovery. In *Foams: Fundamentals and Applications in the Petroleum Industry* (Vol. 242, pp. 201-234): American Chemical Society.

Hirasaki, G. J., & Lawson, J. B. (1985). Mechanisms of Foam Flow in Porous Media: Apparent Viscosity in Smooth Capillaries. *Society of Petroleum Engineers Journal, 25*(02), 176-190. doi:10.2118/12129-PA

Holm, L. W. (1986). Miscibility and Miscible Displacement. *Journal of Petroleum Technology, 38*(08), 817-818. doi:10.2118/15794-PA

Holm, L. W., & Josendal, V. A. (1974). Mechanisms of Oil Displacement By Carbon Dioxide. *Journal of Petroleum Technology, 26*(12), 1427-1438. doi:10.2118/4736-PA

Huh, D. G., & Handy, L. L. (1989). Comparison of Steady and Unsteady-State Flow of Gas and Foaming Solution in Porous Media. *SPE Reservoir Engineering, 4*(01), 77-84. doi:10.2118/15078-PA

Huntsman. (2005). Huntsman Metalworking Chemicals Retrieved from http://www.huntsman.com/performance_products/Media%20Library/a_MC348531CFA3EA9A2E040EBCD2B6B7B06/Products_MC348531D0B9FA9A2E040EBCD2B6B7B06/Amines_MC348531D0BECA9A2E040EBCD2B6B7B06/Morpholine%20%20%20DGA_R_MC348531D0D20A9A2E040EBCD2B6B7B06/DIGLYCOLAMINE_R%20agen_MC348531D0DBAA9A2E040EBCD2B6B7B06/files/metalworking_brochure.pdf

IPCC. (2005). *IPCC Special Report on Carbon Dioxide Capture and Storage. Prepared by Working Group III of the Intergovernmental Panel on Climate Change [Metz, B., O. Davidson, H. C. de Coninck, M. Loos, and L. A. Meyer (eds.)]*. United Kingdom and New York, NY, USA: Cambridge University Press.

IPCC. (2018). *Global Warming of 1.5° C: An IPCC Special Report on the Impacts of Global Warming of 1.5° C Above Pre-industrial Levels and Related Global Greenhouse Gas Emission Pathways, in the Context of Strengthening the Global Response to the Threat of Climate Change, Sustainable Development, and Efforts to Eradicate Poverty*: Intergovernmental Panel on Climate Change.

Jensen, J. A., & Friedmann, F. (1987). *Physical and Chemical Effects of an Oil Phase on the Propagation of Foam in Porous Media*. Paper presented at the SPE California Regional Meeting, Ventura, California. https://doi.org/10.2118/16375-MS

Jha, K. N. (1985). *A Laboratory Study Of Heavy Oil Recovery With Carbon Dioxide*. Paper presented at the Technical Meeting / Petroleum Conference of The South Saskatchewan Section, Regina. https://doi.org/10.2118/SS-85-04

Johns, R. T., & Dindoruk, B. (2013). Chapter 1 - Gas Flooding. In J. J. Sheng (Ed.), *Enhanced Oil Recovery Field Case Studies* (pp. 1-22). Boston: Gulf Professional Publishing.

Kahrobaei, S., Li, K., Vincent-Bonnieu, S., & Farajzadeh, R. (2018). Effects of compositional variations on CO2 foam under miscible conditions. *AIChE Journal, 64*(2), 758-764. doi:10.1002/aic.15938

Kovscek, A. R. (2002). SCREENING CRITERIA FOR CO2 STORAGE IN OIL RESERVOIRS. *Petroleum Science and Technology, 20*(7-8), 841-866. doi:10.1081/LFT-120003717

Kovscek, A. R., & Radke, C. J. (1994). Fundamentals of Foam Transport in Porous Media. In *Foams: Fundamentals and Applications in the Petroleum Industry* (Vol. 242, pp. 115-163): American Chemical Society.

Kuehne, D. L., Frazier, R. H., Cantor, J., & Horn, W., Jr. (1992). *Evaluation of Surfactants for CO2 Mobility Control in Dolomite Reservoirs*. Paper presented at the SPE/DOE Enhanced Oil Recovery Symposium, Tulsa, Oklahoma. https://doi.org/10.2118/24177-MS

Kuhlman, M. I. (1990). Visualizing the Effect of Light Oil on CO2 Foams. *Journal of Petroleum Technology, 42*(07), 902-908. doi:10.2118/17356-PA

Kulkarni, M. M., & Rao, D. N. (2004). *Experimental Investigation of Various Methods of Tertiary Gas Injection*. Paper presented at the SPE Annual Technical Conference and Exhibition, Houston, Texas. https://doi.org/10.2118/90589-MS

Lake, L. W. (2014). *Fundamentals of enhanced oil recovery* ([2. utg.]. ed.). Richardson, Tex: Society of Petroleum Engineers.

Laumb, J. D., Kay, J. P., Holmes, M. J., Cowan, R. M., Azenkeng, A., Heebink, L. V., Hanson, S. K., Jensen, M. D., Letvin, P. A., & Raymond, L. J. (2013). Economic and Market Analysis of CO2 Utilization Technologies – Focus on CO2 derived from North Dakota lignite. *Energy Procedia, 37*, 6987-6998. doi:https://doi.org/10.1016/j.egypro.2013.06.632

Le Gallo, Y., Couillens, P., & Manai, T. (2002). *CO2 Sequestration in Depleted Oil or Gas Reservoirs*. Paper presented at the SPE International Conference on Health, Safety and Environment in Oil and Gas Exploration and Production, Kuala Lumpur, Malaysia. https://doi.org/10.2118/74104-MS

Lee, S., & Kam, S. I. (2013). Chapter 2 - Enhanced Oil Recovery by Using CO2 Foams: Fundamentals and Field Applications. In J. J. Sheng (Ed.), *Enhanced Oil Recovery Field Case Studies* (pp. 23-61). Boston: Gulf Professional Publishing.

Lemmon, E., McLinden, M., & Friend, D. (2012). Thermophysical Properties of Fluid Systems in NIST Chemistry WebBook, NIST Standard Reference Database Number 69, Eds. PJ Linstrom and WG Mallard, National Institute of Standards and Technology, Gaithersburg MD, 20899. In.

Leung, D. Y. C., Caramanna, G., & Maroto-Valer, M. M. (2014). An overview of current status of carbon dioxide capture and storage technologies. *Renewable and Sustainable Energy Reviews, 39*, 426-443. doi:https://doi.org/10.1016/j.rser.2014.07.093

Li, R. F., Yan, W., Liu, S., Hirasaki, G., & Miller, C. A. (2010). Foam Mobility Control for Surfactant Enhanced Oil Recovery. *SPE Journal, 15*(04), 928-942. doi:10.2118/113910-PA

Lien, J. (2004). PTEK211-Grunnleggende reservoarfysikk (Kjerneanalyse og logging). . *Bergen: University of Bergen*.

Ma, H., Luo, M., & Dai, L. L. J. P. C. C. P. (2008). Influences of surfactant and nanoparticle assembly on effective interfacial tensions. *10*(16), 2207-2213.

Mac Dowell, N., Fennell, P. S., Shah, N., & Maitland, G. C. (2017). The role of CO2 capture and utilization in mitigating climate change. *Nature Climate Change, 7*(4), 243-249. doi:10.1038/nclimate3231

Maini, B. B., & Ma, V. (1986). Laboratory Evaluation Of Foaming Agents For High-Temperature Applications — I. Measurements Of Foam Stability At Elevated Temperatures And Pressures. *Journal of Canadian Petroleum Technology, 25*(06), 6. doi:10.2118/86-06-05

Mandal, A., & Bera, A. (2015). Modeling of flow of oil-in-water emulsions through porous media. *Petroleum Science, 12*(2), 273-281. doi:10.1007/s12182-015-0025-x

Mangalsingh, D., & Jagai, T. (1996). *A Laboratory Investigation of the Carbon Dioxide Immiscible Process*. Paper presented at the SPE Latin America/Caribbean Petroleum Engineering Conference, Port-of-Spain, Trinidad. https://doi.org/10.2118/36134-MS

McAuliffe, C. D. (1973). Oil-in-Water Emulsions and Their Flow Properties in Porous Media. *Journal of Petroleum Technology, 25*(06), 727-733. doi:10.2118/4369-PA

Mo, D., Yu, J., Liu, N., & Lee, R. L. (2012). *Study of the Effect of Different Factors on Nanoparticle-Stablized CO2 Foam for Mobility Control*. Paper presented at the SPE Annual Technical Conference and Exhibition, San Antonio, Texas, USA. https://doi.org/10.2118/159282-MS

Muller, T., & Lake, L. W. (1991). Theoretical Study of Water Blocking in Miscible Flooding. *SPE Reservoir Engineering, 6*(04), 445-451. doi:10.2118/20206-PA

Mungan, N. (1981). Carbon Dioxide Flooding-fundamentals. *Journal of Canadian Petroleum Technology, 20*(01), 7. doi:10.2118/81-01-03

Niu, B., Al-Menhali, A., & Krevor, S. (2014). A Study of Residual Carbon Dioxide Trapping in Sandstone. *Energy Procedia, 63*, 5522-5529. doi:https://doi.org/10.1016/j.egypro.2014.11.585

Ogolo, N. A., Olafuyi, O. A., & Onyekonwu, M. O. (2012). *Enhanced Oil Recovery Using Nanoparticles*. Paper presented at the SPE Saudi Arabia Section Technical Symposium and Exhibition, Al-Khobar, Saudi Arabia. https://doi.org/10.2118/160847-MS

Parra-Ramirez, M., Peterson, B., & Deo, M. D. (2001). *Comparison of First and Multiple Contact Carbon Dioxide Induced Asphaltene Precipitation*. Paper presented at the SPE International Symposium on Oilfield Chemistry, Houston, Texas. https://doi.org/10.2118/65019-MS

Peksa, A. E., Wolf, K.-H. A. A., & Zitha, P. L. J. (2015). Bentheimer sandstone revisited for experimental purposes. *Marine and Petroleum Geology, 67*, 701-719. doi:https://doi.org/10.1016/j.marpetgeo.2015.06.001

Perkins, T. K., & Johnston, O. C. (1963). A Review of Diffusion and Dispersion in Porous Media. *Society of Petroleum Engineers Journal, 3*(01), 70-84. doi:10.2118/480-PA

Picha, M. S. (2007). *Enhanced Oil Recovery By Hot CO2 Flooding*. Paper presented at the SPE Middle East Oil and Gas Show and Conference, Manama, Bahrain. https://doi.org/10.2118/105425-MS

Pichot, R., Spyropoulos, F., Norton, I. J. J. o. c., & science, i. (2012). Competitive adsorption of surfactants and hydrophilic silica particles at the oil–water interface: Interfacial tension and contact angle studies. *377*(1), 396-405.

Poettmann, F. H., Christiansen, R. L., & Mihcakan, I. M. (1991). Discussion of Methodology for the Specification of Solvent Blends for Miscible Enriched-Gas Drives. *SPE Reservoir Engineering, 6*, 154-155. doi:10.2118/20205-PA

Ransohoff, T. C., & Radke, C. J. (1988). Mechanisms of Foam Generation in Glass-Bead Packs. *SPE Reservoir Engineering, 3*(02), 573-585. doi:10.2118/15441-PA

Raza, S. H. (1970). Foam in Porous Media: Characteristics and Potential Applications. *Society of Petroleum Engineers Journal, 10*(04), 328-336. doi:10.2118/2421-PA

Rognmo, A. U. (2019). *CO2-foams for enhanced oil recovery and CO2 storage.* University of Bergen, Bergen.

Rognmo, A. U., Heldal, S., & Fernø, M. A. (2018). Silica nanoparticles to stabilize CO2-foam for improved CO2 utilization: Enhanced CO2 storage and oil recovery from mature oil reservoirs. *Fuel, 216*, 621-626. doi:https://doi.org/10.1016/j.fuel.2017.11.144

Rognmo, A. U., Horjen, H., & Fernø, M. A. (2017). Nanotechnology for improved CO2 utilization in CCS: Laboratory study of CO2-foam flow and silica nanoparticle retention in porous media. *International Journal of Greenhouse Gas Control, 64*, 113-118. doi:https://doi.org/10.1016/j.ijggc.2017.07.010

Romero-Zerón, L. (2012). Advances in Enhanced Oil Recovery Processes. In *Introduction to Enhanced Oil Recovery (EOR) Processes and Bioremediation of Oil-Contaminated Sites.*: InTech.

Ross, S., & McBain, J. W. (1944). Inhibition of Foaming in Solvents Containing Known Foamers. *Industrial & Engineering Chemistry, 36*(6), 570-573. doi:10.1021/ie50414a019

Rossen, W. R., & Gauglitz, P. A. (1990). Percolation theory of creation and mobilization of foams in porous media. *AIChE Journal, 36*(8), 1176-1188. doi:10.1002/aic.690360807

Sanchez, J. M., & Hazlett, R. D. (1992). Foam Flow Through an Oil-Wet Porous Medium: A Laboratory Study. *SPE Reservoir Engineering, 7*(01), 91-97. doi:10.2118/19687-PA

Saunes, A. S. (2018). Establishing a homogeneous and stable sand pack to study parameters during spontaneous imbibition. In: The University of Bergen.

Schramm, L. L. (1994a). Foam Sensitivity to Crude Oil in Porous Media. In *Foams: Fundamentals and Applications in the Petroleum Industry* (Vol. 242, pp. 165-197): American Chemical Society.

Schramm, L. L. (1994b). *Foams: fundamentals and applications in the petroleum industry*: American Chemical Society.

Schramm, L. L. (2000). *Surfactants: Fundamentals and Applications in the Petroleum Industry* (L. L. Schramm Ed.). Cambridge: Cambridge University Press.

Schramm, L. L., Society, A. C., & Institute, P. R. (1992). *Emulsions: Fundamentals and Applications in the Petroleum Industry*: American Chemical Society.

Sehbi, B. S., Frailey, S. M., & Lawal, A. S. (2001). *Analysis of Factors Affecting Microscopic Displacement Efficiency in CO2 Floods*. Paper presented at the SPE Permian Basin Oil and Gas Recovery Conference, Midland, Texas. https://doi.org/10.2118/70022-MS

Sheng. (2011). *Modern Chemical Enhanced Oil Recovery: Theory and Practice*: Elsevier Science.

Sheng. (2013). Chapter 11 - Foams and Their Applications in Enhancing Oil Recovery. In J. J. Sheng (Ed.), *Enhanced Oil Recovery Field Case Studies* (pp. 251-280). Boston: Gulf Professional Publishing.

Shi, J.-Q., Imrie, C., Sinayuc, C., Durucan, S., Korre, A., & Eiken, O. (2013). Snøhvit CO2 Storage Project: Assessment of CO2 Injection Performance Through History Matching of the Injection Well Pressure Over a 32-months Period. *Energy Procedia, 37*, 3267-3274. doi:https://doi.org/10.1016/j.egypro.2013.06.214

Shrivastava, V. K., Moore, R. G., & Nghiem, L. X. (2002). *A New Physical Dispersion Model for Miscible Displacement*. Paper presented at the Canadian International Petroleum Conference, Calgary, Alberta. https://doi.org/10.2118/2002-071

Shukla Potdar, R., & Vishal, V. (2016). Trapping Mechanism of CO2 Storage in Deep Saline Aquifers: Brief Review. In V. Vishal & T. N. Singh (Eds.), *Geologic Carbon Sequestration: Understanding Reservoir Behavior* (pp. 47-58). Cham: Springer International Publishing.

Sibree, J. (1934). The viscosity of froth. *Transactions of the Faraday Society, 30*, 325-331.

Singh, R., Mohanty, K. K. J. E., & Fuels. (2015). Synergy between nanoparticles and surfactants in stabilizing foams for oil recovery. *29*(2), 467-479.

Skauge, T., Spildo, K., & Skauge, A. (2010). *Nano-sized Particles For EOR*. Paper presented at the SPE Improved Oil Recovery Symposium, Tulsa, Oklahoma, USA. https://doi.org/10.2118/129933-MS

Skjelsvik, E. B. (2018). Synergy of Nanoparticles and Surfactants for CO2 Foam Enhanced Oil Recovery and CO2 Storage in Carbonates. In: The University of Bergen.

Skjæveland, S. M., & Kleppe, J. (1992). SPOR Monograph, Recent advances in improved oil recovery methods for north sea sandstone reservoirs. *Norwegian Petroleum Directorate, Norway*.

Smithells, C. J., & Ransley, C. E. (1936). The Diffusion of Gases through Metals. III. The Degassing of Nickel and the Diffusion of Carbon Monoxide through Nickel. *Proceedings of the Royal Society of London. Series A, Mathematical and Physical Sciences, 155*(884), 195-212.

Song, Y.-C., Ning-Jun, Z., Yu, L., Jia-Fei, Z., Wei-Guo, L., Yi, Z., Yue-Chao, Z., & Lan-Lan, J. (2011). Magnetic resonance imaging study on the miscibility of a CO2/n-decane system. *Chinese Physics Letters, 28*(9), 096401.

Svorstol, I., Vassenden, F., & Mannhardt, K. (1996). *Laboratory Studies for Design of a Foam Pilot in the Snorre Field*. Paper presented at the SPE/DOE Improved Oil Recovery Symposium, Tulsa, Oklahoma. https://doi.org/10.2118/35400-MS

Tadros, T. F. (2017). *Basic Principles of Dispersions : Basic Principles of Dispersions*. Berlin/Boston, GERMANY: De Gruyter, Inc.

Talebian, S., Masoudi, R., Tan, I. M., & Zitha, P. L. (2013). *Foam assisted CO2-EOR; concepts, challenges and applications.* Paper presented at the SPE Enhanced Oil Recovery Conference.

Talebian, S. H., Masoudi, R., Tan, I. M., & Zitha, P. L. J. (2014). Foam assisted CO2-EOR: A review of concept, challenges, and future prospects. *Journal of Petroleum Science and Engineering, 120*, 202-215. doi:https://doi.org/10.1016/j.petrol.2014.05.013

Veeningen, D., Zitha, P. L. J., & van Kruijsdijk, C. P. J. W. (1997). *Understanding Foam Flow Physics: The Role of Permeability*. Paper presented at the SPE European Formation Damage Conference, The Hague, Netherlands. https://doi.org/10.2118/38197-MS

Verma, M. K. (2015). *Fundamentals of carbon dioxide-enhanced oil recovery (CO2-EOR): a supporting document of the assessment methodology for hydrocarbon recovery using CO2-EOR associated with carbon sequestration* (2015-1071). Retrieved from Reston, VA: http://pubs.er.usgs.gov/publication/ofr20151071

Warner, H. R. (2015). *The reservoir engineering aspects of waterflooding* (2nd. ed. Vol. vol. 3). Richardson, Tex: Society of Petroleum Engineers SPE.

Yellig, W. F., & Metcalfe, R. S. (1980). Determination and Prediction of CO2 Minimum Miscibility Pressures (includes associated paper 8876). *Journal of Petroleum Technology, 32*(01), 160-168. doi:10.2118/7477-PA

Yu, G., Rossen, W. R., & Vincent-Bonnieu, S. (2018). *Foam Generation with Flow Rate: Effect of Surfactant Concentration and Gas Fraction*. Paper presented at the SPE EOR Conference at Oil and Gas West Asia, Muscat, Oman. https://doi.org/10.2118/190398-MS

Zhang, D., & Song, J. (2014). Mechanisms for Geological Carbon Sequestration. *Procedia IUTAM, 10*, 319-327. doi:https://doi.org/10.1016/j.piutam.2014.01.027

Zhang, K., Seetahal, S., Alexander, D., He, R., Lv, J., Wu, K., Hu, Y., & Chen, Z. (2016). *Correlation for CO2 Minimum Miscibility Pressure in Tight Oil Reservoirs*. Paper presented at the SPE Trinidad and Tobago Section Energy Resources Conference, Port of Spain, Trinidad and Tobago. https://doi.org/10.2118/180857-MS

Zhang , T., Espinosa, D., Yoon, K. Y., Rahmani, A. R., Yu, H., Caldelas, F. M., Ryoo, S., Roberts, M., Prodanovic, M., Johnston, K. P., Milner, T. E., Bryant, S. L., & Huh, C. (2011). *Engineered Nanoparticles as Harsh-Condition Emulsion and Foam Stabilizers and as Novel Sensors*. Paper presented at the Offshore Technology Conference, Houston, Texas, USA. https://doi.org/10.4043/21212-MS

Zhang, Z., Freedman, V. L., & Zhong, L. (2009). *Foam Transport in Porous Media-A Review*. Retrieved from

Zolotuchin, A. B. U., Jann-Rune. (2000). *Introduction to petroleum reservoir engineering*. Kristiansand: Høyskoleforl.

Appendix

A. Core Analysis

A1. Core Saturation

Following procedure was conducted to saturate the core plug with brine. A container with a dry core plug was connected to a vacuum pump and vacuumed until the pressure was approx. 600 mTorr and stable for at least 10 minutes. The pressure was measured with a vacuum gauge connected to the system. The saturation fluid was vacuumed and then injected into the container with the core plug and left overnight to ensure full saturation of the sand pack. A schematic drawing of the air evacuation apparatus used for saturation of the core plug is shown in Figure A.1.

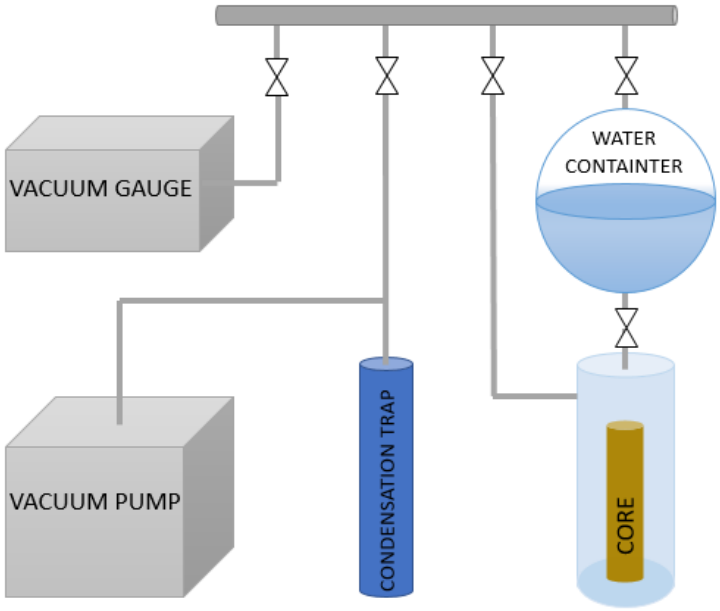

Figure A.1 Experimental setup for air evacuation apparatus.

A2. Porosity Measurements

Porosity is a dimensionless quantity, φ, defined as the ratio of the pore volume V_P and the bulk volume V_B. Porosity can be defined as:

$$\varphi = \frac{V_P}{V_B} \cdot 100\% \qquad A1$$

Porosity can be divided into effective and residual porosity. Effective porosity is the fraction of connected pores in a media where fluid can flow through and residual porosity represents isolated pores in the media. Porosity depends on several factors such as rock type, grain size, shape and distribution (Zolotuchin, 2000).

The effective porosity of the core plug can be measured by using the saturation method. The method involves weighting of the porous media in dry (gas saturated) and brine saturated conditions. The

weight difference corresponds to the weight of brine in the pores (Barnes, 1936). When the density of the brine, ρ, and the weights are known, the pore volume can be calculated using the equation below

$$V_P = \frac{m_{sat} - m_{dry}}{\rho} \qquad A2$$

The effective porosity can be calculated by combining Eq. and $V_P = \frac{m_{sat}-m_{dry}}{\rho}$ A2

.

A3. Permeability Measurements

Permeability, K, is the ease of which fluid flows through a porous media. Permeability divides into absolute, effective and relative permeability. The absolute permeability is the permeability at 100% saturation of a single fluid and was measured in the core plug and sand pack used during this thesis. The absolute permeability is defined and calculated by using Darcy's law:

$$Q = \frac{KA}{L}\frac{\Delta P}{\mu} \qquad A3$$

where Q is the flow rate, K is the absolute permeability, A is the cross sectional area of the porous media, L is the length of the porous media, μ is the viscosity of the injected fluid and ΔP is the differential pressure across the porous media (Lien, 2004).

The absolute permeability of the core plug was measured by injecting brine with a constant injection rate through the porous media. The differential pressure was measured and the permeability, K, was calculated using Eq. $A3$. The process was performed at different injection rates to reduce the uncertainties. Brine was injected through a Quizix QX6000 Pump and the pressure difference was measured using a differential pressure transmitter connected to a computer. The experimental setup for permeability measurements in a core plug is similar to the experimental setup illustrated in Figure 5.1.

B. Permeability Variations

Foam generation and apparent viscosity calculations depends on the permeability of the porous media. Permeability of the core plug was therefore measured between the injections for accurate results. Results show that the permeability varied between the initial value of 1.476 D to 1.142 D (Table B.1). Permeability reduction is probably caused by residual CO_2 inside the core. Although the core plug was cleaned after each experiment, the CO_2 might have been trapped in the pores. Studies of CO_2 trapping mechanisms show that CO_2 can be trapped in a porous media due to capillary pressure and dissolution with the brine (Zhang et al., 2014).

Table B.1 Measured absolute permeability in a single core plug between the injections

Measurement	Permeability [D]	Standard Deviation [D]
1	1.476	0.050
2	1.346	0.022
3	1.272	0.002
4	1.285	0.005
5	1.338	0.006
6	1.303	0.009
7	1.237	0.008
8	1.205	0.020
9	1.209	0.007
10	1.142	0.013
11	1.212	0.012
12	1.476	0.043
13	1.333	0.003
14	1.414	0.007
15	1.234	0.005
16	1.276	0.003
17	1.261	0.004
18	1.378	0.004
19	1.339	0.001
20	1.368	0.010
21	1.409	0.005
22	1.347	0.020
23	1.227	0.028

Prior to permeability measurements a total of 8-10 PV cleaning solvent and brine were injected into the core as described in Chapter 5.6. The fluids were injected at different rates and results showed a correlation between the injection rate and permeability (Figure B.1). Injections at low rates (5-10 ml/h) over a longer period resulted in higher permeabilities, thus better cleaning compared to injections at high rates (100 ml/h). Although permeability varied between the injections, it was lowest during injections using anionic surfactant (SFB) and this might have affected the results (see Chapter 7.2).

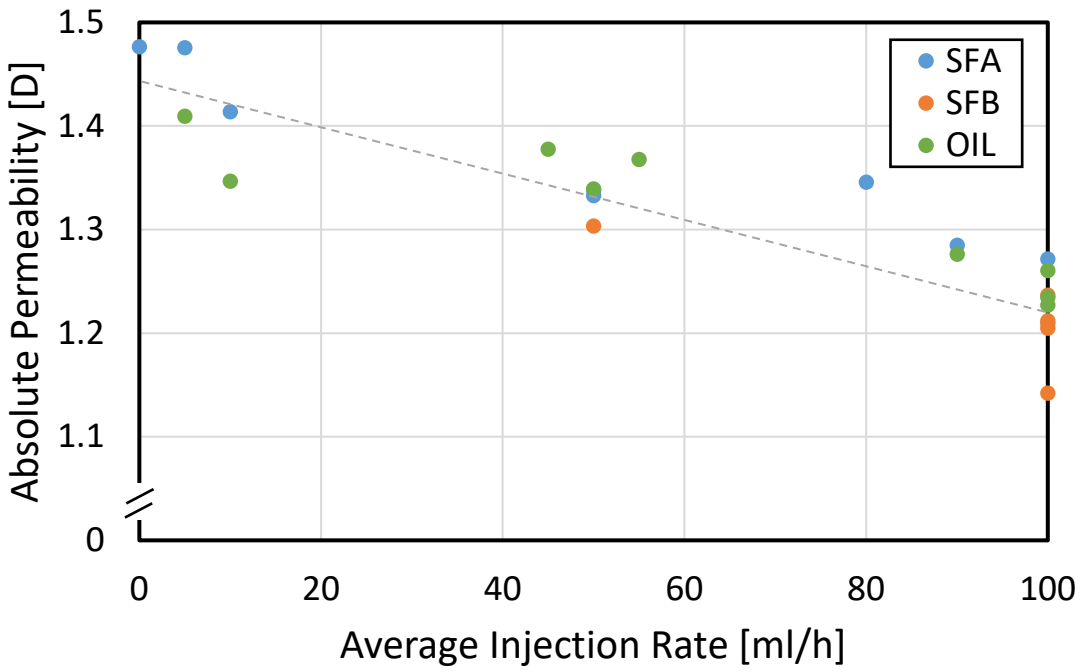

Figure B.1 Absolute permeability of the core as a function of average injection rate during cleaning procedure. Cleaning at low injection rates (5-10 ml/h) resulted in higher permeability compared to injections at high rates (90-100 ml/h). Absolute permeability was lowest during injections using anionic surfactant (SFB).

C. Surfactant and Nanoparticle Concentration Calculations

To create a desired foaming agent solution, the amount of surfactants and nanoparticles was carefully calculated and weighted. The anionic surfactant and nanoparticles used during the experimental work were dispersed in brine and the weight of the solution needed to get the desired concentration was calculated following Eq. C1 and C2.

$$Mass\ NP/SF\ needed = \frac{Desired\ concentration\ [mPPM] \times Amount\ of\ brine\ [g]}{1 - Desired\ concentration\ [mPPM]} \qquad C1$$

$$Weight\ NP/SF\ solution = \frac{Mass\ NP/SF\ needed}{NP/SF\ activity} \qquad C2$$

The anionic surfactant solution was 38.95% active and the nanoparticle solution was 30% active. Nonionic surfactants were in solid phase (100% active) and in a condition to directly be placed on the scale for weighing. Table C.1 show the amount of nanoparticles and surfactants needed to create 1 L of desired foaming agent solution.

Table C.2 Weight of foaming agent needed to make desired foaming agent solution

	5000 PPM	**3500 PPM**	**1500 PPM**	**150 PPM**
Nanoparticles	-	-	4.8 [g]	0.48 [g]
Anionic Surfactant	12.4 [g]	8.7 [g]	-	-
Nonionic Surfactant	5.0 [g]	3.5 [g]	-	-

D. Rate Scan Results

The apparent viscosity is proportional to the differential pressure across the core. During steady state co-injections, differential pressure was measured to investigate foam generation using different foaming agents, injection rates and gas fractions. Injection rates (u) were 16, 8, 4 and 1 feet/day and gas fractions (f_g) were 0.6 and 0.9. Results using all three foaming agents (SFA500, SFA3500 NP1500 and SFA3500 NP150) show identical trends. Differential pressure increased as the CO_2 and the foaming agent entered the core and stabilized after several PV injected. As the injection rate decreased, the differential pressure also decreased. Fluctuations caused by BPR at lower rates were observed and were discussed in Chapter 6.1.

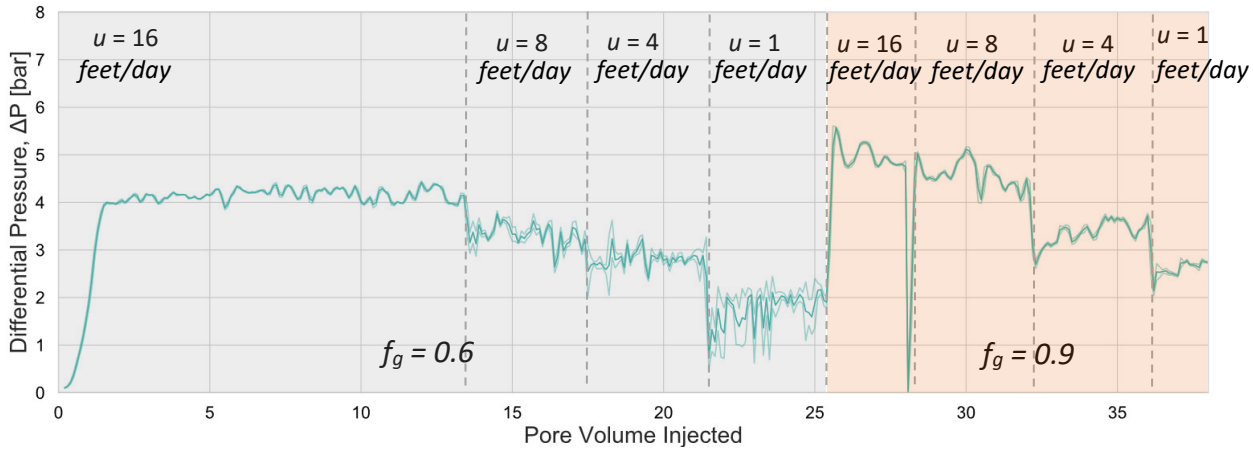

Figure D.1 Differential pressure during co-injection of CO_2 and SFA5000. Gray and orange areas represent injections at fg = 0.6 and fg = 0.9, respectively.

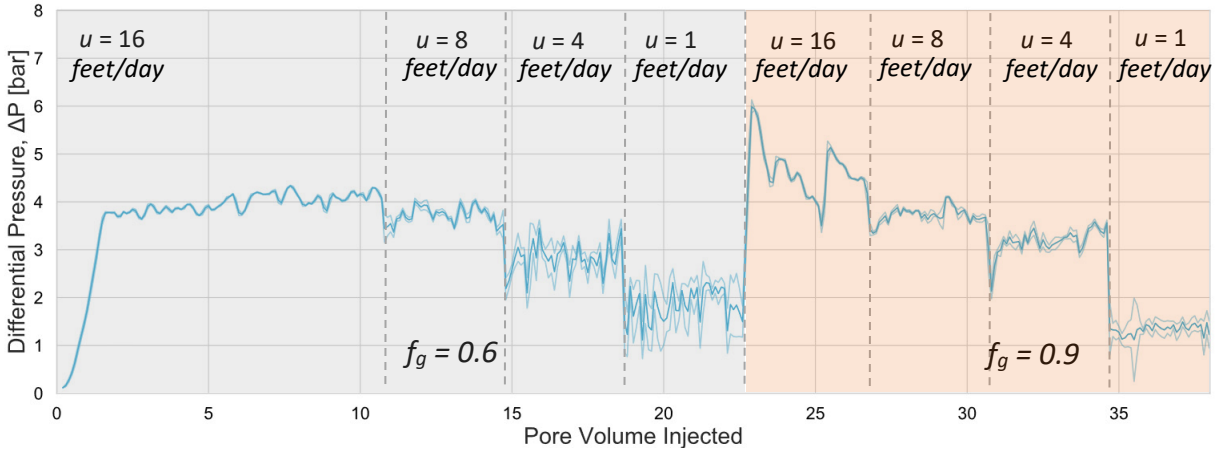

Figure D.2 Differential pressure during co-injection of CO_2 and SFA3500 NP1500. Gray and orange areas represent injections at fg = 0.6 and fg = 0.9, respectively.

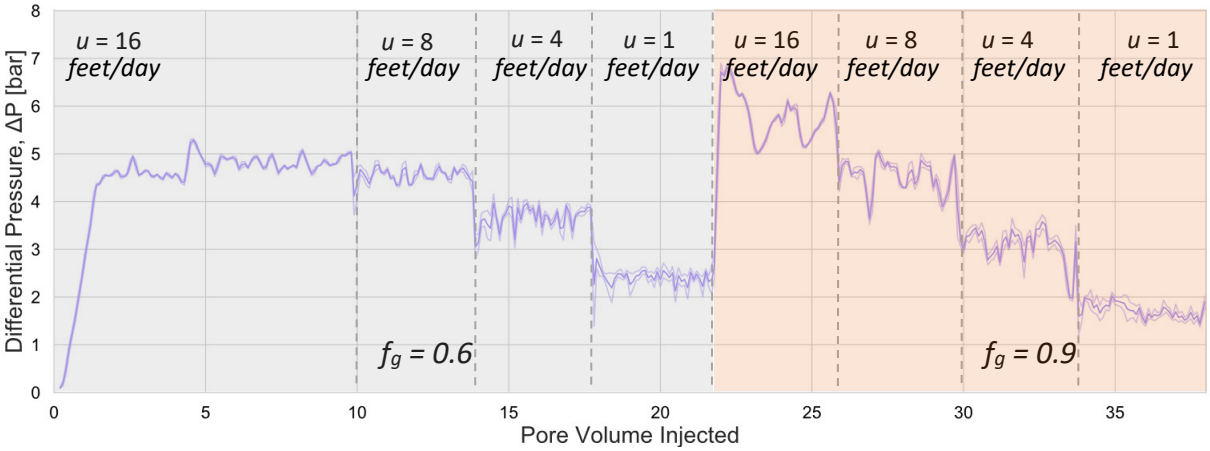

Figure D.3 Differential pressure during co-injection of CO_2 and SFA3500 NP150. Gray and orange areas represent injections at fg = 0.6 and fg = 0.9, respectively.

E. Sand Packs

Investigation of CO_2 foam in unconsolidated systems has been proposed to study foam behavior as a function of length. The idea was to perform injections on sand packs and measure differential pressure at different length to investigate CO_2 foam generation, coalescence and re-generation. In addition, visual analysis of front movement was suggested.

There was developed a new experimental setup for investigation of fluid flow and foam generation in sand packs during this thesis. This section describes the preparation of sand packs, experimental setup, results from porosity and permeability measurements and the challenges observed during this work.

E1. Sand Preparation

To make a homogenous, unconsolidated porous media, the sand was accurately prepared. Sand used in this thesis is quartz-rich sand. Firstly, the sand was flushed with tap water to remove organic content and other impurities. Then it was sifted using several geological sieves. First with a sieve with large mesh size and then by gradually decreasing the mesh size to 125 µm. Afterwards, the sand was dried at 60 °C for 5 days. The final sand consisted of a grain size distribution of sand grains ranging from 250 µm to 125 µm. Due to the preparation process the wettability of the sand is considered water wet. The wettability of the same sand was previously checked by Saunes (2018) using a floating method suggested by Anderson (1986).

E2. Packing Procedure

Sifted and dried sand was packed into glass tubes of different lengths to create sand packs. The sand packs were made performing a combination of a shaking procedure suggested by Brattekås et al. (2019) and sand compression by water injections. A vertically positioned glass tube with an end piece, mesh and paper filter at the bottom was filled with approximately 3 grams of sand using a funnel. The glass tube was gently shaken before more sand was added into the glass. The process was repeated until the glass tube was filled to the rim with sand. The glass tube was then closed with a hydraulic end piece (end pieces are described in Section E3). Distilled water was injected through a Quizix QX1500 pump into the sand pack to compress the sand. As the sand moved toward the outlet, the hydraulic end piece moved in the same direction compressing the sand. When no more movement could be observed, more sand was filled into the sand pack and water was injected into it. The process was repeated until no end piece movement was observed and the sand pack was considered well packed. The setup for water injections is illustrated in Figure E.1. The same setup was used during the permeability measurements.

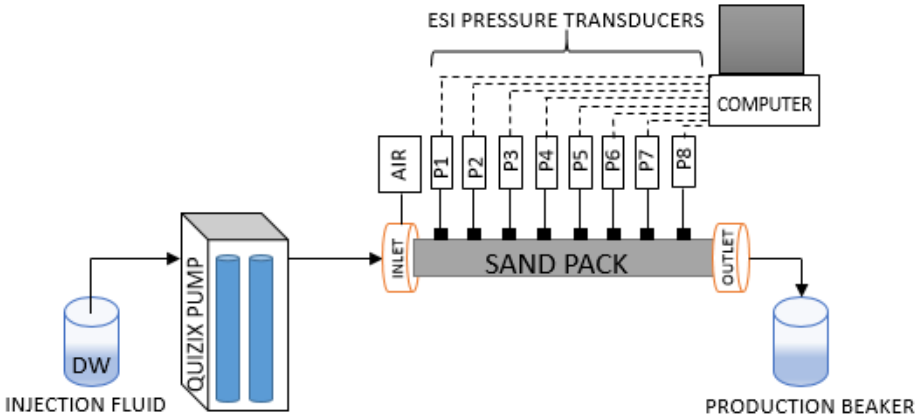

Figure E.1 Experimental setup for sand compression and permeability measurements.

E3. Equipment for Assembling the Sand Pack

The sand packs were closed in both ends using two specially designed end pieces. An inlet piece was attached to one side of the glass tube and an outlet piece to the other. Four steel rods secured by locknuts on the inlet side and regular nuts on the outlet side connected the end pieces. The inlet end piece consisted of two parts made of polyoxymethylene (POM) (Figure E.2). An end piece with a tubing to allow inflow of fluids into the sand pack and a bigger piece around it with a tubing connected to air. The purpose of the second piece was to push the end piece further into the glass tube in case of sand compression and sand movement. This hydraulic end piece acted like a piston and prevented changes in sand pack properties due to sand compression. The outlet end piece consisted of one part made of POM with a PEEK tubing to allow fluids to flow out from the sand pack (Figure E.3). Both a paper filter and a mesh were placed at the end of both sides of the tube to keep the sand in place. The paper filter used during the experiments was Whatman 41 filter with pore size of 20 – 25 µm. Figure E.4 illustrates an assembled sand pack with all parts that are necessary. All the parts are listed in Table E.1 .

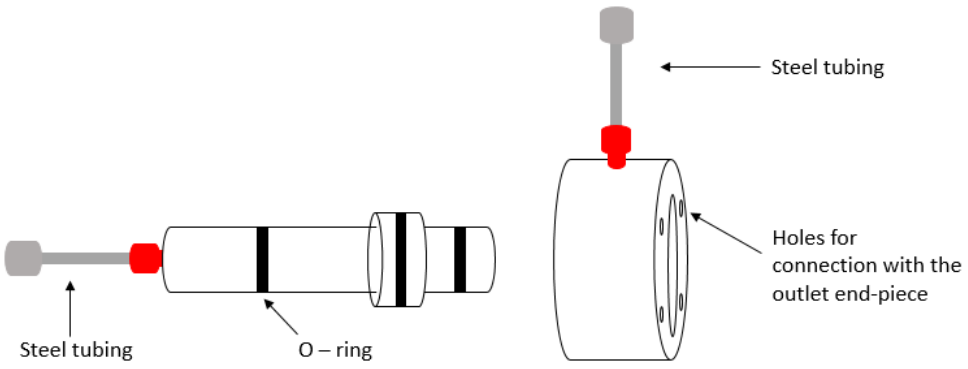

Figure E.2 Hydraulic inlet end piece consisting of two parts. Inner part (left) and outer part (right).

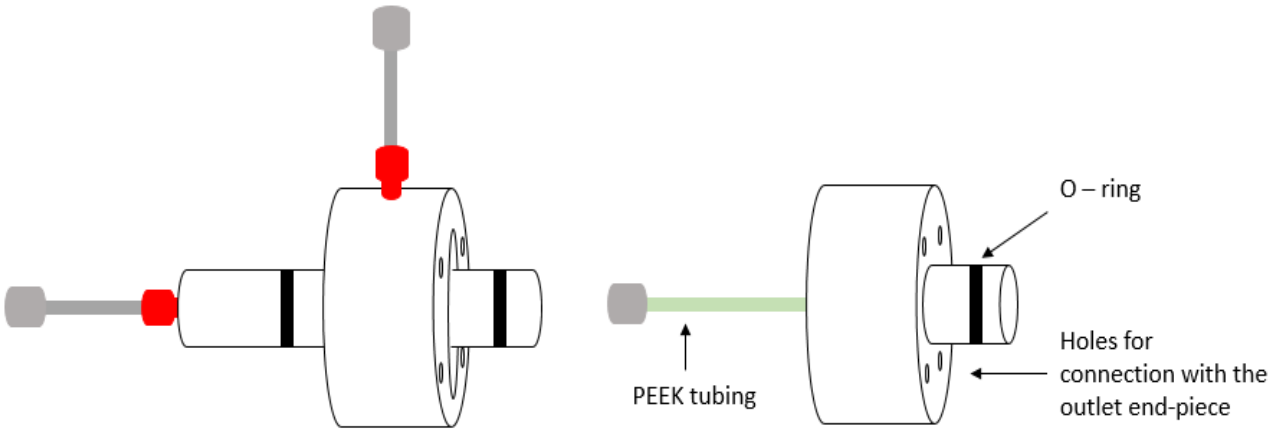

Figure E.3 Inlet end piece consisting of two parts (left), outlet end piece (right).

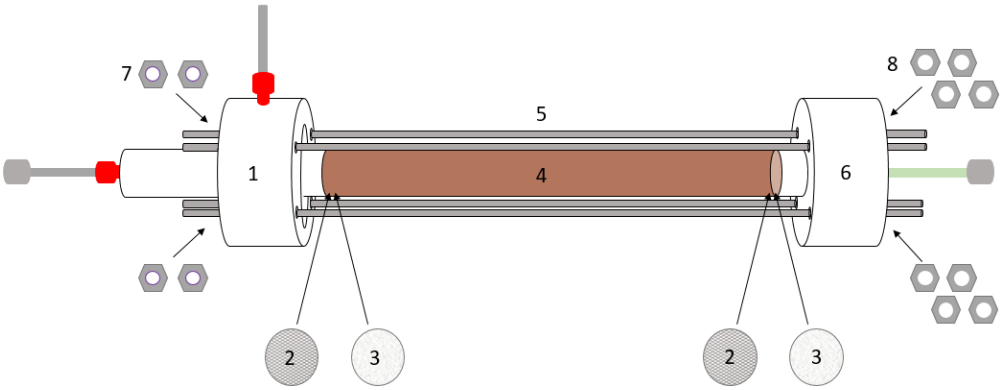

Figure E.4 Parts needed for assembling glass tube.

Table E.1 List of equipment used to assemble sand pack

	Part
1	Hydraulic inlet end piece
2	Metal mesh
3	Paper filter
4	Glass tube
5	Threaded rods
6	Outlet end piece
7	Locknuts
8	Nuts

E4. Experimental Procedure

Figure E.5 represents the experimental setup for foam generation and foam stability studies in a sand pack at 25 °C and 2 bar. A pre-packed sand pack was placed on a scale, connected to an inlet and outlet tubing and eight ESI pressure transducers. Both the scale and the pressure transducers were connected to a computer for measurements. An aqueous solution was injected into the sand pack through a Quizix QX1500 Pump and gas was injected through a Bronkhorst EL-Flow Mass Flow Controller (MFC). Gas used in the first stage of the experiments was nitrogen (N_2). The setup allowed injection of one or two fluids simultaneously. To prevent liquid from flowing into the MFC, a check valve and a water trap was attached as shown in the illustration bellow. The production fluids were collected in a pressurized container to maintain a desired pressure of 2 bar in the sand pack and to reduce the compressibility effects of the gas. Table E.2 describes the equipment that the setup contained.

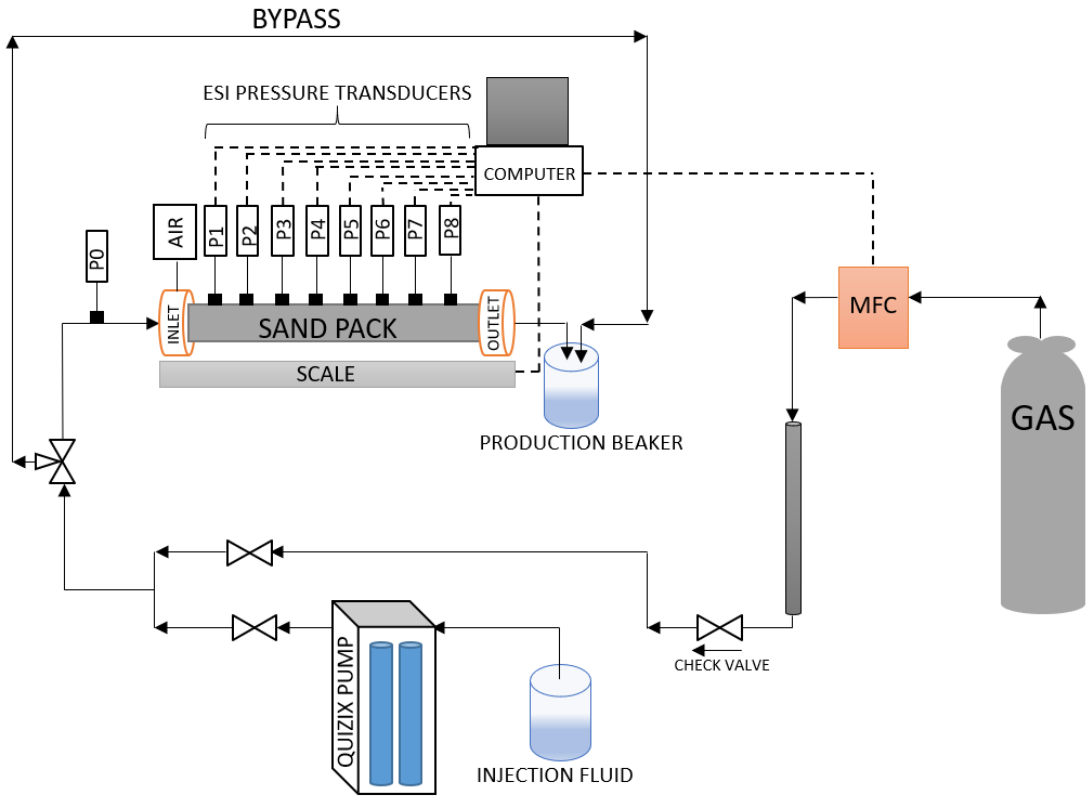

Figure E.5 Experimental setup for investigation of fluid flow and foam generation in unconsolidated system.

Table E.2 List of equipment used during experiments in sand packs

Assembled Sand Pack
Quizix QX1500 pump for injection of aqueous solutions
ESI Pressure Transducers for pressure measurements (range 0 – 4 bar)
Bronkhorst EL-Flow Mass Flow Controller for gas injection
Scale for saturation measurements
Pressurized production beaker
N_2 tank used for gas injection
Cylindrical tube used as a water trap
Swagelock tubing and valves
Computer to operate Quizix pump, ESI Pressure Transducers and scale

E5. Sand Pack Analysis

Porosity and permeability of two sand packs was measured as described in Appendix A. Since eight pressure transducers were connected to the sand pack (as shown in Figure E.), permeability was measured at different lengths. Section 1, referred to as S1, was the section close to the inlet end piece. The distance between the following sections was 5 cm. The measurement was repeated twice. First, the fluid was injected from inlet to outlet, secondly from outlet to inlet. The results are represented in Table E.3.

Table E.3 Porosity and Permeability of sand packs

	Sand pack 1	**Sand pack 2**
Porosity [%]	33.7 ± 0.2	34.4 ± 0.2
Permeability S1 [D]	22.5 ± 0.1	22.5 ± 0.4
Permeability S2 [D]	22.2 ± 0.1	25.4 ± 0.8
Permeability S3 [D]	22.7 ± 0.1	18.6 ± 0.2
Permeability S4 [D]	22.3 ± 0.1	24.2 ± 0.8
Permeability S5 [D]	21.9 ± 0.2	22.6 ± 0.8
Permeability S6 [D]	21.9 ± 0.2	24.8 ± 0.4
Permeability S7 [D]	20.6 ± 0.2	26.9 ± 0.4
Average Permeability [D]	22.0 ± 0.7	23.6 ± 2.6

E6. Experimental Challenges

During development of the new setup, there were observed some experimental challenges. The main challenge was due to the packing procedure as the glass tube was thin and would break easily. To ensure sufficient sand compaction, the sand pack was disassembled by removing the inlet end piece to add more sand. Repeated disassembling weakened the glass tube and caused breakage. Additionally, it was difficult to create a stable sand pack with no sand movement inside. When distilled water was injected, sand grains moved forward, and some migrated through pressure ports towards ESI pressure transducers, resulting in uncertainties in porosity and permeability and poor compaction. Sand movement could also affect the fluid flow inside the porous media. Figure E.6 show voids inside the sand pack as a result of sand movement.

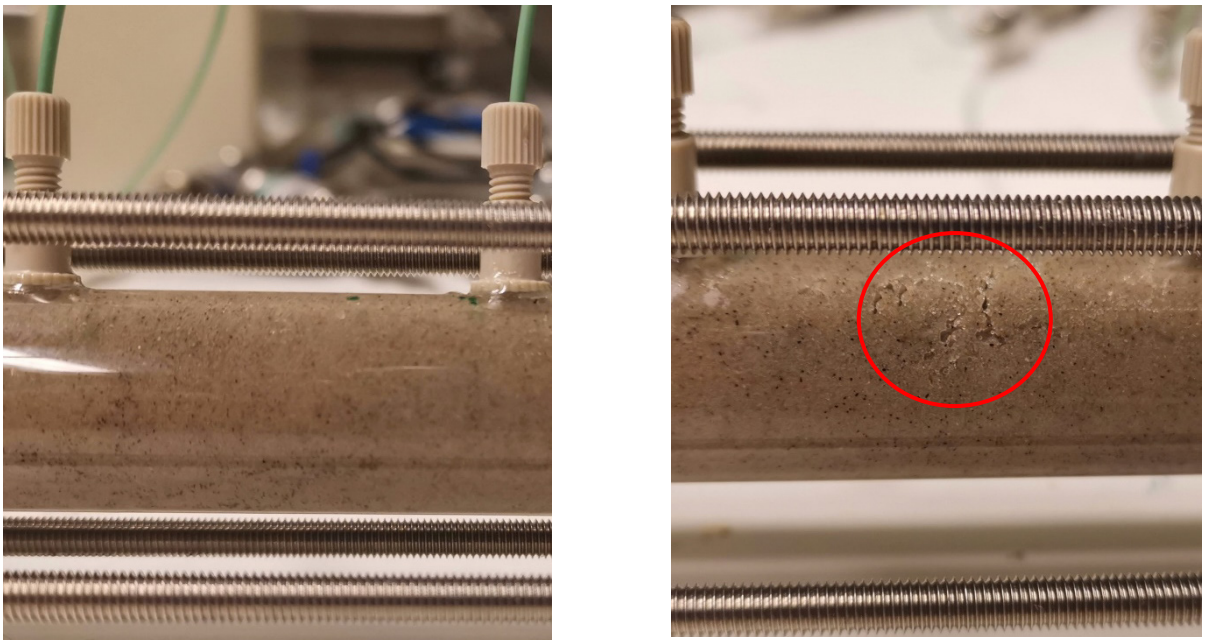

Figure E.6 A section of sand pack prior to water flood (left) and after water flood (right) show voids as a result of sand movement causing uncertainties in porosity and permeability measurements.

To measure the pressure inside the sand pack, ESI pressure transducers were connected to pressure ports on top of the sand pack. Pressure ports were attached using epoxy resin and after several PV water injected, leakage was observed. It would be desirable if a better method of attaching the pressure ports would be developed in future work.

F. Uncertainties

The uncertainty in experimental measurements is caused by two sources: the uncertainty of instruments used during the experiment, e.g. uncertainty of the scale, and the experiment itself, e.g. the method used to measure the porosity. The total uncertainty of a measured value depends on the uncertainty of all the instruments used during the measurement. The instrumental uncertainties are found in Table F.1. The following equations were used to calculate uncertainties during the experimental work.

Addition and Subtraction

When several independent variables $x, y, z \dots, i$, were added or subtracted to calculate a value

R, the uncertainty in R, S_R, was calculated based on the uncertainty of each variable ($S_x, S_y, S_z, \dots, S_i$) :

$$S_R = \sqrt{\left(\frac{\delta R}{\delta x} S_x\right)^2 + \left(\frac{\delta R}{\delta y} S_y\right)^2 + \left(\frac{\delta R}{\delta z} S_z\right)^2 + \cdots + \left(\frac{\delta R}{\delta i} S_i\right)^2} \qquad F1$$

Multiplication and Division

If the value R is calculated as the product or quotient of a set variables $a^2x, b^2y, c^2z, \dots, n^2i$, where $x, y, z, \dots, i$ are variables with an uncertainty $S_x, S_y, S_z, \dots, S_i$ and $a^2, b^2, c^2, \dots, n^2$ are constants the uncertainty S_R can be calculated by:

$$S_R = R\sqrt{\left(a\frac{S_x}{x}\right)^2 + \left(b\frac{S_y}{y}\right)^2 + \left(c\frac{S_z}{z}\right)^2 + \cdots + \left(n\frac{S_i}{i}\right)^2} \qquad F2$$

Standard Deviation

The variation of a set of data, S, can be calculated by following equation:

$$S = \sqrt{\frac{1}{N-1}\sum_{i=1}^{N}(x_i - \bar{x})^2} \qquad F3$$

where N is the number of samples values x and $\bar{x}$ is the sample mean.

Table F.1 Instrumental uncertainties for equipment used during the experimental work

Instrument	Parameter	Uncertainty
Scale	Mass	± 0.01 g
Caliper	Length	± 0.002 cm
Ruler	Length	± 0.1 cm
Measuring Cylinder	Volume	± 0.1 ml
ESI Pressure Transducer	Pressure	± 0.1 % of full scale
Differential Pressure Transducer	Pressure	± 0.075 % of full range
EL-FLOW Mass Flow Controller	Rate	± 0.02 ml/h